Relaxation phenomena in dense glassy polymer membranes

R.H.B. Bouma

RELAXATION PHENOMENA IN DENSE GLASSY POLYMER MEMBRANES

PROEFSCHRIFT

ter verkrijging van
de graad van doctor aan de Universiteit Twente,
op gezag van de rector magnificus,
prof. dr. Th.J.A. Popma,
volgens besluit van het College voor Promoties
in het openbaar te verdedigen
op vrijdag 27 januari 1995 te 15.00 uur.

door

Richard Hendrik Bouke Bouma

geboren op 23 september 1967

te Zuidhorn

Dit proefschrift is goedgekeurd door de promotoren

prof. dr. ing. H. Strathmann,
prof. dr. C.A. Smolders

en de assistent promotor

dr. ir. Th. van den Boomgaard.

aan Tea en Mathijs

SON/NWO is gratefully acknowledged for their financial support.

CIP-DATA KONINKLIJKE BIBLIOTHEEK, DEN HAAG

Bouma, Richard Hendrik Bouke

Relaxation phenomena in dense glassy polymer membranes /
Richard Hendrik Bouke Bouma. - [S.l. : s.n.]. - Ill.
Thesis Enschede. - With ref. - With summary in Dutch.
ISBN 90-9007846-0
Subject headings: polymers / membranes

Printed in the Netherlands by Ponsen & Looijen B.V., Wageningen.

Contents

Chapter 1

Introduction

1.1. Penetrant transport in glassy polymers

Experimental observations made on physical or chemical processes may be biased by the time-scales involved in executing the experiments. Especially when the transient state of a process is studied, the measurement time has to be small compared to the time-scale of changes in the process. On the other hand when the steady-state of a process is studied, the observation may start only when the effects of a previous transient state have faded away.
The diffusion of penetrants in thin films of glassy polymers is studied in this thesis. The transient diffusion processes in films of various thicknesses, but under the same experimental conditions, can only be related to each other when the experimental time-scale is corrected according to the dimensions of the polymer film. In Fickian diffusion, or so-called case I transport, the experimentation time divided by the square of the film thickness is a characteristic parameter. Usually the curves, describing for example the kinetics of a sorption or desorption experiment, or the time-lag of the flux through a membrane in a transient permeation experiment, plotted as a function of this characteristic parameter then converge into a mastercurve. This occurs only when two conditions have been met:

1) Mass transfer in the polymer film is the rate determining step of the process.
2) The polymer and penetrant remain locally in an equilibrium state throughout the diffusion process.

The first condition implies that the diffusion coefficient of a penetrant in the polymer film should be at least substantially lower than its corresponding diffusion coefficient in the adjacent phase(s) of the polymer film. Furthermore the mass transfer coefficient of the penetrant in the adjacent phase of the membrane should be so high, that no or negligible depletion of the penetrant does occur near the membrane. Usually the first condition is fulfilled when the transport of penetrants in polymers is studied.

The second condition, however, needs careful attention. The response of a glassy polymer to a change of the penetrant activity in its environment, is in general (extremely) slow. The relaxation times in glassy polymers associated with the transition from glasslike to rubberlike consistency are of the order of one hour or even more. The transient state in a diffusion process should therefore exceed these relaxation times. Performing diffusion experiments while maintaining local equilibrium, can be accomplished by increasing the film thickness. The use of thick films may not link up with the need for relatively fast experiments, or with the

application of thin membranes in practice. An estimate of the transport regime encountered, i.e. an equilibrium or a non-equilibrium diffusion process, is given by the so-called Deborah number for diffusion, $(DEB)_D$ [1]. This number is defined as the ratio of the characteristic relaxation time of a material, and the characteristic time of a transient diffusion process.

$$(DEB)_D = \frac{\tau}{\theta_D} = \frac{D\tau}{L^2},$$

with τ the characteristic relaxation time of the polymer corresponding to the level of penetrant activity in the diffusion process, and θ_D the characteristic time of the transient diffusion process which is equal to the square of film thickness L, divided by the diffusion coefficient D, corresponding to the same level of penetrant activity.
The Deborah number for diffusion is implicitly a function of the penetrant activity, because the activity influences relaxation times and diffusion coefficients, and it is an explicit function of the thickness of a film. Therefore the Deborah number for diffusion is applicable only to a diffusion process in which the applied change in penetrant activity is relatively small.
The Deborah number for diffusion will be (much) smaller than 1, when the polymer structure responds fast to changes of the penetrant activity in its environment, and the equilibrium state of the polymer-penetrant system is maintained. In this situation Fickian diffusion applies.
The Deborah number for diffusion will be (much) larger than 1, when the polymer structure responds not at all, or very slowly, to changes of the penetrant activity in its environment, and the polymer and the penetrant are not in an equilibrium state during the transient diffusion process. Experimentally case I transport is observed too, if the polymer does not respond to changes in penetrant activity. The transient diffusion processes can be related to each other by dividing the experimental time-scale by the square of the film thickness, but the diffusion coefficients are not representative for the final equilibrium state of the system. Therefore this transport regime is sometimes called pseudo-Fickian diffusion instead of Fickian diffusion. The momentary state depends on previous heat-treatments, preswelling in solvents, physical aging, etc. Pseudo-Fickian diffusion is an exception from the second condition, mentioned before.

The concept of the Deborah number for diffusion, that can predict the mode of transport, is valid only when small (stepwise) changes in penetrant activity are applied. If the changes in penetrant activity are large, then a situation may arise where a gradient in the Deborah number for diffusion is established [1]. Concentration dependent diffusion and anomalous diffusion, in which polymer relaxation proceeds at a time-scale comparable to the time-scale of the transient diffusion process, can be found frequently. The kind of transport depends on the polymer-penetrant combination, the change in penetrant activity, and the temperature. Various transport phenomena have been depicted globally in the Hopfenberg-Frisch chart [2], including

concentration independent Fickian diffusion, concentration dependent Fickian diffusion, time dependent diffusion anomalies, case II transport and solvent crazing-stress cracking.
An extreme case of non-Fickian diffusion is the situation in which part of the film is characterized by a Deborah number for diffusion much smaller than 1, and in another part by a value much larger than 1 [1,3]. The resulting transport regime is called case II transport, and can easily be distinguished from case I transport, because the transient diffusion processes scale with the film thickness instead of the squared film thickness. In the kinetics of sorption a penetration front can be identified which travels with a constant velocity through the polymer film. According to literature [3], there is a concentration gradient and a pressure gradient at the penetration front. A large amount of penetrant can be transported through the swollen part of the film towards the penetration front. There it will penetrate the unswollen part of the film, even though polymer relaxation is too slow to keep pace with the penetrant uptake. The absorbed amount of penetrant will therefore deform the polymer matrix. The so-called swelling pressure balances the tensile stress induced in the polymer.
At large volume deformation and therefore at large tensile stress, the swelling may induce mechanical failure in the polymer. The phenomenon of crazing or cracking is an extreme situation of case II transport.

1.2. Scope of the thesis

In membrane technology dense polymer films are used as permeation selective barriers that can change the composition of a fluid. Due to activity differences across the membrane, molecules will adsorb at the upstream side of the membrane and diffuse through the membrane, where they desorb at the downstream side. The selective permeation is based on differences in solubility and diffusivity in the membrane, of the components in the feed mixture.
Membranes prepared from glassy polymers usually show good selectivities, but low fluxes. A simple solution to the low fluxes is to diminish the membrane thickness. In practice, however, this does not always work.
Even if one can prepare defect-free thin membranes the transient permeation of these thin membranes may result in unexpected mass transport properties and thus transient membrane selectivity behaviour. By decreasing the membrane thickness the Deborah number for diffusion increases drastically, because its magnitude is inversely proportional to the square of the film thickness. The steady-state will be reached only after the complete membrane has attained its equilibrium state. Therefore polymer relaxation times can have a significant effect on the transient permeation through a membrane.

In chapter 2 the transient permeation behaviour of thin membranes, prepared from a glassy polymer, is studied. The membranes are used in the pervaporation process. In this process a liquid mixture is applied to the upstream or feed side of the membrane.

A vacuum or a sweeping gas is applied at the downstream or permeate side of the membrane. At the feed side of the membrane, often relatively large swelling is obtained, which decreases the polymer relaxation times and increases the diffusion coefficients of the penetrants. At the permeate side of the membrane, however, the penetrant activities are maintained at a level that is (almost) zero. In general the gradient in Deborah number for diffusion, in a membrane, will be large in pervaporation, compared to vapour permeation and gas separation.
Transient phenomena in the pervaporation process are studied in this chapter for differently prepared membranes.
In chapter 3 the description of transient diffusion processes in glassy polymers will be looked at in more detail. Attention is paid to the application of large changes in penetrant activity. The implications of non-steady state permeation to membrane processes applying dense membranes of glassy polymers will be discussed.

The membranes used in pervaporation are prepared by dissolving the polymer in a suitable solvent, casting the solution on a support, followed by evaporation of the solvent in an inert atmosphere. Both the dissolution and the drying step are transient diffusion processes. In this work the drying step is studied, because it might have a significant influence on the obtained membrane prepared from a glassy polymer.

In chapter 4 the drying of a cast polymer solution is numerically simulated. The time-scale of the drying process is compared with polymer relaxation times. When the initial thickness of a cast polymer solution is decreased, the time-scale of the drying process will be decreased too. During the evaporation the total film thickness decreases, and the polymer matrix will compact. The compaction or densification may be slow, compared to the evaporation of solvent and excess free volume can be frozen into the polymer matrix. In permeation experiments the available free volume is accessible to the penetrants. A large free volume decreases the membrane selectivity, when the separation is based on differences in diffusivity, because of differences in the free volume distribution. Excess free volume will decrease in time, a process called physical aging.
In chapter 5 the drying of cast polymer solution is followed by monitoring the changes in its dielectric properties. The interdigitated or comb electrodes are used as the electrode geometry in the dielectric experiments, because they do not disturb the drying process. Both the polymer and the solvent contribute to the complex dielectric permittivity of a material. Significant changes in the amount of solvent in the glassy state of the polymer can be seen, in case the solvent has a high dipole moment compared to the dipole moment of the polymer.
In chapter 6 the changes in mechanical properties of a drying polymer solution are monitored. The drying-film torsion-pendulum is sensitive to changes in the mechanical impedance, exerted by a polymer solution or polymer film, onto the torsion-pendulum. The mechanical impedance is determined, amongst others, by the complex shear modulus of the dissolved or diluted polymer.

1.3. References

1. J.S. Vrentas, C.M. Jarzebski, J.L. Duda, A Deborah number for diffusion in polymer-solvent systems, AIChE Journal 21 (1975) 894-901.
2. H.B. Hopfenberg, H.L. Frisch, Transport of organic micromolecules in amorphous polymers, Journal of Polymer Science, Part B, 7 (1969) 405-409.
3. J.C. Wu, N.A. Peppas, Modeling of penetrant diffusion in glassy polymers with an integral sorption Deborah number, Journal of Polymer Science: Part B: Polymer Physics 31 (1993) 1503-1518.

Chapter 2

Pervaporation using Thin Membranes made of Glassy Polymers

2.1. Introduction

Pervaporation is a technique competitive to distillation, liquid-liquid extraction and crystallization. The preference for a specific technique depends on the physical and chemical properties of the components in the liquid mixture, and the economics of the process.

In pervaporation a liquid mixture is brought into contact with a dense membrane. The permeate side of the membrane contains a vacuum or a carrier gas, providing a driving force for transport. The properties of the membrane influence the separation efficiency and transport rates that can be achieved [1].

One can distinguish membranes made of glassy polymers from membranes made of rubbery polymers. Membranes of the latter category have the advantage of rather high fluxes, but usually provide only low separation factors. Membranes prepared from glassy polymers usually show high separation factors and low fluxes. In general these membranes are at the same time more resistant to harsh conditions like high temperatures and agressive chemicals. A lot of research has been carried out to improve the fluxes through membranes of glassy polymers, while maintaining the selective properties of the membrane at the same level. A very simple concept, though still difficult to realize in commercial applications, is the reduction of membrane thickness. Although not anticipated, the increase in flux with decreasing thickness is often accompanied by a decrease in separation factor [2-3].

In pervaporation with glassy polymers as the membrane material, the history of the membrane is very important, because the glassy state is a metastable state. In thermodynamics the glass transition is called a second order transition. At the glass transition the derivatives of the thermodynamic properties like enthalpy, entropy and volume, with respect to temperature and pressure, are discontinuous whereas these thermodynamic properties themselves are continuous [4]. Experimentally it is noticed that the presence of plasticizers in a glassy polymer depresses the glass transition temperature [5], and influences the glassy state itself [6]. Struik [7] found that all glasses 'age' in a similar way, after a temperature quench into the glassy state. He explained the physical aging by stating that the excess free volume in a glass, frozen into the structure at the vitrification of the material, disappears at a rate depending on the segment mobility in the glass. This segment mobility decreases with decreasing amount of excess free volume, and therefore aging is proceeding at a self-decreasing rate.

In permeation experiments with glassy polymers, differences in diffusion coefficients often determine the selective permeation of gas or liquid mixtures through the

membrane. The movement of small molecules in an undiluted polymer matrix is related to the free volume available for diffusion [8]. The experiments presented in this chapter with polyacrylonitrile as the glassy polymer are very sensitive to the history of the membrane because of the dependency of the very low diffusion coefficients on pretreatment. In gas separation polyacrylonitrile is not used, because of its extremely low gas permeabilities [9]. In pervaporation the solubility of permeants can influence permeation selectivity. The permeate side of the membrane however, remains 'dry', which means that at this place permeant fluxes are the product of the diffusion coefficients at permeant concentrations approaching zero, and the respective local concentration gradients of the permeating components. In pervaporation the morphology at the permeate side of the membrane is of extreme importance.
Spitzen *et al.* [2] gave a number of possible explanations for the decrease in separation factor in pervaparation with thin membranes: defects in the membrane, dependence of membrane morphology on thickness, non-steady state behaviour, sorption resistance, concentration polarization and temperature effects. Of these explanations only the dependence of membrane morphology on thickness and the non-steady state behaviour will be addressed in this work in detail, as they prevail against the other possible explanations. Koops *et al.* [3] propose that the decline in separation factor for pervaporation using thin membranes is due to the presence of cracks and crazes, induced by large swelling stresses. The concentration profile in the membrane will be accompanied by gradients in swelling of the polymer and (large) stress gradients are the result for thin layers. In case the polymer cannot resist the (large) stress gradients, macroscopic failure will be invoked. Except for the decline in separation factor with decreasing membrane thickness, no further experimental support has been found yet for this hypothesis.
In this chapter the behaviour of thin, glassy membranes in the pervaporation process is the subject of investigation. The dependence of pervaporation performance on the thickness of so-called homogeneous, dense membranes, and the time-dependence of fluxes and separation factors will be examined. Dense membranes of polyacrylonitrile are used as a model system, with thicknesses varying from a few μm up to about 20 μm. The feed mixture consists of ethanol and water, and as diffusion is generally the selectivity determining parameter for glassy polymers, water will be permeated preferentially. The feed mixture is therefore rich in ethanol, in order that we are able to measure both component fluxes.

2.2. Theory of pervaporation

There is a variety of techniques that can change the composition of liquid mixtures. Differences in chemical potentials give rise to driving forces, needed in all processes. In pervaporation processes gradients in chemical potentials are created by applying a vacuum at the permeate side of a membrane. One can also sweep a carrier gas along the permeate side. At the feed side solvent activities are determined by the composition of the solvent mixture, at the permeate side activities are (almost) zero if

the permeating components are removed effectively. The relation between the molar chemical potential μ of a component in a mixture, and its activity a is given by:

$$\mu_i(p,T,\text{composition}) = \mu_i^*(p,T) + RT \ln(a_i), \qquad (1)$$

with μ^* the chemical potential of the pure substance at pressure p and temperature T, the subscript i denoting the component considered, and R the gas constant.
For a pure liquid substance the activity is always one. Mixing it with another substance is only successful if the Gibbs free energy of the system is lowered. Activities therefore range from zero to one.
The chemical potential of a component in a liquid mixture, apart from a constant value, can be measured, for example from vapour-liquid equilibrium data, or estimated from models for binary liquids. Some models are empirical (Van Laar, and Margules), others are based on statistical thermodynamics (for example Wilson, NRTL and UNIQUAC).

In this work mixtures of ethanol and water are used. Data are available on vapour-liquid equilibria for this system, as a function of temperature and pressure [10]. Solvent activities are determined by calculating the solvent vapour pressures from experimentally determined vapour pressures and vapour compositions, applying the ideal gas law and Dalton's law, and dividing the solvent vapour pressures by the respective saturated vapour pressures at corresponding temperatures. Saturated vapour pressures are calculated with the Antoine equation. In figures 1 and 2 the activities of water and ethanol are given as a function of the respective weight fractions in an ethanol/water mixture.
Activities are not only a function of composition, but also of pressure and temperature. In figures 1 and 2 these variables are not recorded; activities are calculated for ethanol/water mixtures with temperatures ranging from 10 °C to 95.5 °C, and total vapour pressures ranging from 14.3 mmHg to 760 mmHg. For this system the activity is hardly any function of temperature and pressure.

In the pervaporation experiments in this study an ethanol/water mixture is used with a 0.9 weight fraction of ethanol. The corresponding ethanol activity is 0.8 to 0.9. Small deviations of the ethanol weight fraction result in a linear deviation of the activity as can be seen in figure 2. The complementary weight fraction of water is accompanied by a high water activity of 0.4 to 0.5, the activity being very sensitive to changes in feed composition.
In pervaporation a vacuum or a sweeping gas is applied at the permeate side of the membrane. Every molecule permeating through the membrane is removed effectively from the permeate side. The activity of the permeants is (almost) zero at the permeate side.

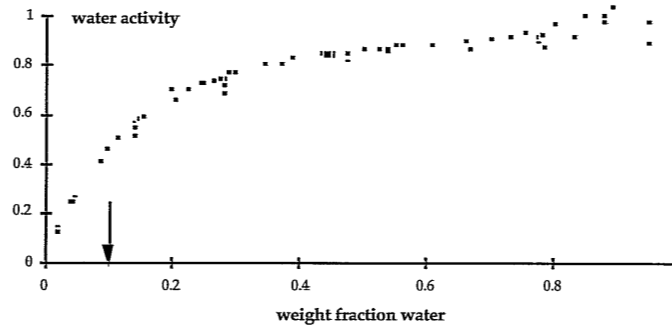

figure 1: Activity of water in a water/ethanol mixture as a function of the weight fraction of water. The arrow indicates feed concentrations used in pervaporation experiments.

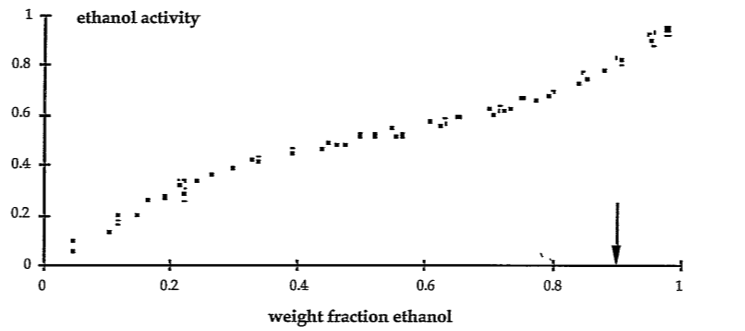

figure 2: Activity of ethanol in a water/ethanol mixture as a function of the weight fraction of ethanol. The arrow indicates feed concentrations in pervaporation experiments.

In terms of solvent activities both the feed and permeate side in pervaporation have been discussed. In pervaporation however, there is a third component involved, which is the membrane material. Essentially there are three steps in the pervaporation process. Sorption of the components from the feed mixture takes place at the feed side of the membrane, followed by diffusion through the membrane because of the applied activity differences between the membrane feed and permeate side, and desorption at the permeate side of the membrane.

If the kinetics of sorption and desorption are fast compared to the overall kinetics of pervaporation then the feed and permeate side of the membrane are in thermodynamic equilibrium with the feed mixture and the permeate respectively. The chemical potentials of the separate components in the feed mixture should be equal to their corresponding chemical potentials at the membrane interface,

$$\mu_{i,\text{ feed mixture}} = \mu_{i,\text{ feed side of membrane}} \qquad (2)$$

The thermodynamic equilibrium ensures a certain concentration of the permeants at the feed side of the membrane.

At the permeate side of the membrane the activities of the permeants are (almost) zero, and therefore the corresponding concentrations in the membrane are (almost)

zero too.

Due to these concentration differences in the membrane itself, a concentration profile will develop during the pervaporation process and a steady-state of permeation is reached. To obtain information on process rates, one can apply the theory of the thermodynamics of irreversible processes. In this chapter the membrane is considered to be homogeneous and the local properties are assumed to be isotropic. In pervaporation one may neglect the hydrodynamic permeability of membranes. This has been verified experimentally by increasing the hydrostatic feed pressure [11-12], which had no effect pervaporation results.

In this theory an expression for the local entropy production σ per unit volume and unit time, at mechanical equilibrium, is derived [13]. The general equation is simplified for the steady-state of the pervaporation process in which no chemical reactions happen, and where no external force fields are applied. Furthermore only the hydrostatic pressure contributes to the total pressure tensor. Then the final equation for the entropy production σ per unit volume and time, in any infinitesimal small volume somewhere in the membrane, contains the vectorial product of the local heat flow $\mathbf{J}_q$ and gradient in reciprocal temperature, and the local, vectorial products of mass flows $\mathbf{J}_i$ and respective gradients in the chemical potentials per unit mass divided by the absolute temperature.

$$\sigma = \mathbf{J}_q \cdot \mathrm{grad}\left(\frac{1}{T}\right) - \sum_{i=1}^{n} \mathbf{J}_i \cdot \mathrm{grad}\left(\frac{\mu_i}{T}\right) \geq 0. \qquad (3)$$

The first term at the right-hand side of this equation arises from heat flow, the second term from diffusive flow. The summation is over all n components present, including the membrane.
The heat flow $\mathbf{J}_q$ in eq. (3) accounts for the heat flow due to conduction and due to mass fluxes. One can correct for this diffusive heat flow by introducing [13],

$$\mathbf{J}'_q = \mathbf{J}_q - \sum_{i=1}^{n} h_i \mathbf{J}_i, \qquad (4)$$

with h_i the partial specific enthalpy of component i.
The mass fluxes $\mathbf{J}_i$ in eq. (3) are those defined with respect to the motion of the centre of mass. So they are interrelated by:

$$\sum_{i=1}^{n} \mathbf{J}_i = 0. \qquad (5)$$

One can incorporate eqs. (4) and (5) into eq. (3).

$$\sigma = J_q' \cdot \text{grad}\left(\frac{1}{T}\right) + \sum_{i=1}^{n-1} J_i \cdot \left[-\frac{1}{T}\{\text{grad}(\mu_i) - \text{grad}(\mu_n)\}_T \right] \geq 0. \qquad (6)$$

It is convenient to rewrite eq. (6) with the membrane, component n, as frame of reference for the mass fluxes [13].

$$\sigma = J_q' \cdot \text{grad}\left(\frac{1}{T}\right) + \sum_{i=1}^{n-1} J_i^n \cdot \left[-\frac{1}{T}\text{grad}(\mu_i)_T \right] \geq 0. \qquad (7)$$

Gradients in temperature may influence diffusive fluxes (the Soret effect) and gradients in chemical potentials may influence the heat flux (the Dufour effect). According to Kedem the Soret effect may contribute to mass fluxes, but it is certainly not essential for pervaporation [14].

A phenomenological approach is used in the theory of the thermodynamics of irreversible processes in which fluxes are considered to be linear functions of the thermodynamic forces, including cross-phenomena [13]. Neglecting the Soret and Dufour effect, the relation between the mass fluxes J_i and the thermodynamic forces X_k, and the relation between heat flux J_q' and the thermodynamic force X_q, are given by:

$$J_i^n = \sum_{k=1}^{n-1} L_{ik}^n X_k, \qquad (8a)$$

and

$$J_q' = L_{qq} X_q, \qquad (8b)$$

with L_{ik} and L_{qq} the phenomenological coefficients. The thermodynamic force X_k is equal to the gradient in chemical potential of component k, multiplied with minus the reciprocal temperature. The thermodynamic force X_q is equal to the gradient in the reciprocal absolute temperature.

In pervaporation the membrane is in contact with a liquid mixture. The molecules permeating through the membrane undergo a phase transition, which requires a certain amount of energy. The molar enthalpy of evaporation for water is 43.9 $kJmol^{-1}$ at 30 °C and 40.7 $kJmol^{-1}$ at 100 °C, and for ethanol 42.3 $kJmol^{-1}$ at 30 °C and 38.7 $kJmol^{-1}$ at 79 °C [13]. Due to the phase transition there can be a temperature drop across the membrane and in the feed mixture [16-17]. Pervaporation of pure water through cellulose acetate membranes shows a temperature drop of less then 10 °C for fluxes of about 0.5 $kg/m^{-2}hr^{-1}$ [17]. Increasing the Reynolds number of the recirculated feed mixture results in a lower temperature drop and higher water flux, indicating that at least part of the temperature gradient is situated in the feed mixture.
In general one cannot neglect the temperature gradient in pervaporation with high flux membranes. If present, a temperature gradient does not necessarily imply that the Soret effect will influence the mass fluxes through the membrane [14]. Diffusion,

however, is a process that results from random molecular motion and therefore it depends directly on the absolute value of temperature.

Reflecting on eq. (1), the gradient in the chemical potential μ_i, depends at a constant temperature, on the pressure gradient and the gradient in the logarithm of activity.

$$\text{grad}(\mu_i) = v_i \, \text{grad}(p) + RT \, \text{grad}(\ln(a_i)), \qquad (9)$$

with v_i the molar volume, p the pressure, R the gas constant, T the temperature and a_i the activity.
In case a gas is swept along the permeate side of the membrane, there is no pressure difference across the membrane, and the first term on the right-hand side of eq. (9) disappears. Very often a vacuum is applied to the permeate side. With an atmospheric pressure at the feed side, a pressure gradient does exist. When the activity differences between feed side and permeate side of the membrane are relatively large, the diffusion along a pressure gradient is usually neglected on the basis of the following inequality:

$$v_i \, \Delta p << RT. \qquad (10)$$

This inequality holds for liquids, applying the usually small pressure differences ($< 1 \cdot 10^7$ Pa), and it does not hold for vapours and gases.

Neglecting the existence of pressure and temperature gradients, there will be only diffusion along a gradient in composition. One can introduce then diffusion coefficients D, which have to be defined with respect to a certain frame of reference, and with respect to a certain measure of composition [13]. Here the membrane and solvent concentration c are adopted for reference.

$$J_i^n = -\sum_{k=1}^{n-1} D_{ik}^{nc} \, \text{grad}(c_k). \qquad (11)$$

All D_{ik}^{nc} depend only on composition and not on gradients in composition.
Eqs (8a) and (11) describe the linear dependence of mass fluxes on the thermodynamic forces and concentration gradients respectively. The diffusion coefficients are related to the phenomenological coefficients by:

$$D_{ik}^{nc} = L_{ik}^n \frac{R}{a_k} \frac{da_k}{dc_k}. \qquad (12)$$

In case the concentration gradient of a component does not contribute to the flux of the other components, then eq. (12) reduces to Fick's first law. The relation between the diffusion coefficient D_{ii} in eq. (12), defining fluxes with respect to the membrane, and Fick's diffusion coefficient D_i defining fluxes with respect to volume-average flux, is

given by:

$$D_{ii}^{nc} = (1-\phi_i)D_i, \tag{13}$$

with ϕ_i the solvent volume fraction.
In the steady-state the fluxes with respect to the membrane do not depend on the place coordinate z. After differentiation of eq. (11) with respect to z, one obtains a set of coupled second order differential equations. For a binary feed mixture this set reduces to two equations.

$$\frac{d^2c_1}{dz^2} = f(z,c_1,c_2,\frac{dc_1}{dz},\frac{dc_2}{dz}) \tag{14a}$$

and

$$\frac{d^2c_2}{dz^2} = g(z,c_1,c_2,\frac{dc_1}{dz},\frac{dc_2}{dz}) \tag{14b}$$

with f and g two functions of indicated variables.
If the boundary conditions of the two concentrations at the feed and permeate side are fixed, the two functions f and g are continuous and their partial derivatives with respect to the arguments are continuous, then there must exist a solution to this set of differential equations and one can prove that this solution for the concentration profiles is unique [18]. The exact solution of the concentration profiles can be drawn relative to the boundaries of the membrane. This implies that all J_i^n relate linearly to the reciprocal membrane thickness d, even when cross-phenomena are present.

$$J_i^n \propto \frac{1}{d}. \tag{15}$$

In pervaporation the quantity flux is easily measured, and corresponds to the chosen frame of reference, i.e. the membrane. The unit of flux used in this work is $kgm^{-2}hr^{-1}$.
The selective properties of a membrane depend on the partial fluxes. One widely used expression is the separation factor of the process, defined for the preferentially permeating component. In a binary mixture the separation factor α of 1 over 2 equals

$$\alpha_{1/2} = \frac{(\frac{w_1}{1-w_1})_p}{(\frac{w_1}{1-w_1})_f} = \frac{J_1/c_{1,f}}{J_2/c_{2,f}}, \tag{16a}$$

or

$$\alpha_{1/2} = \frac{(\frac{x_1}{1-x_1})_p}{(\frac{x_1}{1-x_1})_f} = \frac{J_1^*/x_{1,f}}{J_2^*/x_{2,f}}, \tag{16b}$$

with w the weight fractions, x the mole fractions, and the subscripts p and f denoting respectively the permeate and feed. In eq. (16a) weight fractions are used as measure of

composition, but one may use mole fractions as well, as in eq. (16b). The mass fluxes should be replaced by the corresponding mole fluxes J*. The separations factors of eqs. (16a) and (16b) have the same value.
From eqs. (15) and (16) one can readily see that the process separation factor should not depend on membrane thickness, in case mass transport due to a temperature gradient can be neglected, and a steady-state situation of pervaporation has been reached.

The process separation factor is a function of both the thermodynamics of the entire pervaporation process, and the kinetics of permeation associated with the membrane. Pervaporation combines evaporation and permeation. The feed mixture will be in equilibrium with a vapour, the composition of which is in general different from that feed mixture. In this way a separation is reached already without any membrane. In pervaporation the membrane is a layer that physically separates the liquid phase from the vapour phase.
The membrane selectivity $S_{1/2}$ is defined as the ratio of the permeabilities of component 1 and 2. The permeability is defined as the volume flux through the membrane, corrected for the membrane thickness and for the driving force. In pervaporation the driving force for permeation are the differences in fugacities across the membrane. Because the volume flux is given with respect to the vapour phase, applying the ideal gas law at standard temperature and pressure, its value is proportional to the mole flux. The membrane selectivity $S_{1/2}$ is then inserted into eq. (16b) [19].

$$\alpha_{1/2} = S_{1/2}\,\alpha_{1/2,\text{evaporation}} = S_{1/2}\,\frac{a_{1f}p_1^0 - x_{1,p}p_p\varphi_{1,p}}{a_{2f}p_2^0 - x_{2,p}p_p\varphi_{2,p}} \cdot \frac{x_{2,f}}{x_{1,f}}, \qquad (17)$$

with x representing the respective mole fractions in the feed and permeate, a the activities in the feed mixture, φ the fugacity coefficients in the permeate, p^0 the saturated vapour pressures and p_p the total vapour pressure of the permeate.
When the permeate vapour pressure approaches zero, which is usually the case in pervaporation, the process separation factor can be simplified into:

$$\alpha_{1/2} = S_{1/2}\,\frac{a_{1,f}p_1^0}{a_{2,f}p_2^0} \cdot \frac{x_{2,f}}{x_{1,f}}. \qquad (18)$$

The process separation factor in eq. (18), divided by the membrane selectivity, is the ideal separation factor of evaporation.
In pervaporation experiments with polyacrylonitrile membranes and an ethanol/water mixture with a 0.9 weight fraction of ethanol, process separation factors larger than 1000 have been measured [2]. The high separation factor is on account of the high membrane selectivity. The contribution of evaporation to the separation factor, calculated from vapour-liquid equilibrium data [10], is in between 0.75 and 0.78, indicating that at this composition ethanol is evaporated preferentially.

Experimentally significant changes in time are seen in the permeation properties of thin films. Before describing the equipment and the experiments a brief review will be given concerning the use of dense, thin membranes made of glassy polymers, in pervaporation.

2.2.1. Time-dependence of pervaporation

So-called homogeneously dense membranes have been investigated for their use in dehydrating ethanol/water mixtures [2]. The polymer polyacrylonitrile is a good candidate since it has a very high separation factor, although its permeability is small. Fluxes can be increased by decreasing the membranes thickness. In the dehydration of ethanol/water mixtures, both the ethanol and water flux increase, but the ethanol flux is increasing more than proportionally to the reciprocal membrane thickness, resulting in a lowered separation factor. The same phenomenon is seen in the dehydration of acetic acid with homogeneously dense polyacrylonitrile, polysulfone and polyvinylchloride membranes [3]. Again the total flux, predominantly determined by the preferentially permeated species, is proportional to the reciprocal membrane thickness. The decrease in separation factor is fully attributed to the more than proportional increase in flux of the species that should be retained by the membrane. A lowering in separation factor is found for membrane thicknesses below 20 μm.

In the introduction of this chapter probable explanations have been mentioned. The statement that the measured values of flux and separation factor may not be the values corresponding to the steady-state situation, is interesting for several reasons. One may think that if pervaporation properties are not yet constant in time, one just has to wait longer until they do. This is not trivial at all. There are two time-dependent effects; first the development of a concentration profile in the membrane, and secondly the occurrence of polymer relaxation.

In the dehydration of ethanol as reported in literature, all membranes were preswollen overnight in the feed mixture of pervaporation. Fluxes are decreasing in time, and reach a stationary state only after three days for a 18 μm thick polyacrylonitrile film. The separation factor is constant already after 6 hours [2]. In the dehydration of acetic acid [3] membranes have not been preswollen, and steady-state is reached after 2 to 3 hours, with membrane thicknesses ranging from 3 to 40 μm.

The development of a concentration profile by diffusion along a concentration gradient can not explain the decrease in separation factor with decreasing membrane thickness. The thicker membranes do reach their so-called intrinsic separation factor within 8 hours of pervaporation whereas thin films do not reach the intrinsic separation factor within 8 hours [2-3]. The time to reach the final concentration profile by Fickian diffusion, however, is proportional to the square of the membrane thickness! A rough measure of the time θ_D needed to reach steady-state permeation by diffusion along a concentration gradient [20], assuming a constant diffusion coefficient, no swelling phenomena and no penetrant present in the membrane at the start of permeation, is:

$$\theta_D \cong \frac{d^2}{3D}, \qquad (19)$$

with D the diffusion coefficient and d the membrane thickness.
For an estimation of the diffusion coefficient one needs to know the permeant concentrations in the membrane, at the feed and permeate side. The latter concentrations are assumed to be zero for both ethanol and water. The volume fractions at the feed side can be estimated with the Flory Huggins theory [21], when the activity of a component in the feed equals its activity at the feed side of the membrane.

$$RT \ln a = RT \{\ln\phi + (1-\phi) + \chi(1-\phi)^2\}, \qquad (20)$$

with a the activity of a component, ϕ its volume fraction, and χ the interaction parameter. Implicitly it has been assumed that the number of monomer units per polymer molecule is large. The interaction parameters for the systems polyacrylonitrile/water and polyacrylonitrile/ethanol are respectively 1.8 and 4.2 [22].
In the system polyacrylonitrile/water a water activity of 0.4 to 0.5 corresponds to a water volume fraction of 0.028 to 0.036. In the same way an ethanol activity of 0.8 to 0.9 corresponds to an ethanol volume fraction of 0.0046 to 0.0052. Multiplication of the volume fractions with respective liquid densities gives their concentrations in the membrane at the feed side.
Spitzen [2] measured the thickness dependence of the water and ethanol fluxes through polyacrylonitrile membranes, with the same feed composition used in this work. Neglecting coupling effects and assuming a linear variation of the concentration with distance in the membrane, an average diffusion coefficient of water and ethanol is estimated from his data using Fick's first law, and the above calculated concentrations.

$$J_i = \overline{D}_i \frac{c_{i,f}}{d}, \qquad (21)$$

with J the mass flux of component i, $\overline{D}$ an average diffusion coefficient, c the concentration of component i in the membrane at the feed side, and d the membrane thickness.
The average diffusion coefficient of ethanol is larger than $3.5 \cdot 10^{-14}$ $m^2 s^{-1}$, and the average diffusion coefficient of water is smaller than $1.8 \cdot 10^{-12}$ $m^2 s^{-1}$. With membrane thicknesses of the order 10 μm and assuming diffusion coefficients of 10^{-13} to 10^{-12} $m^2 s^{-1}$, the time θ in eq. (19) ranges from 33 to 330 s. Decreasing the membrane thickness should drastically lower this time.

Diffusion coefficients can have a very strong dependence on solvent concentration. In the glassy state they can vary over decades [23]. In a glassy polymer the polymer matrix is very tight and permeation is diffusion-controlled. A slight increase in solvent concentration can significantly enhance the diffusion processes. Sometimes polymer relaxation interferes with diffusion processes. An increase in solvent concentration is

hindered to some extent by the tight polymer matrix, and further swelling is only possible when relaxation of the polymer chains in their packing proceeds. Solvent swelling in turn might decrease polymer relaxation times, and when the time-scale of polymer relaxation is of the same order as the time-scale of diffusion processes, often 'anomalous' sorption and desorption processes are observed. Typical examples are two-stage sorption curves [23] and non-coinciding sorption and desorption curves [24]. Although in general diffusion controls the selective permeation in glassy polymer membranes, sorption is of importance. The influence of swelling a membrane prior to pervaporation has been verified, with the separation of methanol/methyl tert-butyl ether mixtures by membranes consisting of a blend of polyacrylic acid and polyvinylalcohol [25]. Enhanced swelling has been obtained using feed mixtures enriched with methanol. Starting pervaporation subsequently with a feed mixture consisting of a lower methanol content, gives initially too high fluxes and too low separation factors. A large discrepancy in swelling of the membrane, due to a preconditioning step, results in a delay of the time needed to reach steady-state pervaporation.

2.3. The pervaporation equipment

Three different set-ups have been used for the pervaporation experiments.
The first set-up applies a vacuum to the permeate side of the membrane. In figure 3 this set-up is schematically drawn.

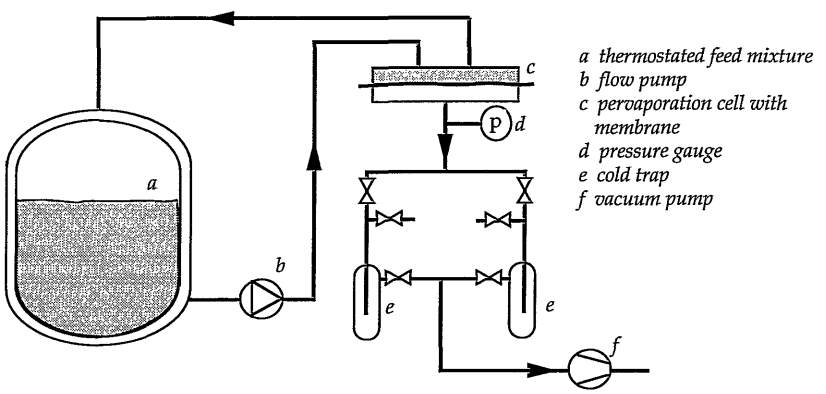

figure 3: Pervaporation set-up with vacuum applied at the permeate side of the membrane.

The ethanol/water feed mixture is continuously circulated with an Iwaki magnet pump (b in figure 3), maximum flow rate 5.5 to 6.0 l/min, to prevent as much as possible concentration polarization near the membrane interface. A rough estimation of the Reynolds number gives a value of 1600, which is about half the critical Reynolds number.

The preferentially permeating component will be depleted in the feed. Due to the large volume of the feed (6 l), the changes in overall feed composition during pervaporation are very small. Besides that the feed composition is monitored regularly. The vessel with the feed mixture (a) has a double wall in which water, with a temperature of 30 °C, is circulated from a thermostat bath.
The membrane is clamped into a stainless steel pervaporation cell (c). The surface of the membrane exposed to the feed has an area of 50.27 cm^2. Because of a 10^5 Pa pressure difference across the membrane it is supported at the permeate side by a sintered metal plate, pore size 40 µm. No capillary condensation can occur in this support.
The pressure at the permeate side should be low enough, i.e. at least four times lower than the saturated vapour pressure of any substance that is permeated [15,17,26]. The vacuum is created with an Edwards E2M2 high vacuum pump (f). The pressure is checked with an Edwards series 1000 vacuum gauge (d) and controller. The highest pressures recorded during pervaporation with highly permeable and extremely thin films are about 100 Pa. The saturated vapour pressures of water and ethanol at 30 °C, calculated with the Antoine-equation [4], are respectively $4.231 \cdot 10^3$ Pa and $1.0456 \cdot 10^4$ Pa.
During pervaporation the permeate is collected in one of the two cold traps (e), cooled with liquid nitrogen. The cold traps are easily disconnected from the pervaporation cell with high-vacuum valves, for determination of the amount of permeant by weighing, and analysis of its composition with a Varian 3400 gas chromatograph. The high-vacuum valves, with double viton O-sealings, are manually operated.

Pervaporation can also be carried out with a sweeping gas at the permeate side. In this way a pressure difference across the membrane can be avoided. A schematic diagram of the set-up used is given in figure 4.
The complete pervaporation cell (c in figure 4) is made out of glass. The membrane is put between two glass parts with just one O-ring as sealing. Although in principal superfluous, the membrane is supported with a 4 mm thick porous glass plate. The support does not influence the experiments. An estimate of the maximum permeant mass transfer coefficient in the membrane ($k_{maximum}=5 \cdot 10^{-4}$ ms^{-1}) is obtained by dividing the maximum permeant diffusion coefficient ($D_{maximum}=10^{-9}$ m^2s^{-1}), which is the diffusion coefficient of water or ethanol in their liquid mixture [27], with the minimum membrane thickness ($d_{minimum}=2 \cdot 10^{-6}$ m). The diffusion coefficient of ethanol and water into air, is of the order 10^{-5} m^2s^{-1} [28] ,which is 4 decades larger than the diffusion coefficient in the liquid phase. Although not the complete support is available for permeation, the mass transfer coefficient in the vapour phase ($\leq 2.5 \cdot 10^{-3}$ ms^{-1}) is larger than in the membrane. In order to obtain a good vapour mass transfer from the permeate side, the volume under the porous plate is as small as possible. With a nitrogen gas flux of 0.25 l/min this volume is replaced 80 times every minute. The membrane area is 10.17 cm^2.
The pervaporation set-up is designed to be operated for a longer period. The membrane area is relatively small and the use of a sweeping gas is less harmful for the equipment in case of leaking membranes.

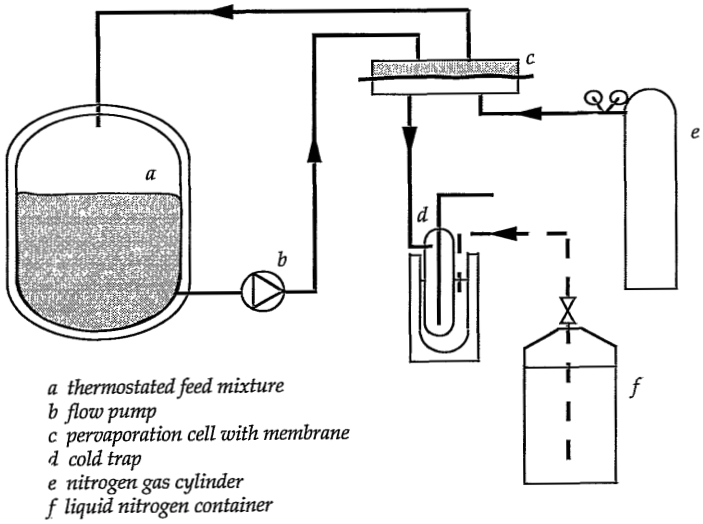

figure 4: Pervaporation set-up with nitrogen sweeping gas flowing along the permeate side of the membrane.

A vessel with a 6 l content is large enough for this set-up with a relatively small membrane area. The feed mixture is circulated with a Masterflex peristaltic pump (b). The liquid nitrogen needed for the collection of the permeate, is supplied automatically. Two Pt 100 temperature sensors are placed in the dewar-vessel. When the liquid nitrogen level has reached the lowest of the two sensors the valve of the liquid nitrogen container (f) is opened by a Mart level control, until the nitrogen level reaches the highest sensor.
For the analysis of the permeate composition a small amount is drawn into a syringe, out of the cold trap that has been heated to lab temperature. This requires a certain amount of permeate, at least 0.1 g, and that in turn determines the minimum permeation time, for each cold trap. For certain glassy polymer membranes it may take more than a few hours, and as high sampling rates are wanted, one has to perform the analysis of the permeate in another way.

The standard set-up which was depicted in figure 3 has been automated. The concept is to let the permeating species increase the pressure in a calibrated volume, for a given time. The increase in pressure per unit of time is then a measure of the total flux through the membrane. The vapour collected in the calibrated volume is immediately passed through the gas chromatograph column for analysis.
Figure 5 gives the outline of the automated pervaporation set-up. Basis of the concept is the pervaporation set-up with a vacuum at the permeate side (figure 3). Originally the calibrated volume was the metal tubing that should connect all eight pervaporation set-ups present in the laboratory, so that one personal computer could control the analysis of up to eight experiments. Only one pervaporation cell has been

drawn in figure 5. Two computer-controlled valves are inserted under each cell to connect the pervaporation cell with the calibrated volume, and to disconnect the pervaporation cell from the cold traps.

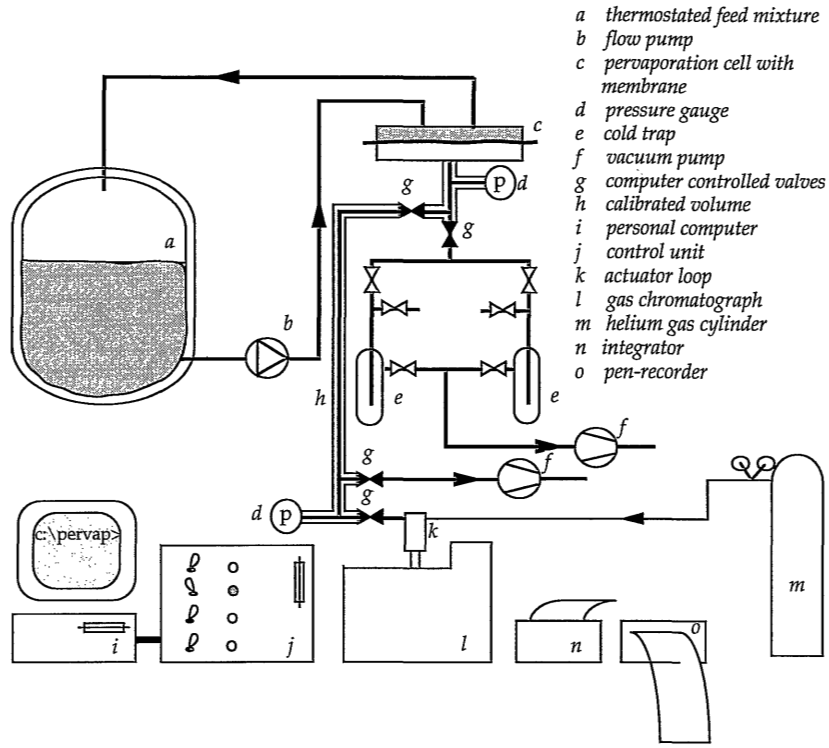

figure 5: Automated pervaporation set-up with vacuum applied at the permeate side of the membrane.

The control unit (j in figure 5) and the computer program can operate the complete pervaporation set-up. The computer program, the software, communicates with the hardware of the control unit via an IEEE 488-cable. The control unit opens and closes valves (g), starts the permeate analysis with a Varian 3300 gas chromatograph (GC) (l), and measures various pressures. At the front of the control unit the operator can indicate, by means of switches, which pervaporation cells should be sampled.
The sequence of sampling one pervaporation-cell is as follows. The permeate flow from the pervaporation cell is shut off from the glass-ware with cold traps and directed towards the pre-evacuated calibrated volume (h); the calibrated volume being specific for each pervaporation cell. After a certain time has elapsed or pressure has been reached, as declared in the input file of the computer program, the calibrated volume is disconnected, and the collected permeate is fed to the pre-evacuated sample loop of the 6-way vacuum valve actuator (k) mounted on top of the GC. The program waits for a defined time, to let the pressure equilibrate throughout the system (calibrated volume and sample loop), and then starts the GC. The integrator and recorder are started at the same time by the GC for the analysis of the permeate. A relay section built in the GC, rotates the sample loop into and out of the helium feed stream of the GC.

On the GC one can program the time after which a ready signal will be given to the control unit. The system waits for this signal before another pervaporation cell is sampled. The sampling rate with the automated set-up is therefore determined by the time needed for a GC-analysis, and/or the time needed to collect enough vapour in the calibrated volume. To speed up the sampling rate the GC can be programmed to give the ready signal as soon as the sample has been rotated into and out of the helium feed stream.
The analysis of the GC measurement signal is done by a LDC/Milton Roy integrator, that determines the area under the water and ethanol peaks, and calculates the percentages with respect to total peak area. The flux can be determined in three ways, by using the cold traps parallel to the automated set-up, by recording the pressure increase in the calibrated volume with a pen-recorder, and by looking at the absolute values of the peak areas as determined by the integrator.
Although the automated pervaporation set-up was designed to monitor up to eight cells, only two cells are connected to the calibrated volume to minimize pressure losses in the system. The permeate vapours should travel a distance as short as possible, and tubing should have an inner radius as big as possible! Also the GC-column should have a large radius to avoid pressure changes in the column when rotating the vacuum valve actuator.

2.4. Pervaporation

In this work attention is directed primarily to the time dependence of the fluxes through the membrane and the resulting (time) effect on the separation factor, for various membrane thicknesses. As shown above the development of a concentration profile cannot explain the decrease in separation factor with decreasing membrane thickness.

2.4.1. Membrane preparation

Membranes are made by dissolving polyacrylonitrile, obtained from Aldrich, in dimethylformamide. The polymer solution is cast onto a cleaned glass plate with a casting knive, followed by drying in an inert atmosphere of nitrogen gas. Membrane thicknesses are varied using casting knives with different slit heights.
The drying and solidification of the polymer solution is asymmetric. The solvent can evaporate only from one side of the cast polymer film and a solvent concentration profile will develop. Since one might expect that residual traces of solvent are very hard to remove from the solidified, glassy polymer film [29], solvent might be present in the membrane when starting pervaporation. With glassy membranes it is therefore better to denote the film as a dense membrane, instead of a 'homogeneously dense' membrane. Attention has been paid to the fact whether the side of the drying polymer film exposed to nitrogen or the side exposed to the glass plate, is facing the

pervaporation feed mixture or especially the permeate side. In this chapter the side of the membrane facing the permeate is always specified with respect to the drying step: the interface through which solvent evaporates is called the nitrogen exposed side and the polymer film/ glass support interface is called the glass plate side. This specification of the orientation of the membrane is given since the large concentration gradient during pervaporation is situated at the permeate side of the membrane.

2.4.2. Pervaporation experiments

Membranes are given no heat treatment prior to pervaporation. In all the experiments an ethanol/water feed mixture has been used with a 0.9 weight fraction of ethanol.
In figures 6a and 6b the separation factor and the total flux, determined after 8 hours of pervaporation, are plotted as a function of membrane thickness. The membranes were prepared by casting a polymer solution on a glass plate, and drying for one day in a nitrogen atmosphere. The membranes are very thin, and are easily torn to pieces when detached from the glass-plate. The capillary force of water has been used to facilitate this process. Out of one cast polymer film, two membranes are cut for use in pervaporation. These two membranes are clamped in pervaporation cells and exposed, overnight, to the lab atmosphere before starting the pervaporation experiments. One membrane is facing the permeate with its nitrogen exposed side and the other one with the glass plate side.
The pervaporation set-up of figure 3, i.e. with a vacuum at the permeate side, has been used to determine pervaporation properties, with the understanding that a duplicate experiment is performed. The same feed mixture is flowing through two pervaporation cells, each with its own glass-ware and cold-traps, and each having a separate vacuum pump. No correlation could be found between the pervaporation properties and the two pervaporation set-ups used.
One can clearly see that a decreasing membrane thickness is accompanied by a decreasing separation factor. This effect is so strong, that a logarithmic scale has been used for the separation factor. There is also a difference between two membranes cut

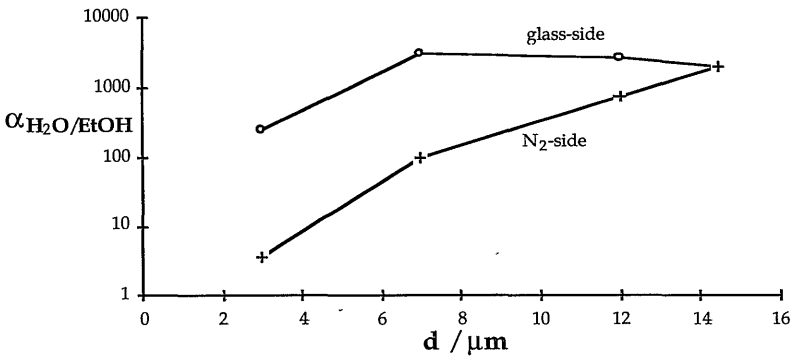

figure 6a: Separation factor for water over ethanol versus membrane thickness, after 8 hours of pervaporation. Open circles and crosses denote respectively membranes with glass plate side and membranes with nitrogen exposed side facing the permeate. Membranes are detached from the glass plate using water. (for explanation see text).

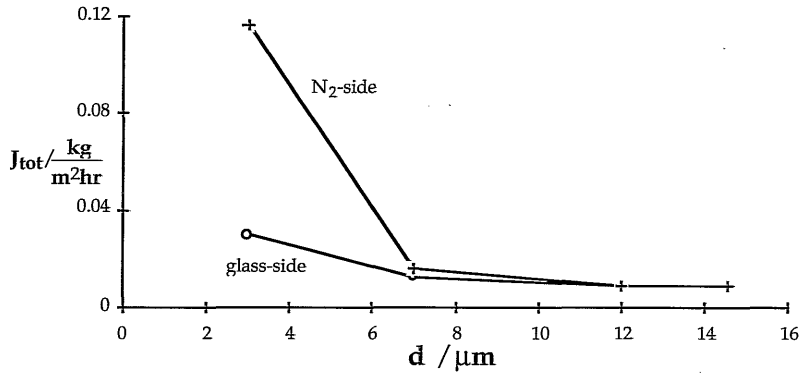

figure 6b: Total flux versus membrane thickness. Open circles and crosses denote respectively membranes with glass plate side and membranes with nitrogen exposed side facing the permeate.

out of the same polymer film, with respect to which side is facing the permeate. When the nitrogen exposed side is facing the permeate lower separation factors and higher fluxes are found. Differences are getting more pronounced with decreasing film thickness.

Separation factors larger than 1000 are not accurate values any more. With the feed mixtures used a separation factor of 1000 corresponds to an ethanol weight percentage of 0.9 in the permeate. A discrepancy in thickness of both films can not explain the observed differences between nitrogen and glass plate side. The error in film thickness is below 0.5 μm.

Due to the pretreatment to get the thin films off the glass plate the membranes used in figure 6a and 6b have been partially swollen by water, penetrating the membrane only from the glass plate side. Therefore a following series of polyacrylonitrile membranes has been detached carefully from the supporting glass plate without the use of water. In table 1 these results are given together with the results of figure 6a.

table 1: Separation factor versus membrane thickness, measured after 8 hours of pervaporation.

membrane thickness (μm)	separation factor α	
	glass plate side facing permeate,	nitrogen side facing permeate
polymer film detached from glass plate using water		
3	240	3.6
7	>1000	95
12	>1000	780
14.5	>1000	>1000
polymer film detached from glass plate without using water		
3	2.9	6
5.5	40	57
7*	590	28

* The membranes have been clamped into a pervaporation cell and a vacuum has been applied for 2-3 days, prior to pervaporation.

For a film, detached from the glass plate using water, separation factors are high when the glass plate side is facing the permeate, whereas for a 'dry' film selectivities are only slightly higher when the nitrogen side is facing the permeate. The 7 μm thick membranes detached from the glass plate without using water, seem an exception to the rule, but these have had a different pre-treatment. All the other membranes are used in pervaporation experiments, within one day after preparation of the dense films, whereas the 7 μm thick membranes have been exposed to a vacuum for another 2 to 3 days.
From the above results it is clear that the presence of water, the preferentially permeating component, in the polymer film prior to the pervaporation experiments, has a tremendous influence on pervaporation properties.

In the following experiments polyacrylonitrile films have always been detached from the glass plate without the use of water. Before the feed is applied to the membrane, care is taken that the vacuum has already been applied to the permeate side and cold traps are cooled already with liquid nitrogen. In figures 7a and 8a the water and ethanol fluxes are given as a function of pervaporation time, for a 5.5 μm thick film. All the fluxes are decreasing in time and separation factors are increasing. After 500 minutes of pervaporation no steady-state is reached. There is a clear, structural difference between the two films: the membrane with the glass plate side facing the permeate, has initially a (very) high water and ethanol flux. After the one day experiment had finished the feed mixture was removed from the membranes, and the membranes are exposed to water. The vacuum pumps are shut down in order to let the permeate side swell with water too. The next day pervaporation is started again immediately after the exchange of the water by the feed mixture and application of the vacuum to the permeate side of the membranes. Both the water and the ethanol fluxes have increased drastically, compared to the day before. Although the decrease of fluxes in time is significant, the separation factor of the pervaporation process is being lost; the initial values of 40 and 57 (see also table 1) drop to a value of only 1.7.
Now the membranes show the same trend of flux decrease in time, for both orientations. It is very probable that just a minor difference in membrane thickness causes the disparities in absolute flux values. The swelling power of water has eliminated the drying history of the polymer membrane, at the expense of selectivity.
The question remains whether the initial high fluxes are caused by the presence of residual solvent dimethylformamide (figures 7a and 8a), or by the permeant water (figures 7b and 8b) in the membrane, at the moment pervaporation is started. Therefore polyacrylonitrile membranes are prepared, 7 μm thick, clamped into the pervaporation cells where for another 2 to 3 days evaporation is enforced by applying a vacuum (see table 1). The fluxes during subsequent pervaporation have been monitored as a function of time (figures 9a and 10a). The separation factors after 8 hours of pervaporation are given in table 1. Comparing for example figures 8a and 10a, the situation has been reversed: now the membrane with the nitrogen side facing the permeate has initially the highest flux. This is due to the vacuum applied to the permeate side of the membrane 2 to 3 days prior to pervaporation.

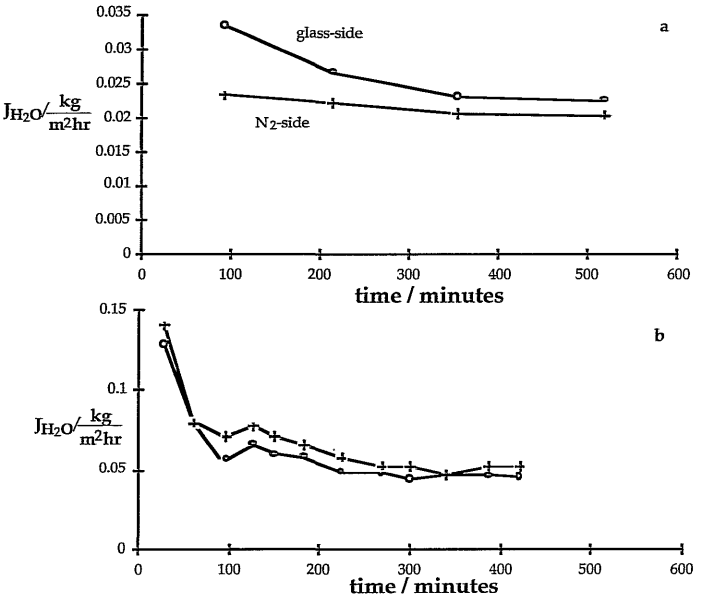

figures 7a and 7b: Water flux versus pervaporation time for a 5.5 μm thick polyacrylonitrile membrane. Open circles and crosses denote respectively membranes with glass plate side and nitrogen exposed side facing the permeate. The membranes are swollen overnight in water between the experiments of figures 7a and 7b (see text).

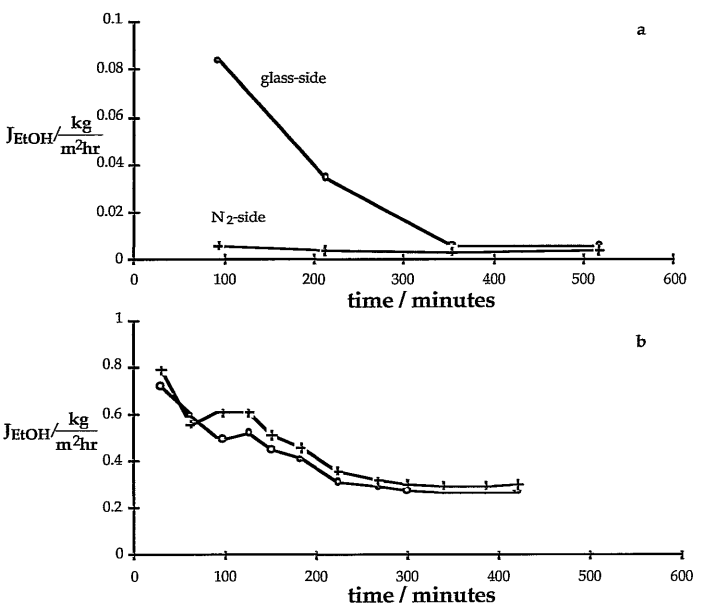

figures 8a and 8b: Ethanol flux versus pervaporation time for a 5.5 μm thick polyacrylonitrile membrane. Open circles and crosses denote respectively membranes with glass plate side and nitrogen exposed side facing the permeate. The membranes are swollen overnight in water between the experiments of figures 8a and 8b (see text).

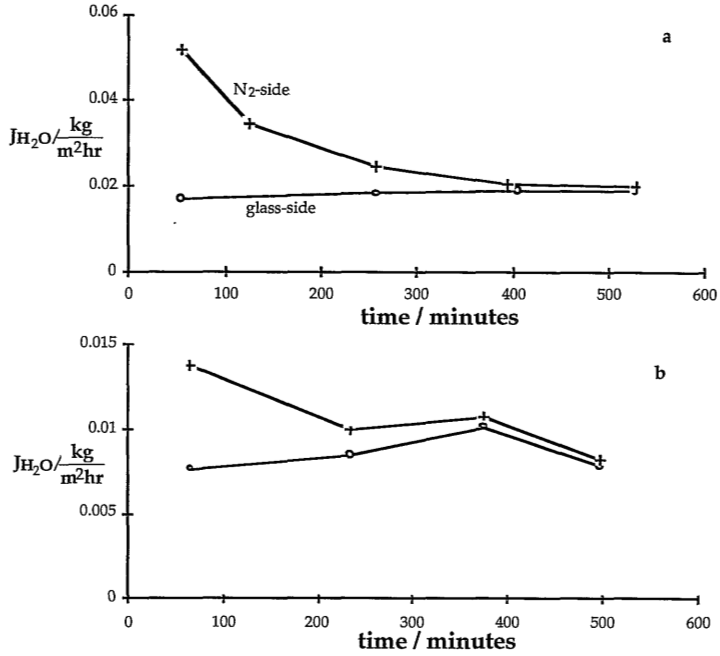

figures 9a and 9b: Water flux versus pervaporation time for a 7 μm thick polyacrylonitrile membrane. Open circles and crosses denote respectively membranes with glass plate side and nitrogen exposed side facing the permeate. The membranes are exposed to vacuum at the permeate side, and the feed mixture is removed, between the experiments of figures 9a and 9b (see text).

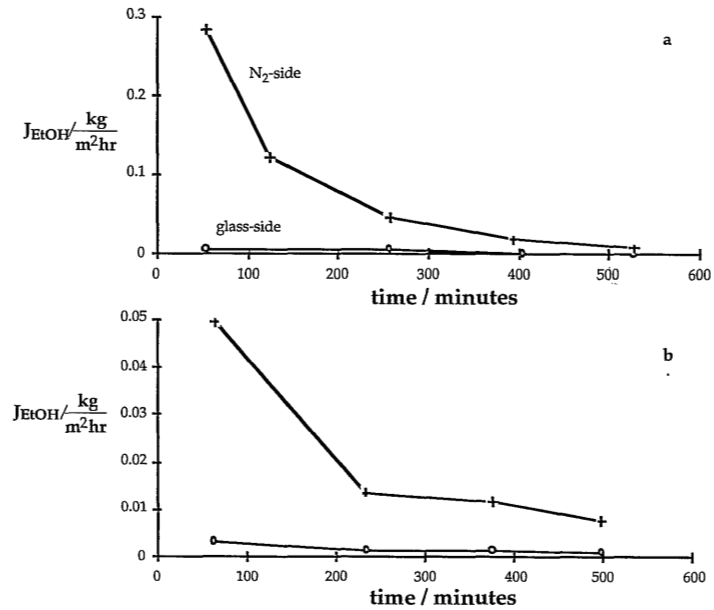

figures 10a and 10b: Ethanol flux versus pervaporation time for a 7 μm thick polyacrylonitrile membrane. Open circles and crosses denote respectively membranes with glass plate side and nitrogen exposed side facing the permeate. The membranes are exposed to vacuum at the permeate side, and the feed is removed, between the experiments of figures 10a and 10b (see text).

At this moment, bearing in mind figures 7 and 8, it still is possible that the presence of residual solvent is the main reason for initially too high fluxes. Therefore the feed mixture has been removed after pervaporation, and a vacuum has been applied at the permeate side of the membrane. The next day pervaporation is started again, and qualitatively the same time-dependence of water and ethanol fluxes is observed as the day before (figures 9b and 10b). In case pervaporation had removed (part of) the solvent, then that should have had a permanent effect. The initial ethanol flux of the membrane with the nitrogen exposed side facing the permeate, is high compared to the last measurements of the day before, and therefore a decrease in flux with time can not be attributed only to a decrease in solvent content of the membrane.
These measurements using the pervaporation set-up with a vacuum at the permeate side (see figure 3) allow the following conclusions:

- during 8 hours of pervaporation it is not possible to get a steady-state in relatively thin films,
- the decrease in fluxes, in contradiction with the development of a concentration profile, show that another important effect must exist,
- and the decrease in separation factor with decreasing thickness of the membrane can not directly be correlated to the amount of solvent (or penetrant) in the membrane.

In the experiments shown next, the pervaporation set-up with nitrogen sweeping gas (see figure 4) is used to see how the separation factor develops over a longer period of time. With the already shown experiments in mind, it is expected that the separation factor will increase with time.
In figures 11a and 11b the separation factor and total flux are shown for a polyacrylonitrile membrane with a thickness of 10 μm. The glass plate side of the membrane is facing the permeate at the start of the experiment. The membrane is turned upside-down in its pervaporation cell almost every day to get rid of residual solvent.
Usually separation factors and fluxes are reported after about 8 hours of pervaporation, and these values are called steady-state values. From figure 11a one can see that the separation factor is increasing in time from 25 on the first day to about 300 after 3 weeks. As three weeks have passed, one can not conclude whether a steady-state is reached already. The separation factors at day 8 and 9 are out of range, without explanation. The flux, plotted in figure 11b, is decreasing in time. Unfortunately the experiment stopped after 22 days. Rubbery particles had deposited on the membrane due to the destructive action of the peristaltic pump, thereby changing the separation factor of the process.

In figures 12a and 12bb similar curves are shown for another membrane, 6 μm thick. The separation factor increases in the first 6 days from 70 to 160, while the flux is decreasing to about one third of its initial value. This strong relative decrease in flux in time is tremendous compared to the thicker film of figure 11b.

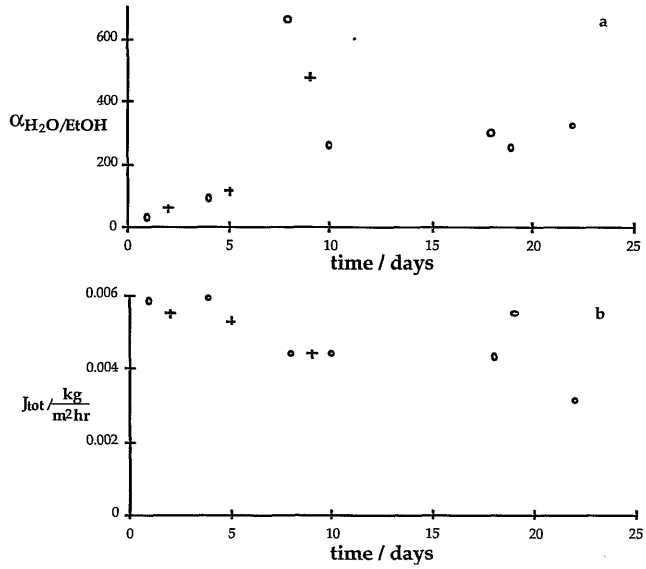

figures 11a and 11b: Separation factor and total flux of a 10 μm thick polyacrylonitrile membrane, versus pervaporation time. Open circles and crosses denote when the glass plate side or the nitrogen exposed side of the membrane is facing the permeate.

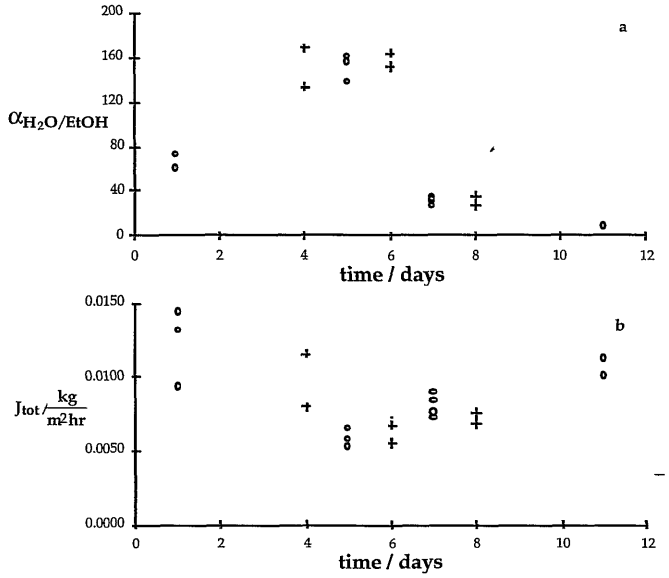

figures 12a and 12b: Separation factor and total flux of a 6 μm thick polyacrylonitrile memrane, versus pervaporation time. Open circles and crosses denote when the glass plate side or the nitrogen exposed side of the membrane is facing the permeate.

After 6 days fluxes increase and separation factors decrease, probably due to the fact that one can not turn these extremely thin films upside-down without mechanical damage. The experiments with the pervaporation set-up of figure 4 with nitrogen as a sweeping gas, presented in figures 11 and 12, show clearly that it may take an extremely long

time before steady-state pervaporation is attained. Unfortunately no experimental evidence is found that the separation factor of these films with thicknesses below 20 μm will increase to their intrinsic value or a value higher than 1000. Also in these experiments it is found that the total flux is decreasing in time and therefore attention is now directed to the first moments of pervaporation.

With the automated pervaporation set-up of figure 5 one can analyze the permeate directly from the vapour phase, and samples can be taken at shorter time-intervals.
In figure 13 the water content of the permeate is shown as a function of pervaporation time. The membrane is 2.5 μm thick, the feed contains 9.7 to 10.0 wt. % of water, and the permeation time to collect each sample is 20 seconds. The water content is shown instead of the separation factor because the latter one is fluctuating too much although there is not so much variation in the water content of the permeate.

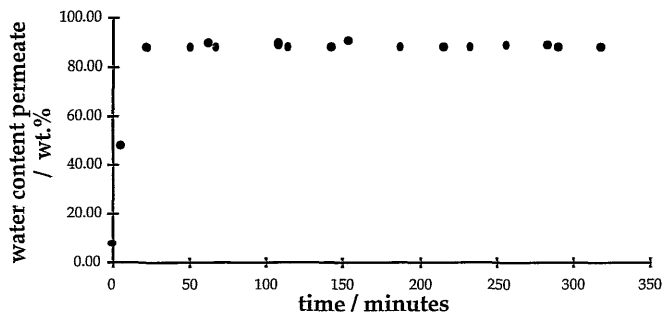

figure 13: Water content of the permeate versus pervaporation time. Measurements are performed with the automated pervaporation set-up. Membrane thickness is 2.5 μm.

Within 23 minutes after starting the experiment the water weight percentage is already 87 and it fluctuates therefrom between 86.2 and 90.5 %. The separation factor varies between 64 and 84. The pressure increase in the calibrated volume divided by the permeation time is taken as a measure of the flux. At the first sampling the pressure increase per unit time is 99 mbar/min, at the second sampling, after 5.7 minutes, its value is already below 18 mbar/min. During the experiment the pressure increase per unit time is slowly decreasing to a value of 15.5 mbar/min. It seems the membrane has reached a steady-state relatively fast when the separation factor is considered, although there is still a noticable and significant decrease in flux through the membrane.

In figures 14a and 14b the separation factor, and the pressure increase per unit time are shown for a 2.0 μm thick membrane. The water weight percentage of the feed is 9.3 to 10.1 %, and the permeation time for each sample is 20 seconds.
Initially the membrane is not selective, the measured separation factor is ca. 0.9! A value smaller than 1 is possible, because the thermodynamic value in the separation factor of the pervaporation process is 0.75 to 0.78. The membrane selectivity is negligible here, see eq. (18). Within 6 minutes the membrane is water selective ($\alpha \approx 3$),

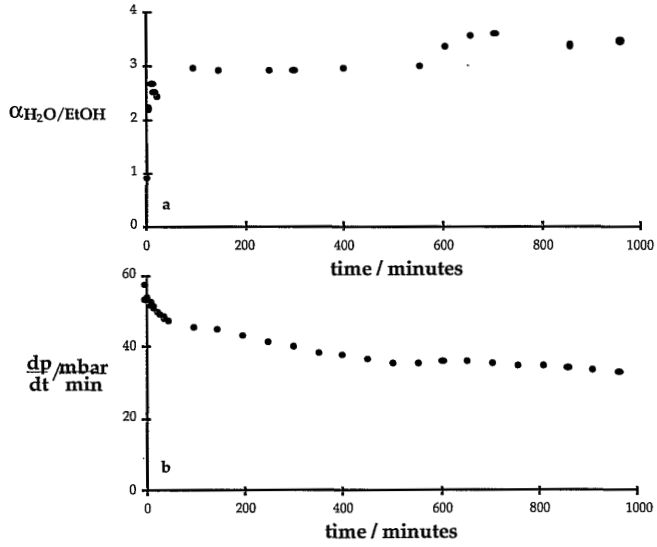

figures 14a and 14b: Separation factor and pressure increase per minute in the calibrated volume, versus pervaporation time. Measurements are performed with the automated pervaporation set-up. Membrane thickness is 2 μm.

the increase of the separation factor in time being very slow thereafter. The decrease of the flux in time is gradual but significant, the initial flux is 57.3 mbar/min and after 1000 minutes the flux is reduced to half its initial value 32.7 mbar/min. The accompanying decrease in mass flux is even more substantial as the water content of the permeate is increasing in time and water has a lower molecular weight than ethanol.

2.5. Discussion

At first glance one might think of a concept in which the absence of any plasticizer, a solvent or a permeant, at the permeate side of the membrane, results in high separation factors. If it is then expected that one can not completely remove the solvent in preparing the membrane with a solvent-cast technique, the solvent should be removed prior to pervaporation by plasticizing the membrane with a suitable plasticizer. According to Hansen [29] small molecules like water and methanol are very effective plasticizers. In case the plasticizing agent swells the polymer it will increase the solvent diffusion coefficient and after completion of the solvent removal the plasticizer is easily removed in a final drying step.
This concept should be used to compare the data presented in table 1. When the polymer film is detached from the glass plate by wetting the glass plate side of the membrane, the solvent dimethylformamide is (easily) extracted from the glass plate side, due to the enhanced mobility of dimethylformamide by the plasticizing action of water. Water present in the film is easily removed thereafter by evaporation. High

separation factors are found when the glass plate side is facing the permeate. When the polymer film is detached from the glass plate without using water, hardly any solvent is present at the nitrogen exposed side of the membrane, like in the case before with the glass plate side of the membrane, and a slightly higher separation factor is found when the nitrogen exposed side is facing the permeate.
Completely wetting the membrane just prior to pervaporation, without drying the membrane, plasticizes the permeate side of the membrane, and separation factors are lost (figure 7b and 8b). The concept of residual solvent removal fails, or is not complete, as can be seen when evacuating the membrane overnight between two pervaporation experiments (figures 9a, 9b, 10a and 10b). The second day of pervaporation shows high initial ethanol fluxes, even higher than the last measured fluxes of the first day. However, the amount of water, ethanol and eventually residual dimethylformamide, in the membrane could only decrease during the evacuation step. Hence there must be another reason for the observed flux behaviour than removal of solvent alone.
The obtained separation factors, for the thin membranes, are not steady-state values and are increasing steadily in time. This is not seen with the 2 and 2.5 μm thick membranes used in the automated pervaporation set-up, but the total fluxes are still decreasing in time. This observation is in contradiction with the development of ethanol and water concentration profiles by diffusion along a concentration gradient. The reasonable assumption that the diffusion coefficient of water is higher than the diffusion coefficient of ethanol must lead to the conclusion that the separation factor should decrease in time, in case the driving force for mass transport is only due to the development of a concentration gradient. Furthermore the low separation factors can not be due to the presence of residual solvent, as the solvent is completely removed when proper measures are taken (figures 11 and 12). One can not explain the high separation factor of the thick membrane from the fact that a thick membrane should contain relatively more solvent than a thin membrane. Residual solvent always enlarges the chances for lowering the membrane selectivity.

Aside from studying instationary permeation experiments, information concerning the diffusion coefficients of solvents and vapours in glassy polymers can also be obtained from the kinetics of sorption. A lot of phenomena have been found in literature describing these kinetics, like strongly concentration dependent diffusion coefficients, polymer relaxation phenomena, and stress induced diffusion. The latter phenomenon can sometimes lead to material failure, by the initiation of cracks or crazes.
A very important parameter in sorption experiments is the sample thickness, because it may influence the kind of transport encountered in glassy polymers. Vrentas *et al.* introduced the Deborah number for diffusion in polymer-solvent systems [30]. This dimensionless number $(DEB)_D$ is defined as the ratio of a characteristic relaxation time of the material, $\tau_{relaxation}$, and a characteristic time for diffusion processes in a sorption experiment, θ_D.

$$(DEB)_D = \frac{\tau_{relaxation}}{\theta_D} \cong \frac{D \cdot \tau_{relaxation}}{d^2}, \qquad (22)$$

with D the diffusion coefficient and d the membrane thickness.
For a given polymer/solvent system, $(DEB)_D$ is a function of temperature, solvent activity, and dimensions of the sample. Whenever $(DEB)_D$ is much smaller than 1, the polymer relaxation is fast enough to adapt to a new situation created by a sorption or desorption experiment. Ideal Fickian diffusion (or Case I transport) is observed. In case $(DEB)_D$ is much larger than 1, the situation is reversed. The polymer matrix will not respond noticably to changes caused by sorption or desorption. Also in this case Fickian diffusion is found. Because the diffusion coefficients do not correspond to the equilibrium state, and therefore are history dependent, the transport regime is sometimes called pseudo-Fickian diffusion. Typically non-Fickian diffusion, so-called anomalous diffusion, is encountered when both time-scales are of the same order.
The characteristic relaxation time of a glassy polymer is large, usually of the order of hours or even more. The characteristic time for diffusion is inversely proportional to the diffusion coefficient and proportional to the square of film thickness [30], see for example eq. (22).

A more complex situation arises when in sorption experiments, large steps in penetrant activities are applied with time [31]. Another transport regime is noticed, especially when part of the polymer is unswollen, and local transport is controlled by diffusion, and part of the polymer is swollen and transport is controlled by polymer relaxation. It is called case II transport. According to refs. [30,32] there is then a gradient in Deborah number for diffusion, including Deborah numbers of the order 1. Crazing of the glassy polymer is an extreme of case II transport, where the stresses induced by the swelling of the polymer matrix are so large that mechanical failure is a result.
In case II transport the penetrant enters the polymeric matrix faster than the polymer can adapt itself by volume relaxation. The kinetics of sorption are then controlled by the gradient in internal pressure, which is equal to the normal stress gradient [32-33]. Mass uptake is linear in time, whereas in Fickian diffusion with a constant diffusion coefficient the mass uptake is proportional to the square root of time.
The description of the solvent transport in glassy polymers and swelling of the polymer matrix due to solvent uptake will be discussed in chapter 3.

Also in pervaporation large differences in penetrant activities are applied to the polymer. The difference, compared to sorption, is that the large differences in penetrant activities across the membrane are maintained. There are two contributions to the fluxes through the membrane. First there is a flux due to concentration gradients in the membrane, and secondly a flux due to a gradient in tensile stress. The latter contribution to the total flux may decrease the observed process separation factor, because the same pressure gradient is a driving force for all permeating components.
The tensile stress σ_{zz} in the z-direction that results from swelling is equal to the Young's modulus E of the polymer, multiplied with the tensile deformation ε_{zz} which

is equal to the volume deformation.

$$\sigma_{zz} = E\varepsilon_{zz} = E\frac{\phi}{1-\phi}, \qquad (23)$$

with ϕ the penetrant volume fraction.
At the feed side of the membrane the solvent volume fraction is determined by the thermodynamic equilibrium. A tensile stress, or swelling pressure, will decrease the activity of the solvent in the membrane. The thermodynamic equilibrium is given by:

$$RT\ \ln a_{feed} = RT\ \ln a_{feed\ side\ membrane} + v\sigma. \qquad (24)$$

For the activity of a solvent at the feed side of the membrane one can apply the Flory Huggins theory, see eq. (20), and for the tensile stress eq. (23). Eq. (24) is evaluated for the binary system polyacrylonitrile/water, with a water activity 0.5 corresponding to the feed mixture in pervaporation, a molar volume of $1.8 \cdot 10^{-5}$ m^3mol^{-1}, an interaction parameter of 1.8 [22], and a Young's modulus of $\approx 10^{10}$ Nm^{-2} [34]. At the moment the water is applied to the membrane, its volume fraction at the feed side will be 0.013 and the corresponding stress will be $1.3 \cdot 10^8$ Pa. The latter value is so large that it may not be neglected anymore in eq. (9). It is not expected that an initial tensile deformation of about 1 % will induce crazing in the polymeric matrix.
The polymer attains its undeformed state by polymer relaxation. Therefore the swelling pressure will disappear in time. Because the equilibrium condition given in eq. (24) will be maintained, the water volume fraction will increase until a maximum of 0.036, which corresponds to the undeformed state in which there is no more tensile stress or deformation.
The expected large concentration gradient near the permeate side of the membrane, implies that there is also a gradient in the polymer relaxation time near the permeate side. As a result the pressure gradient will be near the permeate side of the membrane. The initially too high fluxes that are observed, will disappear as the polymer accomodates to the local, unstressed state. Wu *et al.* [32-33] use the Maxwell model as a stress-strain constitutive equation to model sorption. The relaxation time involved is related to the degree of swelling of the polymer matrix. At the permeate side, the membrane is unswollen, and as polyacrylonitrile is a glassy polymer, large relaxation times are expected. In general these relaxation times are of the order of 1 hour or even more.

With the large swelling at the feed side of the membranes, accompanied by large stresses in the glassy polymer, it is shown that case II transport is expected to occur. In time the transport regime will gradually shift to diffusion along a concentration gradient. This transition is controlled by polymer relaxation, and therefore can be slow. The initial case II transport may explain the initially high fluxes and low separation factors found in thin films. The same transport mechanism would be expected in thick films, but as it is difficult to remove residual solvent from the polymer matrix, some

amount is still present in thick polymer films, thereby enhancing polymer relaxation.

In explaining the effects observed in pervaporation of ethanol/water mixtures through thin films of polyacrylonitrile, some explanations for the decrease in selectivity with decreasing membrane thickness have been neglected. Concentration polarization might occur due to high fluxes, but it can not explain initially too high fluxes. The same applies to a temperature drop across the bulk of the feed mixture and the permeate side of the membrane. Although these effects are not discussed, they still might happen, as well as imperfections in the membrane structure and sorption resistances.

2.6. Acknowledgement

The electronics service group of the faculty of electronic engineering at the University of Twente is acknowledged for designing and constructing the control unit of the automated pervaporation set-up and writing the computer program.
Z. Borneman is acknowledged for making the automated pervaporation set-up work, and performing the experiments with the automated pervaporation set-up and the pervaporation set-up with nitrogen as a sweeping gas.

2.7. List of symbols

a	activity
c	solvent concentration
d	membrane thickness
f	feed
h	enthalpy
i,k	index or subscript indicating a specific component
n	total number of components
p	pressure or permeate
p^o	saturated vapour pressure
q	heat
v	molar volume
w	weight fraction
x	mole fraction
z	place coordinate
f, g	functions
α	separation factor
ε	tensile strain or deformation
θ_D	time to reach steady-state permeation
μ	chemical potential
σ	entropy production, and tensile stress
τ	relaxation time
φ	fugacity
ϕ	penetrant volume fraction
χ	interaction parameter
D	diffusion coefficient
E	Young's modulus
L	phenomenological coefficient
R	gas constant
S	membrane selectivity
T	absolute temperature

J	flux
X	thermodynamic force
$(DEB)_D$	Deborah number for diffusion

2.8. References

1. J. Néel, Introduction to pervaporation, Pervaporation membrane separation processes, ed. by R.Y.M Huang, Elsevier 1991.
2. J.W.F. Spitzen, G.H. Koops, M.H.V. Mulder, C.A. Smolders, The influence of membrane thickness on pervaporation performance, Proceedings of third international conference on pervaporation processes in the chemical industry, ed. by R. Bakish, Nancy, France, 1988.
3. G.H. Koops, J.A.M. Nolten, M.H.V. Mulder, C.A. Smolders, Selectivity as a function of membrane thickness: gas separation and pervaporation, Journal of Applied Polymer Science 53 (1994) 1639-1651.
4. J.H. Gibbs, Nature of the glass transition and the vitreous state, Modern aspects of the vitreous state, ed. by J.D. Mackenzie, Butterworths 1960.
5. E. Jenckel, R. Heusch, Die Erniedrigung der Einfriertemperatur organische Gläser durch Lösungsmittel, Kolloid Zeitschrift 130 (1953) 89.
6. M. Wessling, Relaxation phenomena in dense gas separation membranes, PhD-thesis, University of Twente, Enschede, the Netherlands, 1993.
7. L.C.E. Struik, Physical aging in amorphous polymers and other materials, Elsevier 1978.
8. J.D. Ferry, Viscoelastic properties of polymers, John Wiley & Sons 1980, Ch. XI.
9. Polymer handbook, ed. by J. Brandrup, E.H. Immergut, John Wiley & Sons 1975, Ch. III, pg. 229.
10. J. Gmehling, U. Onken, Vapor-liquid equilibrium data collection, aqueous-organic systems, Chemistry data series vol.I, part 1, ed. by D. Behrens, R. Eckermann, Dechema 1977.
11. R.C. Binning, R.J. Lee, J.F. Jennings, E.C. Martin, Separation of liquid mixtures by permeation, Industrial and Engineering Chemistry 53 (1961) 45-50.
12. P. Aptel, J. Cuny, J. Jozefonvicz, G. Morel, J. Néel, Liquid transport through membranes prepared by grafting of polar monomers onto poly(tetrafluoroethylene) films. II. Some factors determining pervaporation rate and selectivity, Journal of Applied Polymer Science 18 (1974) 351-364.
13. S.R. de Groot, P. Mazur, Non-equilibrium thermodynamics, North-Holland Publishing Company 1962.
    - Ch. III, § 2
    - Ch. III, § 3
    - Ch. XI, § 2
    - Ch. IV, § 1
14. O. Kedem, The role of coupling in pervaporation, Journal of Membrane Science 47 (1989) 277-284.
15. K. Stephan, H. Hildwein, Recommended data of selected compounds and binary mixtures, Chemistry data series vol. IVm parts 1+2, ed. by D. Behrens, R. Eckermann, Dechema 1987.
16. R. Rautenbach, C. Herion, U. Meyer-Blumenroth, Engineering aspects of pervaporation: calculation of transport resistances, module optimization and plant design, Pervaporation membrane separation processes, ed. by R.Y.M. Huang, Elsevier 1991.
17. R. Rautenbach, R. Albrecht, Separation of organic binary mixtures by pervaporation, Journal of Membrane Science 7 (1980) 203-223.
18. R. Courant, Differential and integral calculus. Vol II, Blackie & Son Limited 1936, Ch. VI, §5.
19. H. Strathmann, C.M. Bell, W. Gudernatsch, K. Kimmerle, Die Entwicklung von lösungsmittelselektiven Membranen und ihre Anwendung in der Gastrennung und Pervaporation, Chem.-Ing.-Tech. 60 (1988) 590-603.
20. J. Crank, The mathematics of diffusion, Oxford University Press 1975, Ch. IV, § 3.
21. P.J. Flory, Principles of polymer chemistry, Cornell University Press 1953, Ch. XII.
22. M.H.V. Mulder, T. Franken, C.A. Smolders, Preferential sorption versus preferential permeability in pervaporation, Journal of Membrane Science 22 (1985) 155-173.
23. H. Fujita, Diffusion in polymer-diluent systems, Fortschr. Hochpolym.-Forsch. 3 (1961) 1-47.
24. J. Crank, A theoretical investigation of the influence of molecular relaxation and internal stress on diffusion in polymers, Journal of Polymer Science 11 (1953) 151-168.
25. H.-C. Park, Separation of alcohols from organic liquid mixtures by pervaporation, PhD-thesis, University of Twente, Enschede, the Netherlands, 1993.
26. F.W. Greenlaw, R.A. Shelden, E.V. Thompson, Dependence of diffusive permeation rates on upstream and downstream pressures. II. Two component permeant, Journal of Membrane Science

2 (1977) 333-348.
27. R.B. Bird, W.E. Stewart, E.N. Lightfoot, Transport phenomena, John Wiley & Sons 1960, Ch. XVI.
28. CRC Handbook of Chemistry and Physics, ed. by R.C. Weast, CRC Press, 1984.
29. C.M. Hansen, Polymer coatings. Concepts of solvent evaporation phenomena, Ind. Eng. Chem. Prod. Res. Develop. 9 (1970) 282-286.
30. J.S. Vrentas, C.M. Jarzebski, J.L. Duda, A Deborah number for diffusion in polymer-solvent systems, AIChE Journal 21 (1975) 894-901.
31. H.B. Hopfenberg, H.L. Frish, Transport of organic micromolecules in amorphous polymers, Journal of Polymer Science, Part B, 7 (1969) 405-409.
32. J.C. Wu, N.A. Peppas, Modeling of penetrant diffusion in glassy polymers with an integral sorption Deborah number, Journal of Polymer Science, Part B: Polymer Physics 31 (1993) 1503-1518.
33. J.C. Wu, N.A. Peppas, Numerical simulation of anomalous penetrant diffusion in polymers, Journal of Applied Polymer Science 49 (1993) 1845-1856.
34. A.S. Kenyon, McC. J. Rayford, Mechanical relaxation processes in polyacrylonitrile polymers and copolymers, Journal of Applied Polymer Science 23 (1975) 717-725.

Chapter 3

Transient diffusion and volume relaxation in glassy membranes

3.1. Introduction

In this chapter the transport of solvents and gases in dense, glassy membranes will be considered. From pervaporation experiments shown in the second chapter it is clear that it may take a long time before a steady-state is reached with thin membranes. The development of a concentration profile is relatively fast compared to polymer relaxation. Also the preparation of the membrane itself influences the membrane properties. The history dependence has been noticed in pervaporation and is expected from the numerical simulations and the dielectric experiments on the drying of solvent-cast polymer films.
The observed transient permeation in pervaporation applying thin, glassy membranes can not be described with Fick's first law, employing a concentration dependent diffusion coefficient. Therefore the transient diffusion processes in glassy polymers will be looked at in more detail. These transient diffusion processes can be of rather complex nature, even if the glassy polymer and the solvent are in thermodynamic equilibrium. In paragraph 3.2. the description of transient diffusion processes will be discussed. It will focus on the solvent transport through glassy polymers in membrane processes. The fundamentals apply of course, to the kinetics of solvent uptake in polymer films as well. The application of dense membranes prepared from a glassy polymer in membrane processes like gas separation, vapour permeation and pervaporation is analysed in paragraph 3.3. There the influence of swelling on transient permeation is discussed, as well as the effect of membrane conditioning and the effect of excess free volume frozen into the polymer matrix due to the membrane preparation method.

3.2. Description of transient diffusion processes

In this paragraph some comments will be given concerning the description of (transient) diffusion processes of a single solvent in a polymer matrix. In general gradients in the chemical potentials are the driving forces for diffusion. The description of diffusion processes will start from the definition of the chemical potential. Then the transport equation is given in paragraph 3.2.1. The tensile stresses that develop in the polymer matrix and polymer relaxation will be discussed in paragraph 3.2.3. In paragraph 3.2.4. the initial and boundary conditions to solvent transport will be given.

Although the diffusion of only a single solvent in the polymer matrix is considered, conclusions are drawn in paragraph 3.3. from the equations developed in paragraph 3.2., with respect to the selective permeation in non-steady state membrane processes and the influence of preswelling of the membrane.

3.2.1. The chemical potential of the solvent

In membrane processes like gas separation and pervaporation a dense membrane is in contact with the feed at the upstream side and the permeate at the downstream side. At the membrane interfaces a thermodynamic equilibrium with the feed and permeate is maintained, i.e. the chemical potential of the solvent in the membrane and near the interface is equal to the chemical potential of the solvent in the adjacent phase (feed or permeate). A change of the solvent activity in the adjacent phase is accompanied by a change in the solvent concentration or solvent volume fraction at the membrane interface. Because diffusive transport is usually based on these latter measures instead of solvent activity it would be convenient to know the relation between the chemical potential of a solvent and for example the solvent volume fraction in the membrane.

$$(\mu_{0,1} + RT \ln a_1)_{\text{adjacent phase}} = (\mu_1(\phi))_{\text{membrane interface}}. \qquad (1)$$

Here $\mu_{0,1}$ is the chemical potential of the pure solvent, R the gas constant, T the temperature, a_1 the activity of the solvent in the feed or permeate and μ_1 the chemical potential of the solvent as a function of solvent volume fraction ϕ in the membrane and near the corresponding interface.
Because the solvent volume fraction in the polymer matrix as a function of the solvent activity in the adjacent phase is not always known for the polymer/solvent system considered, one often reflects upon equations for the chemical potential derived from the theory of statistical thermodynamics.

The chemical potential of the solvent can be derived from the Gibbs free energy. Here only one solvent, indicated by subscript 1, and a polymer, indicated by subscript 2, are considered. The chemical potential of the solvent μ_1 is defined by:

$$\mu_1 \equiv \left(\frac{\partial G}{\partial n_1}\right)_{n_2,p,T}. \qquad (2)$$

Here G is the Gibbs free energy, p the pressure, T the temperature, and n_1 and n_2 the number of moles of solvent and polymer respectively.
By changing the amount of solvent in a polymer/solvent system the enthalpy and entropy of the system also change. This affects the chemical potential in the following way [1]:

$$\mu_1 = \mu_{0,1} - T\left(\frac{\partial S_{ath}}{\partial n_1}\right) + \Delta\mu_{1,inter}. \qquad (3)$$

Here $\mu_{0,1}$ is the molar chemical potential of the pure solvent, S_{ath} the entropy in the athermal case and $\Delta\mu_{1,inter}$ accounts for the heat of mixing. Athermal means that from energy considerations there is no preference for a polymer segment to be close to another polymer segment or to a solvent molecule. The same argument applies for a solvent molecule. The specific interactions are accounted for in the third term at the right-hand side of eq. (3).
If it is possible to count the number of realizable conformations that constitute the macroscopically observed system of polymer and solvent, then the entropy is known. At this point a clear distinction must be made between a polymer solution, a polymer gel and a plasticized glassy polymer. In a polymer solution the average expectancy to find a polymer segment anywhere in the solution is equal to the polymer volume fraction when that volume fraction is reasonably large. In a swollen polymer gel, the expectancy to find a polymer segment close to a chemical crosslink of the gel is of course larger than the average polymer volume fraction. This argument applies to a plasticized polymer too, which is also considered to be a polymer network. The entanglements in a glassy polymer restrain the motion of polymer chains and are regarded as temporary crosslinks. The variable expectancy to find a polymer segment somewhere in a swollen polymer network directly influences the number of realizable conformations in the (temporary) polymer network, when compared to the number of realizable conformations in a polymer solution at equal polymer and solvent volume fraction.
There is another difference between a polymer solution and a (temporary) polymer network. In both systems a solvent will swell the dry polymer because of the lower chemical potential of the solvent in the dry polymer. In the polymer network, however, the swelling is counter-acted by the stretching of the network due to the action of swelling [2]. The latter effect is absent in the case of a polymer solution.

For a polymer solution one can use the Flory-Huggins expression for the chemical potential of the solvent. This expression is derived by counting the number of realizable conformations in which polymer and solvent molecules can be arranged on a lattice in order to the determine the entropy of mixing and by counting the number of polymer-solvent contacts in the lattice in order to determine the heat of mixing [3].

$$\mu_{1,Fl.H.}(\phi) = \mu_{0,1} + RT\{\ln(\phi) + (1-\phi)\} + RT\chi(1-\phi)^2. \qquad (4)$$

Here $\mu_{1,Fl.H.}$ is the chemical potential of a polymer solution according to the Flory-Huggins lattice theory, ϕ the solvent volume fraction and χ the so-called interaction parameter. In eq. (4) it has been assumed that the molar volume of the polymer is much larger than the molar volume of the solvent. The successive terms at the right-hand side of eq. (4) correspond to the successive terms in eq. (3). Eq. (4) is valid only under certain assumptions. These assumptions, specified by Flory [3], are:

1) the same lattice applies to the pure solvent, the polymer segments and mixtures from them,

2) the expectancy that, during the successive insertion of polymer molecules in the lattice, a neighbouring lattice site of a previously vacant site is occupied by already inserted polymer molecules, is equal to the expectancy that a lattice site chosen at random is occupied by the already inserted polymer molecules,
3) the conformation of the polymer chains in the solution is random,
4) when adding successively polymer molecules to the lattice the polymer segments of previously added molecules are distributed at random.

As already mentioned a swollen polymer network differs from a polymer solution in the number of realizable conformations. Therefore both the entropy and heat of mixing that led to eq. (4) are not the same in a (temporary) polymer network. With an additional assumption the discrepancy may be neglected [1].

5) The average end-to-end distance of the polymer chains in between crosslinks or entanglements is small compared to the contour length of the polymer chains between those crosslinks or entanglements.

The discrepancy in the entropy and heat of mixing between a polymer solution and a polymer network can be stated more precisely.

$$-T\left(\frac{\partial S_{ath}^{\text{polymer network}}(\phi)}{\partial n_1}\right) > RT\{\ln(\phi) + (1-\phi)\}, \qquad (5a)$$

and

$$\left|\Delta\mu_{1,inter}^{\text{polymer network}}(\phi)\right| \leq \left|RT\chi(1-\phi)^2\right|. \qquad (5b)$$

The notation with absolute values can be omitted in eq. (5b) when the interaction parameter is positive. In that case the decreased entropy of the polymer network with respect to the polymer solution is counterbalanced to some extent by the decreased heat of mixing.
Often the interaction parameter is used as a fitting parameter because the theoretical value of the interaction parameter, calculated from solubility parameters, is correct only for nonpolar polymer-solvent combinations [4]. The interaction parameter can be determined experimentally by applying a solvent with activity one to the dry polymer and measuring the increase in volume of the polymer sample. The relationship between the interaction parameter χ and solvent volume fraction is found then by equating the left-hand side of eq. (1) with the Flory-Huggins expression for the chemical potential.

$$\chi = \left(\frac{-\ln\phi - (1-\phi)}{(1-\phi)^2}\right)_{a_1=1} \qquad (6)$$

In a polymer network the contribution to the Gibbs free energy of volume deformation due to swelling has to be taken into account. In order to give a physical interpretation

of the swelling of a polymer network Hill introduces the concept of an osmotic pressure to describe the tendency of a pure solvent to swell the dry polymer network [2].

$$\Pi = \frac{\mu_{0,1} - \mu_1(\phi)}{v_1}. \qquad (7)$$

Here Π is the osmotic pressure which represents the swelling tendency and v_1 is the molar volume of the solvent. For the chemical potential of the solvent as a function of solvent volume fraction one can take for example eq. (4). The so-called osmotic pressure is balanced in equilibrium by the tensile stress induced in the polymer network that tries to contract the network when it is being expanded.
From continuum mechanics Wu *et al.* [5] showed that for a system with a polymer and a single solvent the tensile stress opposes the osmotic pressure when shear stresses are not present and the inertial terms in the momentum balance of the system can be neglected. These conditions are generally true in the transport of solvents in glassy polymers.
If the entropy and heat of mixing derived from the Flory-Huggins lattice theory are assumed to be valid then the following expression for the chemical potential of the solvent in a polymer network is derived:

$$\mu_{1,\text{polymer network}}(\phi) = \mu_{0,1} + v_1\sigma + RT\{\ln(\phi) + (1-\phi)\} + RT\chi(1-\phi)^2. \qquad (8)$$

Here σ is the tensile stress and v_1 the solvent molar volume.
Although one might argue upon the validity of the Flory-Huggins expression to describe the sorption of solvents in a glassy polymer, eq. (8) is instructive in explaining the transport phenomena and it will therefore be used in the remainder of paragraph 3.2.

3.2.2. The transport equation

The negative gradient in chemical potential is the driving force for transport; transport is in the direction from the higher chemical potential towards the lower chemical potential. With transport in only one direction the gradient of the chemical potential can be derived in a straightforward way.

$$\frac{\partial \mu_1(z,t)}{\partial z} = v_1 \frac{\partial \sigma(z,t)}{\partial z} + RT\{\frac{1}{\phi} - 1 - 2\chi(1-\phi)\}\frac{\partial \phi(z,t)}{\partial z}. \qquad (9)$$

Here z is the directional coordinate in which solvent transport occurs and t the time. Gradients in hydrostatic pressure p and temperature T are neglected.
From eq. (9) it is clear that solvent transport can occur due to a gradient in solvent volume fraction and/or a gradient in the tensile stress. The transport of both the polymer and the solvent is completely described by the gradient in the chemical

potential of the solvent if locally the equilibrium between polymer and solvent is maintained.
Assuming a linear relationship between solvent flux and the driving force, then

$$J_1(z,t) = -L\frac{\partial \mu_1(z,t)}{\partial z}. \qquad (10)$$

Here L is a phenomenological coefficient, which is related to the mutual diffusion coefficient $D(\phi)$ by the following equation:

$$L \cdot RT\{\frac{1}{\phi} - 1 - 2\chi(1-\phi)\} = D(\phi). \qquad (11)$$

The mutual diffusion coefficient $D(\phi)$ is determined by the solvent volume flux with respect to volume-average flow and the gradient in solvent volume fraction [6]. Now the final transport equation, describing solvent volume flux J_1 as a function of the directional coordinate z and time t, can be obtained by combining eqs. (9) through (11).

$$J_1(z,t) = -D(\phi)\{\frac{v_1\phi}{RT(1-\phi)(1-2\chi\phi)} \cdot \frac{\partial \sigma(z,t)}{\partial z} + \frac{\partial \phi(z,t)}{\partial z}\}. \qquad (12)$$

The solvent volume fraction varies with time in a transient diffusion process. The rate of increase or decrease in solvent volume fraction in a finite volume is given by the difference between the flux to and from this finite volume.

$$\frac{\partial \phi(z,t)}{\partial t} = -\frac{\partial J_1(z,t)}{\partial z}. \qquad (13)$$

The combination of eqs. (12) and (13) can be used to solve the transient diffusion processes. As input parameters the temperature, the solvent molar volume, the polymer/solvent interaction parameter and the concentration dependent diffusion coefficient have to be known. Furthermore the development of the tensile stress profile has to be known.

3.2.3. The tensile stress and polymer relaxation

Due to solvent uptake the polymer matrix will expand. The volume changes can be related to the solvent volume fraction. Applying flat membranes in membrane processes swelling or deswelling can be realized in one direction only, i.e. in the direction of permeation.

$$\frac{\Delta V}{V_0} = \frac{\Delta L}{L_0} = \frac{\phi}{1-\phi}. \qquad (14)$$

The symbol Δ represents the variation in volume V or thickness L with respect to volume V_0 or thickness L_0 of the dry polymer.
The tensile stress in a polymer gel with chemical crosslinks is proportional to the length deformation or tensile strain. The proportion is given by the tensile or Young's modulus. In a glassy polymer however, the crosslinks have a temporary character. In time the tensile stress will fade away by polymer relaxation. The stress-strain relation is given by the Maxwell model if polymer relaxation is controlled by one distinct relaxation time.

$$\frac{\partial\sigma(z,t)}{\partial t} = -\frac{\sigma(z,t)}{\tau(\phi)} + E(\phi)\frac{\partial(\frac{\phi}{1-\phi})}{\partial t}. \qquad (15)$$

Here τ is the polymer relaxation time and E the tensile or Young's modulus. The first term on the right-hand side represents polymer relaxation and the second term the relation between the development of tensile stress and the tensile strain rate.
The solvent volume fraction is known to have a large influence on polymer relaxation times. The tensile modulus is also a function of the solvent volume fraction although Wu *et al.* considered it to be a constant [5].
According to Ferry it is possible to obtain one master curve for the shear relaxation modulus of concentrated polymer solutions or gels in the transition zone [7]. The transition zone represents the transition from glass-like to rubber-like mechanical behaviour and therefore it corresponds to the volume relaxation looked at in this paragraph. When the Poisson's ratio is 1/2, regardless of the solvent volume fraction, then a master curve can be established for the tensile or Young's relaxation modulus as well. The master curve is obtained by reducing the tensile relaxation modulus at a certain volume fraction to the pure polymer and correcting the time-scale for the polymer relaxation times at different solvent volume fractions, i.e. by plotting:

$$E(t,\phi=0) = \frac{1}{1-\phi}E(t,\phi) \quad \text{vs.} \quad t\frac{\tau(\phi=0)}{\tau(\phi)}. \qquad (16)$$

For the relation between the relaxation times at various solvent volume fractions one can take for example the following equation which is based on the Doolittle equation for the viscosity of liquids as a function of fractional free volume, and the linear increase of fractional free volume in a concentrated polymer solution with solvent volume fraction [7].

$$\tau(\phi) = \tau(\phi=0)\exp\left(\frac{-B\beta'\phi}{f\,(f+\beta'\phi)}\right). \qquad (17)$$

B is a constant in the Doolittle equation which is usually taken as unity, f is the

fractional free volume of the polymer and β' the parameter relating fractional free volume to the volume fraction of solvent. A variation of the fractional free volume volume f of the polymer changes both the exponent in eq. (17) and the relaxation time of the pure polymer $\tau(\phi=0)$.
The dependence of the diffusion coefficient on solvent volume fraction can be based on the same approach that led to eq. (17), see ref. [8].

$$D(\phi) = D(\phi=0)\exp\left(\frac{B\beta'\phi}{f\,(f+\beta'\phi)}\right). \qquad (18)$$

Comparing eqs. (17) and (18) one can see that, at equal solvent volume fractions, the relative decrease in relaxation time with respect to the dry polymer is the same as the relative increase in solvent diffusion coefficient with respect to the dry polymer.

Combining eqs. (15) through (17) and taking B as unity will give the development of the tensile stress as a function of the directional coordinate z and time t.

$$\frac{\partial\sigma(z,t)}{\partial t} = -\frac{\sigma(z,t)}{\tau(\phi=0)}\exp\left(\frac{\beta'\phi}{f\,(f+\beta'\phi)}\right) + \frac{E(\phi=0)}{1-\phi}\frac{\partial\phi}{\partial t}. \qquad (19)$$

The fractional free volume f in a glassy polymer below the glass transition temperature is smaller than the fractional free volume at the glass transition, i.e. smaller than 0.025 ± 0.005 [6]. The parameter β' varies from 0.1 to 0.3 which are values comparable to the fractional free volume of a pure solvent [7]. The tensile modulus of a glassy polymer is in general of the order 10^9 - 10^{10} Nm^{-2}. The relatively large value of the tensile modulus is the reason why tensile stresses may not be neglected in the advance in the transient diffusion processes.

The designation "glassy state" or "glassy polymer" is rather ambiguous and refers to the non-equilibrium nature of vitrification, see for example ref. [7] and paragraph 4.5. In the description of solvent transport and polymer relaxation in glassy polymers it has been assumed that local equilibrium is maintained. The plasticized polymer is considered to be a concentrated polymer solution.

3.2.4. The initial and boundary conditions to solvent transport

The boundary conditions at both sides of a membrane have already been given in eq. (1). The thermodynamic equilibrium is given by putting eq. (8) at the right-hand side of eq. (1).

$$(RT\ln a_1)_{\text{adjacent phase}} = (v_1\sigma + RT\{\ln(\phi) + (1-\phi) + \chi(1-\phi)^2\})_{\text{membrane interface}}. \qquad (20)$$

When the temperature, activity, molar volume of the solvent and the interaction parameter are known, there are two unknown variables left: the tensile stress and the solvent volume fraction. For the interrelation between these two variables eq. (15) will be used. This equation depends on the history and therefore an initial boundary condition is needed.
For simplicity one may assume that the initial boundary condition is given by the stepwise change of the solvent activity in the adjacent phase. This corresponds to sorption experiments in which the kinetics of the sorption process are studied, and it corresponds to the application of a feed mixture to the membrane in a separation process. Apart from applying a feed mixture to a dry membrane, one can also apply a vacuum instantaneously to the permeate side of a membrane preswollen in the feed mixture. Wu *et al.* [5,9] assume that the tensile stress at the membrane interface remains zero and the equilibrium solvent volume fraction is then uniquely determined by eq. (20) with $\sigma=0$. This assumption is not correct because a change in solvent volume fraction must be accompanied by a change in the tensile stress. Therefore the correct initial boundary condition to the stepwise change in activity is given by incorporating eq. (15) in eq. (20) and stating that no polymer relaxation can occur in an infinitesimally small time.

$$RT\Delta\ln a_{1,\text{adjacent phase}} = v_1 E(\phi)\Delta\{\frac{\phi}{1-\phi}\} + RT\Delta\{\ln\phi + (1-\phi) + \chi(1-\phi)^2\}. \quad (21)$$

The symbol Δ represents a stepwise change. The change in solvent volume fraction is known from eq. (21) and therefore the corresponding change in tensile stress is known from the thermodynamic equilibrium given in eq. (20).
When after a stepwise change in solvent activity its value is maintained constant, then both the solvent volume fraction and the tensile stress will change in time. This boundary condition is given combining the time-derivative of eq. (20) which must be equal to zero, and eq. (15).

$$\frac{d\sigma}{dt} = -\frac{\sigma}{\tau(\phi)} \cdot \frac{1}{1 + \dfrac{E(\phi)v_1\phi}{RT(1-\phi)^3(1-2\chi\phi)}}, \; a_1 = \text{constant}, \quad (22a)$$

and

$$\frac{d\phi}{dt} = \frac{-v_1\phi}{RT(1-\phi)(1-2\chi\phi)} \cdot \frac{d\sigma}{dt} = \frac{\sigma}{\tau(\phi)} \cdot \frac{1}{\dfrac{RT}{v_1\phi}(1-\phi)(1-2\chi\phi) + \dfrac{E(\phi)}{(1-\phi)^2}}, \; a_1 = \text{constant}. \quad (22b)$$

Eqs. (22a) and (22b) are the boundary conditions that apply to the developed equations and a constant activity of the solvent in the adjacent phase of the membrane. For simplicity the concentration dependence of the tensile modulus and relaxation time is not incorporated in eqs. (21) and (22), but one can apply of course eqs. (16) and (17).

In time the tensile stress will disappear and a constant solvent volume fraction will be obtained. The concept of a variable surface concentration has been proposed intuitively in literature in order to explain sigmoid and two-stage sorption curves, see for example ref [8]. The variable surface concentration is introduced on the consideration that the sorption of solvents requires a rearrangement of the polymer molecules, and therefore depends on the segmental motion of polymer chains. This argument agrees with the concept presented in this paragraph that swelling is restrained to a certain extent due to the entangled polymer chains. The restricted swelling is gradually relieved in time because of polymer relaxation and will be noticed as volume relaxation.
The assumed variable surface concentration, reproduced from ref. [8], is:

$$c_1^s = c_1^i + (c_1^\infty - c_1^i)(1 - \exp(-\beta t)). \qquad (23)$$

Here is c_1^s the variable surface concentration, c_1^i the surface concentration immediately after applying a stepwise change in activity, c_1^∞ the surface concentration after an infinitely long time and β a rate constant. In a sorption experiment the value of c_1^i is assumed to be larger than the initial surface concentration just before applying the stepwise change in solvent activity [8].
Apart from the variable surface concentration and diffusion along a gradient in concentration or solvent volume fraction as in ref. [8], one has to take into account the diffusion of solvent along a gradient in tensile stress.
As an example how the surface volume fraction and tensile stress vary with time eqs. (21) and (20) have been evaluated for the system polyacrylonitrile/water. The interaction parameter of this system is 1.8 [10], the tensile modulus is estimated to be 10^{10} Nm^{-2} [11], the molar volume of water is $1.8 \cdot 10^{-5}$ m^3mol^{-1} and the temperature is here 300 K. The activity changes stepwise from 0.0 to 0.5, which corresponds to the water activity of the feed mixture in the pervaporation experiments described in chapter 2. The combination of tensile stress and solvent volume fraction that belongs to the thermodynamic equilibrium at the membrane interface is plotted in figure 1.

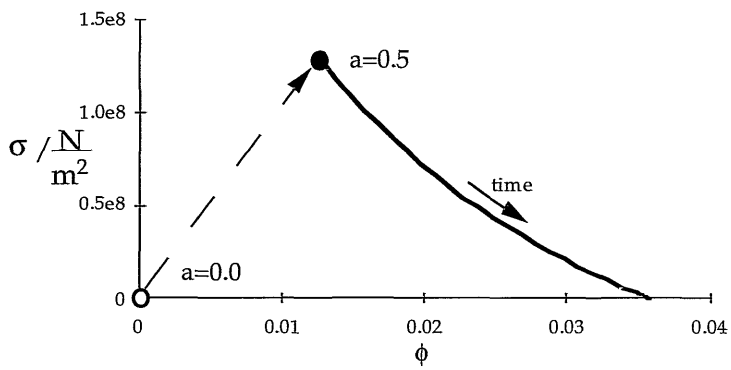

figure 1: The unique combination of tensile stress σ and water volume fraction ϕ in polyacrylonitrile is given for the situation in which the water activity a is changed stepwise from 0.0 to 0.5.

Initially the polymer contains no water and is free from tensile stresses. After changing

the water activity from 0.0 to 0.5 the water volume fraction at the membrane interface increases instantaneously from 0.0 to 0.013. This is accompanied by an increase in the tensile stress to $1.28 \cdot 10^8$ Nm^{-2}. In time the stress will fade away due to polymer relaxation and gradually the water volume fraction at the interface increases to the final value 0.036. The increase of solvent volume fraction at the membrane interface is accompanied by an increase of the solvent diffusion coefficient and a decrease of the relaxation time. In the pervaporation experiments described in chapter 2 the flux through the membrane decreases in time which seems to contradict the enhanced diffusion coefficient. The initial and boundary conditions discussed in this paragraph, however, are only part of the described transport process. Therefore one has to solve the partial differential equations of solvent volume fraction and tensile stress as a function of time and place in the membrane.

The description of the transient diffusion processes consist of two coupled partial differential equations. The first differential equation describes the local change of solvent volume fraction with time, i.e. the combination of eqs. (12) and (13). The second differential equation describes the local change of tensile stress with time, i.e. eq. (15) or eq. (19). Due to the complex nature of these differential equations they cannot be solved analytically and therefore numerical simulation is the only way to check experimental results with the developed equations.
The boundary condition that corresponds to a stepwise change of the solvent activity in an adjacent phase of the membrane is given in eq. (21). The boundary conditions are given by eqs. (22a) and (22b) when the solvent activity of the adjacent phase is constant.

3.3. Transient permeation in membrane processes

Swelling and polymer relaxation are of extreme importance in the transient diffusion processes in glassy polymers. In membrane processes like pervaporation, vapour permeation and gas separation at elevated pressures, a significant degree of swelling is encountered at the upstream side of the membrane, whereas the downstream side of the membrane is in general unswollen. Due to the large tensile moduli of glassy polymers it is anticipated that tensile stresses build up because of the swelling or deswelling that has to be realized in the polymer matrix when starting the membrane process. These tensile stresses are inherent to the application of a feed mixture to the upstream side of a dry membrane or applying a vacuum to the downstream side of a preswollen membrane. The tensile stresses disappear in the course of time due to the segmental motion of polymer chains. At the same time there is volume expansion or contraction of the membrane because of the gradual change of solvent volume fraction at the membrane interface(s) and in the membrane.
In paragraph 3.3.1. the effect of swelling a dry membrane will be compared with deswelling of a preswollen membrane. Also the effect of tensile stresses on selective

permeation will be discussed.
Except for the changes in the swollen state of the membrane inherent to the start of a separation process, a history dependence of membrane properties has been observed. The effect of residual solvent in the membrane due to slow evaporation of solvent during membrane preparation, and the effect of excess free volume in the polymer matrix due to very fast evaporation of solvent during membrane preparation, will be discussed in paragraph 3.3.2.

3.3.1. The influence of swelling

In membrane processes permeation is usually started by applying a feed mixture to an initially dry polymer. Due to the applied feed mixture swelling occurs near the feed side of the membrane. In pervaporation the membrane is sometimes preswollen in the feed mixture prior to the pervaporation process because the conditioning history is important in diffusion experiments [12]. Pervaporation is started then by applying a vacuum at the permeate side of the membrane. The membrane will shrink due to the decrease in solvent volume fraction near the permeate side. Both ways of starting a membrane process will be compared.
First a dry membrane is considered in which the solvent volume fraction and tensile stress are zero throughout the membrane. At a certain moment a feed mixture is applied at the upstream side of the membrane. The change in time of solvent volume fraction and tensile stress near the feed and permeate side of the membrane is drawn schematically in figure 2.

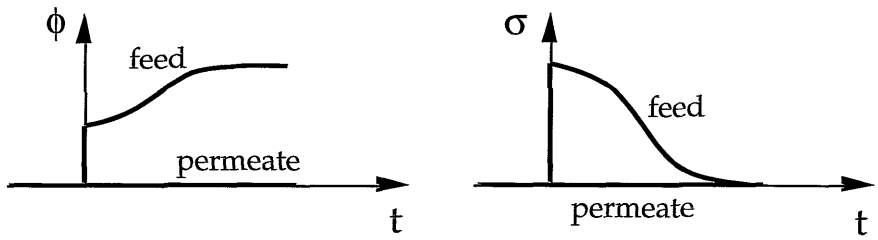

figure 2: Schematic drawing of solvent volume fraction ϕ and tensile stress σ at the feed and permeate side of an initially dry polymer free from tensile stresses, as a function of time t. The activity is changed stepwise at the feed side of the membrane.

The permeate side of the membrane remains dry and therefore the solvent volume fraction and the tensile stress remain zero. At the feed side however, an instantaneous solvent uptake is realized according to eq. (21). The same instance a tensile stress develops in the polymer due to swelling accompanying the solvent uptake. In time the tensile stress will fade away according to boundary condition (22a) and at the same time the solvent volume fraction increases towards a finite value according to boundary condition (22b).
In figure 3 the membrane is preswollen and a vacuum is applied instantaneously to the permeate side of the membrane. The change in time of solvent volume fraction and tensile stress near the feed and permeate side of the membrane is drawn

schematically in figure 3.
The feed side of the membrane remains swollen and therefore the solvent volume fraction is constant in time and the tensile stress remains zero. At the permeate side an instantaneous desorption is realized according to eq. (21). The activity changes from a finite value to zero and therefore the solvent volume fraction becomes zero immediately. The same instance a negative tensile stress develops in the polymer. In time the negative tensile stress will fade away according to boundary condition (22a) in which $\phi=0$.

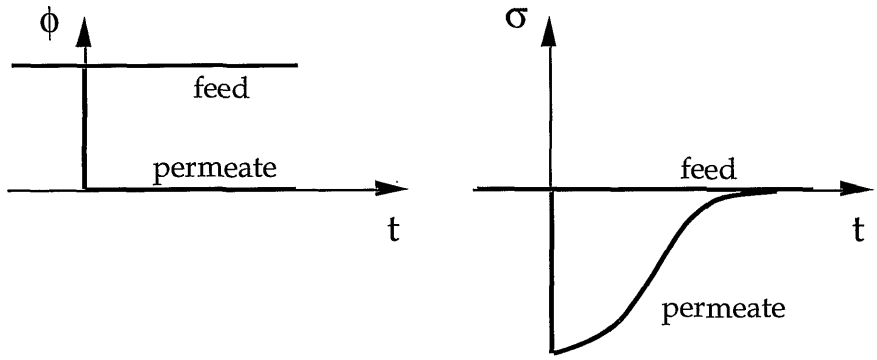

figure 3: Schematic drawing of solvent volume fraction ϕ and tensile stress σ at the feed and permeate side of an initially preswollen polymer free from tensile stresses, as a function of time t. The activity is changed stepwise to zero at the permeate side of the membrane.

There is no large difference in applying a feed to a dry membrane or applying a vacuum to a membrane preswollen in the same feed. The differences ($\phi_{\text{feed side}} - \phi_{\text{permeate side}}$) and ($\sigma_{\text{feed side}} - \sigma_{\text{permeate side}}$) across the membrane are of the same order. In case of a vacuum applied at the permeate side of a preswollen membrane the instantaneous change in solvent volume fraction is larger when solvent is removed effectively from the permeate side of the membrane. In both cases the tensile stress is relieved by polymer relaxation, which means that it may take hours or even years before the membrane is free from tensile stresses.
The time-scales involved in the attainment of steady-state permeation are of the same order when comparing initially dry membranes with membranes initially swollen in the feed mixture. Therefore one may compare the experimental results of chapter 2, table 1, on the dehydration of ethanol/water mixtures applying initially dry polyacrylonitrile membranes with the results obtained by Spitzen [13], who uses exactly the same system with the only difference that membranes have been preswollen in the feed mixture. The same trend is observed: the separation factor decreases with decreasing membrane thickness, as measured after 8 hours of pervaporation.
The general observation in pervaporation applying glassy membranes is that the separation factor is too low for thin membranes, regardless of the initial state of the membrane. Spitzen [13] and Park [14] apply preswollen membranes in the dehydration of ethanol and the removal of methanol from mixtures with methyl tert-butyl ether respectively, whereas Koops [15] applies initially dry membranes in the dehydration of

acetic acid. The separation factors in these references were determined after the pervaporation process had reached a seemingly steady-state and diffusion is controlled by slow polymer relaxation processes.

Due to the complexity of the transport equations the transient permeation of solvent through a membrane can be solved numerically only. In paragraph 3.2. the transport of one solvent has been considered. In membrane processes interest is directed towards the competitive transport of solvent mixtures. Although the transport equations are not numerically simulated some statements concerning the (selective) transient permeation and the driving forces for solvent transport can be made.

In paragraph 3.2.4., figure 1, an example has been given of the variable solvent volume fraction and variable tensile stress at the membrane interface when the activity in the adjacent phase is changed stepwise. In the example, which corresponds to the applied activity of water in the pervaporation experiments of chapter 2, the initial stress is $1.3 \cdot 10^8$ Nm^{-2}. In pervaporation the permeate side remains dry and therefore the initial stress at the feed side is also the maximum stress difference across the membrane.
In general diffusion due to a pressure gradient may be neglected on basis of the following inequality:

$$v\Delta p << RT. \qquad (24)$$

Here v is the molar volume of the solvent, Δp the pressure gradient across the membrane, R the gas constant and T the temperature. In pervaporation the difference in hydrostatic pressure across the membrane is usually 1 bar and its influence of diffusion may therefore be neglected. The initial difference in tensile stress at both interfaces of the membrane, however, may become so large that diffusion along a concentration gradient (Fickian diffusion) does not describe solvent transport properly. In the given example the product of instantaneous tensile stress and molar volume of water is $2.3 \cdot 10^3$ $Jmol^{-1}$ and the product of the gas constant and temperature is $2.5 \cdot 10^3$ $Jmol^{-1}$. The inequality (24) does not hold and therefore, in the beginning of the experiment one may not neglect the contribution of tensile stress to the chemical potential of the solvent in this example.

In a membrane separation process a feed is applied of various solvents, vapours or gases. The thermodynamic equilibrium at the membrane interface is evaluated here for a three component system which means that the feed is restricted to a binary mixture and a polymer membrane. The Flory-Huggins expression for the chemical potential of two solvents in a polymer will be used [16]. In this expression the interaction between the two solvents in the polymer is neglected on the basis of the justified assumption that the solvent volume fractions are small. The tensile stress contributes to the chemical potential of both solvents and is due to the total sorption of solvent. The equivalence of eq. (21) is given for the case that the polymer is initially dry and free from tensile stresses and in case the feed mixture is applied stepwise.

$$RT\ln a_{1a} = v_{1a}E(0)\frac{\phi_{1a}+\phi_{1b}}{1-\phi_{1a}-\phi_{1b}} + RT\left\{\ln(\phi_{1a})+1-\phi_{1a}-\frac{v_{1a}}{v_{1b}}\phi_{1b}+\chi_{1a}(1-\phi_{1a})\phi_2-\frac{v_{1a}}{v_{1b}}\chi_{1b}\phi_{1b}\phi_2\right\}, \quad (25a)$$

and

$$RT\ln a_{1b} = v_{1b}E(0)\frac{\phi_{1a}+\phi_{1b}}{1-\phi_{1a}-\phi_{1b}} + RT\left\{\ln(\phi_{1b})+1-\phi_{1b}-\frac{v_{1b}}{v_{1a}}\phi_{1a}+\chi_{1b}(1-\phi_{1b})\phi_2-\frac{v_{1b}}{v_{1a}}\chi_{1a}\phi_{1a}\phi_2\right\}. \quad (25b)$$

The subscripts 1a and 1b refer to the first and second solvent respectively and subscript 2 refers to the polymer.
Eqs. (25) are applied to the equilibrium between a water/ethanol mixture and a polyacrylonitrile polymer. The situation corresponds to the pervaporation process in chapter 2. The water activity changes instantaneously from 0.0 to 0.5 and at the same moment the ethanol activity becomes 0.9. The molar volumes of water and ethanol are $1.8 \cdot 10^{-5}$ $m^3 mol^{-1}$ and $5.8 \cdot 10^{-5}$ $m^3 mol^{-1}$ respectively. The tensile modulus of polyacrylonitrile is $\approx 10^{10}$ Nm^{-2} [11]. The interaction parameters χ that account for the interaction between water and polyacrylonitrile and between ethanol and polyacrylonitrile are 1.8 and 4.2 respectively [10].
In table 1 the calculated initial volume fractions and tensile stress are given, as well as the final volume fractions that will be obtained when the stress has faded away.

table 1: *The initial volume fractions of water and ethanol and the initial stress in a polyacrylonitrile membrane after applying the liquid mixture to a membrane. The data compares to the pervaporation experiments described in chapter 2. The final volume fractions are obtained after polymer relaxation. The volume fractions and tensile stresses are calculated with eqs. (25).*

	$\phi_{initial}$	ϕ_{final}	$\sigma_{initial}$ (Nm^{-2})	σ_{final}·(Nm^{-2})
water	0.0127	0.0385	$1.3 \cdot 10^8$	0
ethanol	0.00026	0.0074	$1.3 \cdot 10^8$	0

One can see from table 1 that initially the swelling is almost fully on the account of the water in the feed mixture. The initial water volume fraction and the initial stress are almost the same as their corresponding values in the binary system water - polyacrylonitrile depicted in figure 1. The large swelling due to the sorption of water is the cause of the low initial sorption of ethanol. In time the polymer will accomodate to the swollen state and further volume expansion will occur. In time the water volume fraction will become about 3 times its initial value whereas the ethanol volume fraction will become about 30 times its initial value! This observation is of extreme importance when the driving forces for permeation are considered.
For the system water - polyacrylonitrile it was already argued that diffusion along a stress gradient could not be neglected with respect to diffusion along a concentration gradient. The same tensile stress is a driving force in the permeation of ethanol. The

product of tensile stress and ethanol molar volume is $7.5 \cdot 10^3$ $Jmol^{-1}$ which is large compared to the product of gas constant and temperature, i.e. $2.5 \cdot 10^3$ $Jmol^{-1}$. On this basis and on the "absence" of an ethanol concentration difference across the membrane, it is even appropriate to neglect initially, for ethanol, the diffusion along a concentration gradient. It is remarkable to notice that in the pervaporation experiments initially high ethanol fluxes are observed although the concentration difference across the membrane is negligible.

It is clear from the above example that one can not apply straightway Fick's first law, describing diffusion due to a concentration gradient, for the transient permeation processes in glassy membranes. Apart from the solvent concentration also swelling contributes the chemical potential of the solvent.

3.3.2. The influence of membrane history

The history of the membrane is of importance to initial permeation properties. In the pervaporation experiments it has been shown that excessive swelling of the membrane in pure water is detrimental when looking at the separation factor, see figures 7 and 8 in chapter 2. The maximum water uptake of polyacrylonitrile is 9 % by volume [9]. The excessive swelling also deleted completely the history of the drying process. The effect of lost separation factors due to excessive swelling has been measured too in the separation of methanol from mixtures with methyl tert-butyl ether (MTBE) [15]. In the latter work the membranes, which were blends of polyacrylic acid (70 %) and polyvinylalcohol (30 %), were swollen in a mixture enriched in methanol prior to pervaporation. The swelling in a methanol enriched feed compares to swelling in ethanol. The measured ethanol volume fraction in an almost similar blend, polyacrylic acid (80 %) and polyvinylalchol (20%), immersed in pure ethanol was 0.81 [15]. Applying a feed mixture in pervaporation with only 10 % by weight of methanol after removal of the methanol enriched liquid mixture will drastically decrease the degree of swelling. These measurements compare with figure 3, with the understanding that the complete membrane has to deswell when the feed mixture of the pervaporation process replaces the liquid in which the excessive swelling has been realized. The total solvent volume fraction will decrease throughout the membrane, but the most near the permeate side of the membrane. The net difference between the solvent volume fraction at the feed and permeate side is responsible for the resulting net difference in temporary tensile stress across the membrane.

In gas separation large swelling can be found too when a gas like carbon dioxide is applied at high pressures. Jordan *et al.* [17] found that at high pressures the carbon dioxide permeation of polycarbonate varies with time. The permeabilities were measured at feed pressures which were gradually increased up to 60 bar. The membrane remained conditioned at this pressure for 5 days. Then permeabilities were measured decreasing the feed pressure gradually down to a few bar. A clear hysteresis phenomenon is seen when plotting the permeability versus CO_2 feed pressure. After

the conditioning at high pressure the membrane permeability is permanently larger at low feed pressures. In the same reference [17] the results of volume dilation are shown for the polycarbonate exposed to the same increase and decrease of CO_2 pressure. Also volume dilation shows a hysteresis when plotted versus pressure. This is a clear indication that the time-dependent permeation of carbon dioxide through a polycarbonate membrane is controlled by the variable surface concentration of carbon dioxide at the feed side.
The observed dilation of polycarbonate due to the presence of carbon dioxide is almost 8 % by volume measured with respect to the dry polymer and at a pressure of 60 bar. This degree of swelling even exceeds the swelling of polyacrylonitrile in contact with the liquid feed mixture employed in the pervaporation experiments of chapter 2. The high degree of swelling enhanced the relaxation of polycarbonate, an effect that would not have been noticed on reasonable experimental time-scales without the conditioning of the membrane at high CO_2 pressure. One should keep in mind that the duration of the experiment described in reference [17] is more than 5 days, that the experiments in chapter 2 show no steady-state within a few hours or weeks depending on the experiment, and that the detrimental effect of excessive swelling on pervaporation of methanol - MTBE mixtures did not give steady-state permeation within 80 hours [14]!

Although the presence of residual solvent in solvent-cast membranes can have a (significant) influence on the transient permeation through the membranes, it can not fully explain the initially high fluxes observed in pervaporation. This is concluded from figures 9 and 10 in chapter 2 and from the work of Koops [15] who made sure that residual solvent was removed from the membrane by exposing the applied membranes, prepared from polyvinylchloride, polyacrylonitrile or polysulfone, to a heat-treatment near the glass transition temperature of the polymer for one week in a vacuum-oven.
Glassy membranes prepared by drying a polymer solution on a non-permeable support like a glass-plate may have an asymmetric structure because evaporation occurs from one interface only. It is anticipated that near the glass plate exposed side of the membrane the solvent volume fraction is larger than near the nitrogen or air exposed side of the membrane. When the glass plate side is directed towards the permeate diffusion is enhanced and separation factors are low compared to the situation in which the nitrogen exposed side is facing the permeate. The differences are only marginal (see chapter 2, table 1).
In the experiments shown in chapter 2 the solvent is probably extracted from one side of the membrane, by detaching the membrane from the supporting glass plate with the use of water, which has a high affinity towards the solvent dimethylformamide. The effect is so large that reasonable separation factors may be obtained when that side of the membrane from which the residual solvent has been extracted, is facing the permeate (also chapter 2, table 1, first part).
The presence of residual solvent may have a positive effect too. Spitzen [13] prepared some solvent-cast membranes from a polyacrylonitrile - dimethylformamide solution,

while retarding the drying process by enforcing a partial vapour pressure of dimethylformamide in the nitrogen flow that should convey the evaporating solvent. These membranes show improved performance and this is probably due to the presence of dimethylformamide in the membrane at the moment pervaporation starts. The sorption of water and ethanol from the feed mixture is (partially) coupled with the replacement of the volume previously occupied by dimethylformamide. The swelling of the membrane is not so large compared with swelling of an initially dry membrane and higher separation factors are found. This does explain then the high separation factors of thick membranes because swelling and the resulting tensile stress is diminished because initially the thick membranes are certainly not dry.

The non-equilibrium nature of the glassy state and the presence of traces of solvent is of importance when the permeation near the permeate side of the membrane in pervaporation and in gas separation applying high feed pressures of gases like CO_2, is considered. The effect of the non-equilibrium nature of the glassy state is seen best applying thin, solvent-cast membranes when performing gas separation with inert gases, like in ref. [18]. Sorption of these gases in glassy polymers is small and therefore the accompanying tensile stress and its effect on permeabilities are small. Initially too high permeabilities were found for helium, oxygen and nitrogen in polyimide and polycarbonate membranes with estimated thicknesses of 0.33 μm and 0.47 μm respectively [18]. No residual solvent is left in these membranes and initially high fluxes are attributed to the excess free volume in the polymer membranes due to fast evaporation of solvent during the preparation of thin membranes of a polymer solution.
It is noteworthy to realize that in gas separation with inert gases initially too high permeabilities can be found due to the presence of excess free volume in the polymer matrix whereas in gas separation with condensable gases initially too low permeabilities can be found due to swelling.

3.4. Symbols

c	surface concentration
f	fractional free volume of pure polymer
n	number of moles
p	pressure
t	time
v	molar volume
z	directional coordinate
β	rate constant
β′	parameter relating fractional free volume to volume fraction of solvent
μ	molar chemical potential
σ	tensile stress
ϕ	solvent volume fraction
χ	interaction parameter
Δ	(stepwise) variation in the variable following this symbol
B	constant in Doolittle equation
D	diffusion coefficient
E	tensile or Young's (relaxation) modulus

G	Gibbs free energy
J	solvent volume flux
L	phenomenological coefficient or length
R	universal gas constant
S	entropy
T	temperature
V	volume
Π	osmotic pressure

3.5. References

1. P.F. Mijnlieff, W.J.M. Jaspers, Thermodynamics of swelling of polymer-network gels. Analysis of excluded volume effects in polymer solutions and polymer networks, Journal of Polymer Science: Part A-2, 7 (1969) 357-375.
2. T.L. Hill, An introduction to statistical thermodynamics, Addison-Wesley Publishing Company 1960, Ch. XXI.
3. P.J. Flory, Principles of polymer chemistry, Cornell University Press 1953, Ch. XII.
4. J.H. Hildebrand, R.L. Scott, Solubility of nonelectrolytes, Dover Publications 1964, Ch. XX.
5. J.C. Wu, N.A. Peppas, Modeling of penetrant diffusion in glassy polymers with an integral sorption Deborah number, Journal of Polymer Science: Part B: Polymer Physics 31 (1993) 1503-1518.
6. J. Crank, The mathematics of diffusion, Oxford Science Publishers 1975, Ch. X (§2).
7. J.D. Ferry, Viscoelastic properties of polymers, John Wiley & Sons 1980, Ch. XI, Ch. XVII.
8. H. Fujita, Diffusion in polymer-diluent systems, Fortschr. Hochpolym.-Forsch. 3 (1961) 1-47.
9. J.C. Wu, N.A. Peppas, Numerical simulation of anomalous penetrant diffusion in polymers, Journal of Applied Polymer Science 49 (1993) 1845-1856.
10. M.H.V. Mulder, T. Franken, C.A. Smolders, Preferential sorption versus preferential permeability in pervaporation, Journal of Membrane Science 22 (1985) 155-173.
11. A.S. Kenyon, McC. J. Rayford, Mechanical relaxation processes in polyacrylonitrile polymers and copolymers, Journal of Applied Polymer Science 23 (1975) 717-725.
12. M.H.V. Mulder, F. Kruitz, C.A. Smolders, Separation of isomeric xylenes by pervaporation through cellulose ester membranes, Journal of Membrane Science 11 (1982) 349-363.
13. J.W.F. Spitzen, G.H. Koops, M.H.V. Mulder, C.A. Smolder, The influence of membrane thickness on pervaporation performance, Proceedings of third international conference on pervaporation processes in the chemical industry, ed. by R. Bakish, Nancy, France, 1988.
14. H.-C. Park, Separation of alcohols from organic liquid mixtures by pervaporation, PhD-thesis, University of Twente, Enschede, the Netherlands, 1993.
15. G.H. Koops, J.A.M. Nolten, M.H.V. Mulder, C.A. Smolders, Selectivity as a function of membrane thickness: gas separation and pervaporation, Journal of Applied Polymer Science 53 (1994) 1639-1651.
16. F.W. Altena, C.A. Smolders, Calculation of liquid-liquid phase separation in a ternary system of polymer in a mixture of a solvent and a nonsolvent, Macromolecules 15 (1982) 1491-1497.
17. S.M. Jordan, W.J. Koros, G.K. Fleming, The effects CO_2 exposure on pure and mixed gas permeation behavior: comparison of glassy polycarbonate and silicone rubber, Journal of Membrane Science 30 (1987) 191-212.
18. M.E. Rezac, P.H. Pfromm, L.M. Costello, W.J. Koros, Aging of thin polyimide-ceramic and polycarbonate-ceramic composite membranes, Industrial & Engineering Chemistry Research 32 (1993) 1921-1926.

Chapter 4

Numerical Simulation of Evaporation from a Solvent-Cast Polymer Film

4.1. Introduction

In the preparation of polymer films by the solvent-cast technique, long drying times are encountered for the removal of solvent when the dry film consists of a glassy polymer. The thickness of the cast film and decreasing diffusion coefficients directly influence the drying times. In the glassy state the solvent diffusion coefficient can vary over several decades and can become so low that it is almost impossible to remove traces of residual solvent from relatively thick, glassy films.
If the transport equations and appropriate boundary conditions are known, and experimental data are available on the paramaters involved in those equations, one may be tempted to find an analytical solution to the drying process mathematically. With increasing complexity of the transport equations and boundary conditions, however, this route may become unattractive. It may even become impossible to solve the set of equations analytically. Numerical simulation is then a more appropriate technique for solving the set of equations.
Numerous equations have been developed for a variety of drying problems. In spin coating deposition of thin solid films, the knowledge of the drying process is needed for controlling the dry film thickness [1]. The reduction of solvent concentration to a desired level determines the size of the drying oven in the production of photographic films, adhesives, etc. [2]. The prediction of evaporation rates of solvents from paint and resin films and the prediction of solvent composition during drying is of importance to paint formulations [3-4].
The pore size and skin thickness of asymmetric membranes prepared by phase inversion, are determined by the coagulation of a polymer solution into a non-solvent bath [5] and an eventual evaporation step prior to coagulation. The final morphology of the membrane is of prime importance for its applicability in a separation process. In order to relate the obtained morphology to the evaporation step, several studies have been directed to the initial phase of drying of a binary or ternary polymer solution [6-11].
All previous references have in common that their interest is mainly directed to the initial phase of drying. There are two phases in drying a polymer solution. In the first phase evaporation is controlled by the kinetics at the polymer solution / gas atmosphere interface. In the second phase solvent is transported by diffusion towards the interface where evaporation occurs [12]. Surface cooling can be significant in the first phase, due to heat loss during evaporation [13-14].
A complicating factor in drying is the non-equilibrium nature of the glassy state. After

the vitrification of the polymer solution, one might expect that further volume relaxation due to continuous evaporation of solvent, is hindered because the glassy polymer matrix cannot adapt fast enough to changes in solvent concentration. This is expected to occur especially in thin films.
In this chapter the drying of a polymer solution will be modelled and numerically simulated. Interest is directed to the second phase of drying, where internal diffusion is the rate determining step for the drying process. In paragraph 4.2. aspects of transport equations and boundary conditions will be treated, thereby defining a model that assumes local equilibrium throughout the drying process. In the next paragraph the numerical implementation of the adopted differential equations, is described in detail. Numerical results obtained are given in paragraph 4.4. Attention is paid to the time-scales involved in the drying process. The effect of the relaxation time of the polymer film and its influence on the drying process, will be discussed in paragraph 4.5. In the following paragraph results are discussed with respect to the non-equilibrium nature of the glassy state, and its influence on the gas permeabilities of thin glassy membranes prepared from a polymer solution.

4.2. Transport equations and boundary conditions

In this paragraph various aspects of the transport equations and boundary conditions used in literature will be described. It is not meant to be an elaborate review; it will only focus the attention to some important aspects, relevant for the drying of a polymer solution. First a transport equation is needed to describe the motion of solvent towards the free surface where it evaporates. Because drying is a transient diffusion process, the transport equation should describe the shrinkage of the polymer as well. The solvent and polymer transport is determined by the diffusion coefficients and the driving forces for the diffusion process. There are two boundary conditions to the transport equations. The first boundary condition is related to the free surface where solvent evaporates into a gas atmosphere. It is assumed that no accumulation of solvent can occur at the interface. The second boundary condition is related to the interface between the solid support and the polymer solution. It is postulated that no solvent transport can occur through this interface.

4.2.1. The transport equation

All transport equations incorporate a solvent diffusion coefficient. The equation depends on the frame of reference and the determination of composition [15-16]. In this work the transport equation, with respect to total volume and based on solvent volume fraction, is:

$$\frac{\partial \phi}{\partial t} = \frac{\partial}{\partial z}\left(D(\phi)\frac{\partial \phi}{\partial z}\right). \qquad (1)$$

Here is D the diffusion coefficient, ϕ the solvent volume fraction, t the time and z the directional coordinate perpendicular to the plane of the film.
In this frame of reference the solvent diffusion coefficient D is equal to the polymer diffusion coefficient, and therefore also called the mutual diffusion coefficient. The diffusion coefficient is in general a function of the solvent volume fraction. With the volume-average velocity as frame of reference, it is implicitly assumed that the partial specific volumina are constant. Furthermore, the use of eq. (1) in the glassy state is allowed only if the system of polymer and solvent is locally always in equilibrium.
The basis of numerical simulations is eq. (1), which will be evaluated iteratively at various depths in an imaginary polymer film. The approximation that in a thin film concentration gradients in case of mass flow, or temperature gradients in case of heat flow, are no function of the place coordinate z [14], is most probably wrong and is therefore rejected.
In the glassy state diffusion coefficients will strongly depend on the solvent volume fraction in case of polymer-solvent, or polymer-diluent systems. In case of negligible interaction between polymer and penetrant, which is usually not the case in a polymer-solvent system, hardly any dependence of diffusion coefficient on volume fraction is noticed [17]. Generally the exponential dependence of the mutual diffusion coefficient on solvent volume fraction is adopted [17-19].

$$D(\phi) = D(0)\exp(\gamma\phi). \qquad (2)$$

D(0) is the diffusion coefficient for zero solvent volume fraction, and the parameter γ is a so-called plasticization constant.
Fujita [17] derived a slightly different equation that can account for the convex shape of the logarithm of the diffusion coefficient versus volume fraction, near the glass transition.

$$D(\phi) = D(0)\exp\left(\frac{\phi}{c_1+c_2\phi}\right). \qquad (3)$$

with c_1 and c_2 two constants. Eq. (3) is based on the Doolittle equation.
The larger the difference between D(0) and the diffusion coefficient at the glass transition, the more the equation derived by Fujita approaches eq. (2). For relatively large solvent molecules, the diffusion coefficient can even vary over six orders of magnitude within the glassy state [18-19]. Above the glass transition, there is no large dependence of diffusion on solvent concentration.
Eq. (2) is used here by the introduction of two different plasticization constants for volume fractions below the glass transition of the binary system and above the glass transition respectively.

4.2.2. The polymer film / gas atmosphere interface

At the surface of the polymer solution or film, solvent evaporates into the surrounding atmosphere. At the interface no accumulation of solvent can occur. The

solvent flux through the polymer film towards the interface must be equal to the solvent vapour flux leaving the interface. The solvent volume flux J towards the interface is given by Fick's first law, which is also the basis of the already given transport equation.

$$J_{\text{to interface}}(t) = \left[-D(\phi)\frac{\partial \phi}{\partial z}\right]_{z=L(t)}. \qquad (4)$$

J is here the volume flux of solvent to the interface and L the film thickness. The interface is situated at z=L, with L the film thickness that is varying in time. The positive direction of the z-coordinate is from the support side of the film towards the gas atmosphere.
The flux from the interface into the atmosphere is determined by the vapour diffusion coefficient and by the convective flow of gases (air, nitrogen) along the surface of the solution. The total vapour mass transfer near the interface is described by a mass transfer coefficient k. Expressions for vapour mass transfer coefficients are described in literature [3,10]. The evaporation step is not considered to be the rate-limiting step in drying. Therefore the mass transfer coefficient is assumed to be constant. In general the mass transfer coefficients under conditions considered in this work range from 10^{-2} to 1 ms^{-1} [20].

$$J_{\text{from interface}}(t) = k\left[\phi\right]_{z=L(t)}. \qquad (5)$$

J is here the volume flux of solvent from the interface and k the vapour mass transfer coefficient. The flux from the interface is proportional to the solvent volume fraction at the interface. During drying the solvent volume fraction at the interface will decrease and therefore the flux from the interface will decrease in time also. The use of a constant evaporation rate [1] can not be applied, because attention is focussed to the final stage of drying where evaporation is limited by solvent diffusion towards the free surface. An immediately zero volume fraction at this interface, at the moment drying starts, presupposes an instantaneous glass transition at this interface which is inconsistent with experimental observations [8]. By equating the flux to the interface in eq. (4) with the flux from the interface in eq. (5), the problem of an immediately zero volume fraction at this interface is avoided elegantly.

4.2.3. The polymer film / support interface

At the interface between the support and the polymer film, the following boundary condition must be met:

$$\left[\frac{\partial \phi}{\partial z}\right]_{z=0} = 0. \qquad (6)$$

Some authors [8,13], however, use the condition that the solvent volume fraction at

the interface does not change, which is the same as stating that evaporation occurs from a semi-infinite polymer solution. Their interest is directed only to the first moments of evaporation and therefore formulating that boundary condition should not be necessary at all.

4.3. Description of the numerical implementation of the model

In this paragraph the numerical equivalences of the transport equation and the two boundary conditions will be given. The solvent volume fraction is a continuous function of time and place. The differential equations (1), (4) and (6) describe the diffusion processes at any time and anywhere in a drying solvent-cast film. These equations can not directly be implemented on a computer. They have to be transformed into finite-difference equations in a proper way. In case of a constant diffusion coefficient, this is done in a straightforward manner. However, the exponential dependence of diffusion coefficient on solvent volume fraction is adopted both for the vitrified and the non-vitrified state as indicated in figure 1. When the diffusion coefficients at zero solvent volume fraction, for the pure solvent, at the glass transition, as well as the solvent volume fraction at the glass transition are known, then the exact dependence of diffusion coefficient on composition is known. The computer program for the numerical simulation needs furthermore a vapour mass transfer coefficient, an initial casting thickness and an initial solvent volume fraction, as external input parameters.

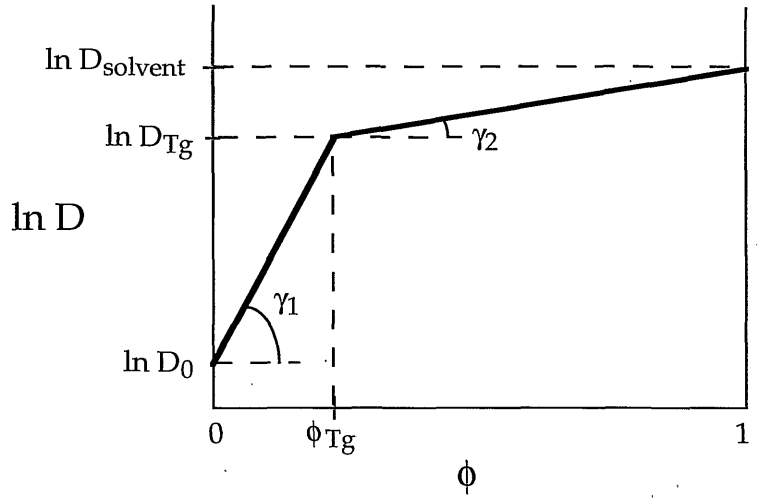

figure 1: The logarithm of the mutual diffusion coefficient D plotted against the solvent volume fraction ϕ. D_0, D_{Tg} and $D_{solvent}$ are the diffusion coefficient at zero solvent volume fraction, at the glass transition and for the pure solvent respectively. The plasticization constants γ_1 and γ_2 apply to the vitrified and non-vitrified state respectively.

Unlike the situation with a constant diffusion coefficient it is not so obvious how to derive the right finite-difference equations in case of a concentration dependent diffusion coefficient, except for a special case. Hansen [19] used the same concentration dependent diffusion coefficient as depicted in figure 1. Because of the exponential relation between the diffusion coefficient and solvent volume fraction the transport equation can be changed, by a transformation of variables, into:

$$\frac{\partial D_m}{\partial T} = D_m \frac{\partial^2 D_m}{\partial Z^2}. \qquad (7)$$

where D_m is a modified diffusion coefficient equal to $\exp(\gamma\phi\phi_0^{-1})$, T is a reduced or dimensionless time equal to $D_0 t L^{-2}$, and Z is a reduced or dimensionless distance equal to zL^{-1}. In these reduced variables ϕ_0 is the initial solvent volume fraction and L the total film thickness. Eq. (7) has almost the same appearance as the diffusion equation, Fick's second law, and is solved numerically in almost the same way. Instead of the solvent volume fraction, the modified diffusion coefficient D_m is determined iteratively as a function of dimensionless time T and dimensionless distance Z. Numerical simulation of only eq. (7) would give a solution to the drying process, for a given concentration dependent diffusion coefficient, irrespective of the initial thickness of the cast polymer solution. However, Hansen [19] also had to introduce a dimensionless variable to account for the boundary condition at the polymer film / gas atmosphere interface. That dimensionless variable is equal to kLD_0^{-1}, the product of film thickness and vapour mass transfer coefficient, divided by the diffusion coefficient at zero solvent volume fraction. The numerical simulation is thereby implicitly a function of film thickness. When the influence of the thickness of the cast polymer solution is investigated, as it is the case in this chapter, the drying process has to be simulated for every initial film thickness, even though the transport equation (7) is based on dimensionless time and distance.

Here the guidelines will be given how to develop the finite-difference equations when the exact form of the concentration dependent diffusion coefficient is known. It is required that the solvent volume fraction ϕ can be solved analytically as a function of the place coordinate z in case of a steady-state diffusion process. Then the following

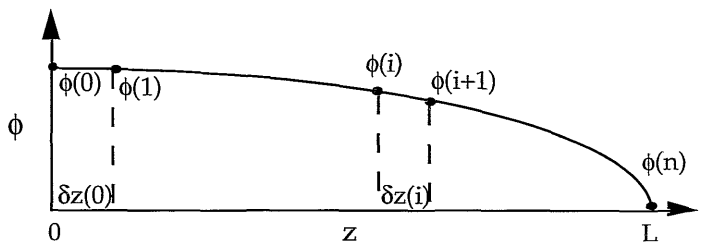

figure 2: Schematic diagram showing the solvent volume fraction at various distances z in the polymer films as n+1 discrete values. The discrete values are separated by n layers with variable thicknesses δz. L is the total film thickness.

relation applies:

$$\frac{\partial}{\partial z}(D(\phi)\frac{\partial \phi}{\partial z}) = 0. \qquad (8)$$

The total film thickness is divided in a number of parallel layers, each of which has a variable thickness δz and a solvent volume fraction that is an average of the volume fractions at both sides of the layer. The schematically drawn curve of solvent content versus distance in the film is shown in figure 2.
The solvent volume fraction ϕ, monitored by the index i, is given by n+1 discrete values. With the index i the thickness $\delta z(i)$ of a specific layer is monitored too.

4.3.1. Constant diffusion coefficient

In the numerical simulations the local volume fluxes are calculated. With a constant diffusion coefficient D the flux J in layer i considered positive in the direction of place-coordinate z, is given by:

$$J(i) = D\frac{\phi(i) - \phi(i+1)}{\delta z(i)}. \qquad (9)$$

During drying the solvent-cast film will shrink. To recalculate during drying all the layer thicknesses δz, it is necessary to know the average volume fractions. With a constant diffusion coefficient D, the average volume fraction is given by:

$$\phi_{av}(i) = \frac{1}{2}(\phi(i) + \phi(i+1)), \qquad (10)$$

where $\phi_{av}(i)$ is the average solvent volume fraction in layer i.
From eqs. (9) and (10) it is clear that in case of a constant diffusion coefficient a steady-state flux through the layer is assumed. Consequently a straight curve represents the solvent volume fraction in this layer.

4.3.2. Concentration dependent diffusion coefficient

In general, with a concentration dependent diffusion coefficient, there will be a gradient of the diffusion coefficient within one layer. It is not so obvious which average diffusion coefficient should be used. But one can of course apply the approach of a steady-state flux within one layer, like in the case of a constant diffusion coefficient. The problem and its solution are drawn schematically in figure 3.

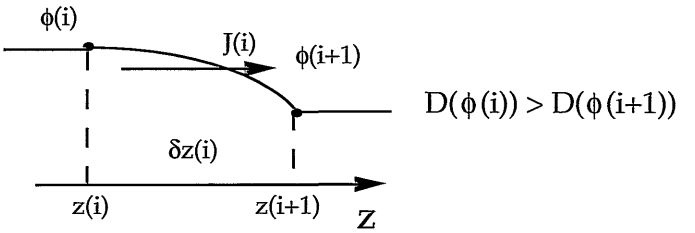

figure 3: The curve of solvent volume fraction ϕ versus place coordinate z. This curve is used to calculate the local flux in case a concentration dependent diffusion coefficient is used.

With the exponential increase of diffusion coefficient with solvent volume fraction, the local curve of solvent volume fraction versus distance under steady-state conditions can be determined by twice integrating eq. (8).

$$\phi(z) = \phi(i) + \frac{1}{\gamma}\ln\left[\frac{z-z(i)}{z(i)-z(i+1)} + \frac{z(i)-z}{z(i)-z(i+1)}\exp(\gamma(\phi(i+1)-\phi(i))\right], \gamma>0. \qquad (11)$$

Here γ is the plasticization constant which has a value larger than zero and which is linked to the volume fractions $\phi(i)$ and $\phi(i+1)$ at both sides of the layer drawn in figure 3 and the corresponding diffusion coefficients, by the following equation.

$$\gamma = \frac{\ln\left(\frac{D(\phi(i))}{D(\phi(i+1))}\right)}{\phi(i) - \phi(i+1)}. \qquad (12)$$

The steady-state volume flux in layer i is determined by combining Fick's first law and eq. (11).

$$J(i) = \left[-D(\phi)\frac{\partial\phi}{\partial z}\right]_{\text{in layer i}} = \frac{D(\phi(i)) - D(\phi(i+1))}{\gamma\,\delta z(i)}, \gamma>0. \qquad (13)$$

The average volume fraction ϕ_{av} of layer i, corresponding to the steady-state flux, is calculated by integration of eq. (11) in layer i, and dividing the obtained value by the thickness $\delta z(i)$ of layer i.

$$\phi_{av}(i) = \frac{1}{\delta z(i)}\int_{z_i}^{z_{i+1}} \phi(z)dz = \frac{\phi(i)D(\phi(i)) - \phi(i+1)D(\phi(i+1))}{D(\phi(i)) - D(\phi(i+1))} - \frac{1}{\gamma}, \gamma>0. \qquad (14)$$

The plasticization constant in eqs. (11), (13) and (14) cannot be zero. If the plasticization constant approaches zero then eqs. (13) and (14) should approach eqs. (9) and (10) respectively. This can be shown by making a Taylor series expansion of the logarithm appearing in eq. (12).

$$\gamma = \frac{\ln\left(\frac{D(\phi(i))}{D(\phi(i+1))}\right)}{\phi(i) - \phi(i+1)} = \frac{1}{\phi(i) - \phi(i+1)}\left\{\left(\frac{D(\phi(i))}{D(\phi(i+1))} - 1\right) + O\left(\left(\frac{D(\phi(i))}{D(\phi(i+1))} - 1\right)^2\right)\right\}. \quad (15a)$$

When the diffusion coefficients at both sides of layer i are almost similar, i.e. the plasticization constant approaches zero, the terms of second order or higher in eq. (15a), denoted by $O(..^2)$, can safely be neglected. Applying then eq. (15b) to eqs. (13) and (14) will show their similarity with eqs. (9) and (10) respectively.

$$\gamma \to 0: \quad \gamma \approx \frac{1}{D(\phi(i+1))} \cdot \frac{D(\phi(i)) - D(\phi(i+1))}{\phi(i) - \phi(i+1)}. \quad (15b)$$

Eqs. (13) and (14) apply to the vitrified and the non-vitrified state respectively. However, during drying locally the glass transition will be traversed whenever the following condition holds:

$$\phi(i) > \phi_{Tg} > \phi(i+1). \quad (16)$$

The local flux and average solvent volume fraction of layer i, are calculated in a similar way as illustrated in eqs. (13) and (14). They are respectively:

$$J(i) = \frac{D(\phi(i)) - D_{Tg}}{\gamma_2\, \delta z(i)} + \frac{D_{Tg} - D(\phi(i+1))}{\gamma_1\, \delta z(i)}, \ \gamma_1 \text{and } \gamma_2 > 0, \quad (17)$$

and

$$\phi_{av}(i) = \frac{1}{\gamma_1(D(\phi(i)) - D_{Tg}) + \gamma_2(D_{Tg} - D(\phi(i+1)))}$$

$$\left\{\gamma_1(\phi(i)D(\phi(i)) - \phi_{Tg}D_{Tg}) - \frac{\gamma_1}{\gamma_2}(D(\phi(i)) - D_{Tg})\right.$$
$$\left. + \gamma_2(\phi_{Tg}D_{Tg} - \phi(i+1)D(\phi(i+1))) - \frac{\gamma_2}{\gamma_1}(D_{Tg} - D(\phi(i+1)))\right\}, \ \gamma_1 \text{and } \gamma_2 > 0. \quad (18)$$

In eqs. (17) and (18) the plasticization constants γ_1 and γ_2 apply to the vitrified and non-vitrified state respectively. D_{Tg} is the diffusion coefficient at the glass transition and ϕ_{Tg} the corresponding solvent volume fraction. When γ_1 is equal to γ_2, then eqs. (17) and (18) become similar to eqs. (13) and (14) respectively.

4.3.3. Iteration of the transport equation and boundary conditions

Now that the finite-difference equations for the fluxes have been derived, the finite-difference form of the transport equation (1) can be given. The local solvent volume

fraction ϕ will change in time because of a difference between the flux to and the flux from its close surroundings. A change in local volume fraction $\phi(i)$ in a discrete time δt is of course realized within those surroundings, the average of the adjacent layer thicknesses $\delta z(i-1)$ and $\delta z(i)$.

$$\phi(i,t+\delta t) = \phi(i,t) + \delta t \frac{J(i-1,t)-J(i,t)}{\frac{1}{2}(\delta z(i-1,t)+\delta z(i,t))}, \qquad i \in [1..n-1]. \tag{19}$$

Eq. (19) is valid for all i in the range of 1 to n-1. The fluxes and layer thicknesses in eq. (19) are the ones at time is t. It implies that the Euler method is used to obtain the finite-difference form of eq. (1).
Because the fluxes are not specified explicitly, eq. (19) may be applied in case of a constant as well as a concentration dependent diffusion coefficient. Introduction of eq. (9) into eq. (19) gives the finite-difference form of the diffusion equation or Fick's second law.
Because of changes in solvent volume fraction within a discrete time-lag δt, according to eq. (19), the layer thicknesses δz must change as well. Both the polymer and the solvent contribute to the layer thickness. The contribution of the polymer is constant, and can be related to the initial solvent volume fraction and the initial layer thickness.

$$\delta z(i,t) = \delta z_p(i) + \delta z_s(i,t) = (1-\phi_{av}(i,t=0))\delta z(i,t=0) + \delta z_s(i,t). \tag{20}$$

Time t=0 indicates that there the initial conditions are valid, and the substripts p and s denote the polymer and solvent respectively.
The relation between the layer thickness and the average solvent volume fraction in that layer is given by eq. (21).

$$\delta z(i,t) = \frac{(1-\phi_{av}(i,t=0))\delta z(i,t=0)}{(1-\phi_{av}(i,t))}, \quad i \in [0..n-1]. \tag{21}$$

A diffusion process can now numerically be solved by applying in alternation eqs. (19) and (21), with index i varying from 1 to n-1 and 0 to n-1 respectively. Performing an iteration with eq. (19) is allowed, subject to the condition that an appropriate iteration time δt is found. During one iteration step it is never possible that the volume fraction with index i gets smaller than the volume fraction with index i+1 (see figure 2). An even more strict condition is:

$$\phi(i,t+\delta t) > \phi(i+1,t). \tag{22}$$

The iteration time δt can be found by evaluating the time that is needed for $\phi(i,t+\delta t)$ to decrease to a value of $\phi(i+1,t)$, using eq. (19). This is done for index i ranging from 1 to n-1. The minimum of these n-1 evaluated times is the maximum allowable iteration time. This value, divided by 10, is taken as the iteration time, and is recalculated every iteration cycle.

The boundary conditions have to be applied at every iteration cycle. At the "air" exposed side the boundary condition is met by the following finite-difference equation, combining eqs. (4), (5) and (13).

$$\phi(n,t+\delta t) = \frac{J(n-1,t)}{k}, \qquad (23)$$

where k is the vapour mass transfer coefficient.
The boundary condition at the supported side of the film, eq. (6), is even more simple. After evaluation of eq. (19), one just equates $\phi(0)$ and $\phi(1)$.

$$\phi(0,t+\delta t) = \phi(1,t+\delta t). \qquad (24)$$

An important remark concerning the numerical scheme is left. The decrease in solvent content is realized in the total film thickness L. Evaluation of eq. (19) is the same as realizing this depletion in a film thickness L - 1/2 $\delta z(0)$ - 1/2 $\delta z(n-1)$. Therefore the outermost layers should have a relatively small thickness. This is done in the initialisation part of the computer program.

$$\delta z(0,t=0) = \delta z(n-1,t=0) = 0.01\frac{L(t=0)}{(2x0.01+n-2)}. \qquad (25a)$$

$$\delta z(i,t=0) = \frac{L(t=0)}{(2x0.01+n-2)}, \quad i \in [1..n-2]. \qquad (25b)$$

The two outermost layers have initially a thickness that is only 1 % of the thickness of the inner layers. The ratio of the initial, total film thickness, and the initial thickness of the film in which solvent depletion is realized, is equal to 1.001248 for n=10. For n=20 the ratio is already 1.000555, a deviation of less than 0.1 % from the ideal case.
The total film thickness during the simulated drying process, is found by summation of all layer thicknesses.

$$L(t) = \sum_{i=0}^{n-1} \delta z(i,t). \qquad (26)$$

It will decrease from the initial film thickness L(t=0) to a final value of $(1-\phi_{av}(t=0))\cdot L(t=0)$.

The Euler method has been applied to obtain the finite-difference form of eq. (1) instead of a Runge-Kutta method. The Euler method is based on a local Taylor's expansion of $\phi(t)$, using only the first derivative $\partial\phi/\partial t(t)$ to get an estimate of $\phi(t+\delta t)$. Therefore its local truncation error is of second order, or $O(\delta t^2)$, which means that terms of second order or higher are neglected. The first-order Runge-Kutta method uses an average of the first derivates $\partial\phi/\partial t$ (t) and $\partial\phi/\partial t$ (t+δt). In this way the first-order

Runge-Kutta method has a local truncation error of third order, or $O(\delta t^3)$, which is of course better than the Euler method [21]. The accuracy of the Euler method, applied in eq. (19), is checked by reducing the iteration time. In eq. (22) a criterion is mentioned by which a maximum iteration time can be found. Usually the maximum allowable iteration time is divided by 10 to obtain the iteration time in the numerical simulations, but in checking the accuracy of the method it is divided by 100. No influence on the simulated drying process is noticed. The same applies for a variation in the number of layers.

In this paragraph a procedure has been developed in which a transport equation with a concentration dependent diffusion coefficient, is solved numerically in exactly the same way as one is used to solve the diffusion equation with a constant diffusion coefficient. The only requirement is that it should be possible to solve analytically the transport equation under steady-state conditions. Instead of the applied Euler method, one can use a Runge-Kutta method, without changing the validity of the developed procedure.

4.4. Numerical simulations

The numerical simulations are performed using the equations derived in the foregoing paragraph. Hansen [19] simulated the drying process, using eq. (7). Results obtained here are slightly different from his findings when the first phase of drying is considered. Here attention is directed to the time-scales involved in the drying process. The experimental data of Hansen [18-19] are taken as starting-point, and they describe the diffusion coefficients, at 25 °C, of methanol, ethylene glycol monomethyl ether, chlorobenzene and cyclohexanone in polyvinylacetate. At low volume fractions of the solvent, the polymer is in the glassy state. The parameters, as presented in table 1, may seem arbitrary, but represent realistic values. Calculations are performed for two cases. Case A represents the system polyvinylacetate / chlorobenzene, whereas case B resembles more or less the system polyvinylacetate / ethylene glycol monomethyl ether.
The diffusion coefficient at zero solvent volume fraction is found by extrapolating the logarithm of measured diffusion coefficients to zero solvent volume fraction [18-19].
A discussion of the glass transition is postponed to paragraph 4.5. The diffusion coefficients reported in table 1 are assumed to be representative for a polymer/solvent system in equilibrium at every solvent volume fraction.
The vapour mass transfer coefficient in table 1 is large but a lower value has no influence on the simulated drying process. This has been verified in a simulation with a vapour mass transfer coefficient of 10^{-2} ms^{-1}, other parameters are taken from case B and the initial casting thickness is 50 μm. In the specific numerical simulation the drying proceeds very fast but the drying curves are not different from applying a vapour mass transfer coefficient of 1 ms^{-1}. This is already an indication that drying is controlled by diffusion of solvent towards the air exposed side of the film.

table 1: Parameter used in the numerical simulation of the drying process resembling the system polyvinylacetate and two different solvents.

	case A	case B
D_0	10^{-18} m^2s^{-1}	10^{-15} m^2s^{-1}
D_{Tg}	10^{-12} m^2s^{-1}	10^{-12} m^2s^{-1}
$D_{solvent}$	10^{-9} m^2s^{-1}	10^{-9} m^2s^{-1}
k	1 ms^{-1}	1 ms^{-1}
ϕ_{Tg}	0.2	0.1
$\phi_{initial}$	0.9	0.9
n	21	21

Figure 4 and 5 give the solvent volume fraction near the supported side of the film, as a function of time. The calculated data are given in a double-logarithmic plot, because of the self-decreasing rate of the drying process. In these figures the initial casting thickness has been varied from 50, 100, 200, 400 to 800 μm. The initial solvent volume fraction is 0.9. Therefore the final film thicknesses are 5, 10, 20, 40 and 80 μm respectively.

The parameters for case A and B are the same, except for the diffusion coefficient D_0, respectively 10^{-18} m^2s^{-1} and 10^{-15} m^2s^{-1}, and the solvent volume fraction at the glass transition ϕ_{Tg}, respectively 0.2 and 0.1. In the first stage of drying, one can hardly see any difference between figures 4 and 5. The variation of only the solvent volume fraction at the glass transition is of no importance.

The time needed to vitrify the entire film, i.e. when $\phi(z=0)$ equals ϕ_{Tg}, is proportional to the square of the initial film thickness, indicating that solvent evaporation is never a limiting factor. This is in contradiction with the results of Hansen [19], where the vapour mass transfer coefficients are considerably lower, about a factor 10^5. A plot of parameters like $\phi(z=0)$ and total film thickness L as a function of the parameter tL^{-2}, the

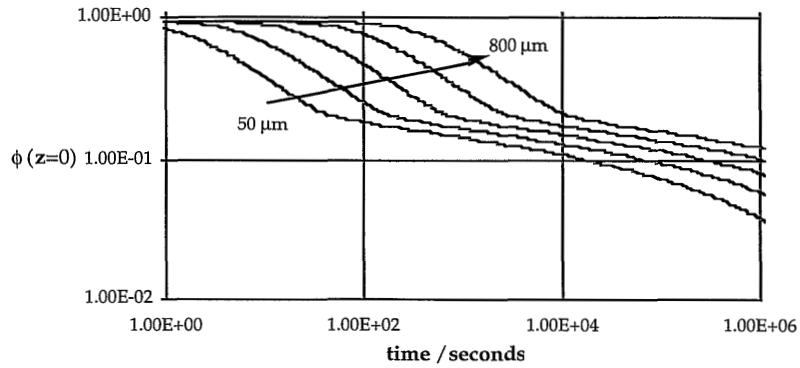

figure 4: The solvent volume fraction ϕ at the supported side of the film, as a function of time, during the numerically simulated drying process. The initial film thickness has been varied from 50 to 800 μm. Parameters used in the simulation are given in table 1, case A.

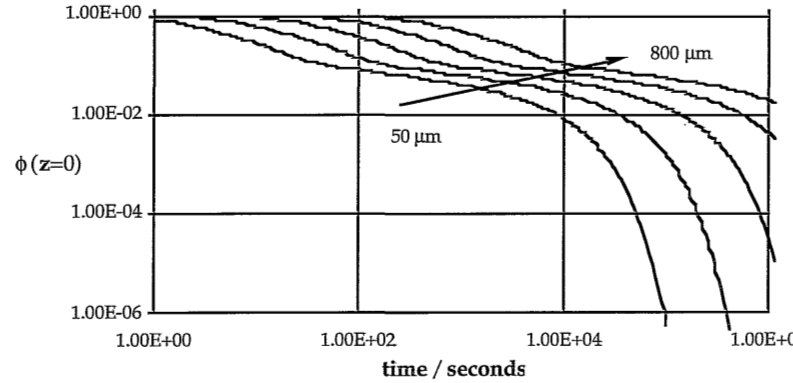

figure 5: The solvent volume fraction ϕ at the supported side of the film, as a function of time, during the numerically simulated drying process. The initial film thickness has been varied from 50 to 800 μm. Parameters used in the simulation are given in table 1, case B.

time divided by the squared film thickness, will yield master curves of the drying process. These master curves are specific for each set of parameters (case A or B).
The variation of D_0 strongly influences the drying process in the glassy state. In figure 4 the solvent volume fraction at the supported side of the film does not get below 0.01 within 10^6 seconds, almost 2 weeks. In figure 5 the value of D_0 is three orders of magnitude higher and except for the thickest film, all do reach a value below 0.01 in 10^6 seconds.

A characteristic time-scale of the diffusion processes involved in drying, depends on the amount of solvent in the film and the rate at which solvent leaves the film. The use of a mutual diffusion coefficient implies that there is no excess volume of mixing. Therefore the momentary film thickness minus the dry film thickness is a measure of the volume of solvent per unit of film area. The rate at which solvent leaves the film, i.e. the solvent volume flux, is given by the time derivative of the film thickness. It is a measure of solvent volume leaving the film per unit of time and per unit of film area. An estimate of the momentary maximum time-scale of the drying process is calculated by dividing the amount of residual solvent in the film by the flux out of the film.

$$\tau_{drying}(t) = \frac{L(t) - L(t=\infty)}{J_{out}(t)} = \frac{L(t) - L(t=\infty)}{-\left(\frac{\partial L(t)}{\partial t}\right)}, \qquad (27)$$

with τ an estimate of the characteristic time of drying and $L(t=\infty)$ the dry film thickness. In figures 6 and 7 these time-scales are evaluated and plotted as a function of the solvent volume fraction near the supported side of the film. The figures represent the drying processes depicted in figures 4 and 5 respectively.

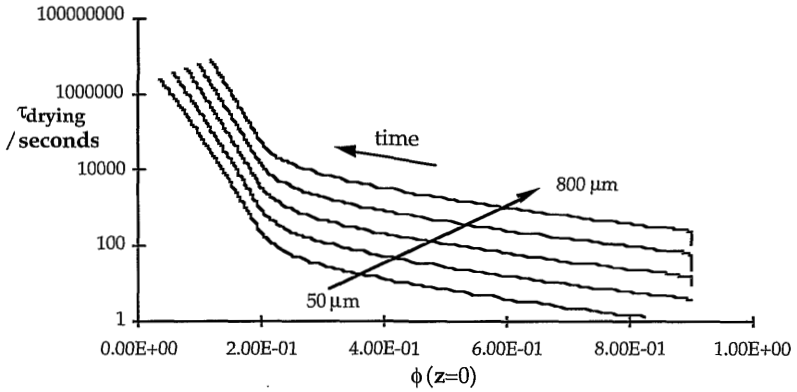

figure 6: The characteristic time τ of the drying process as a function of solvent volume fraction ϕ at the supported side of the film. The initial film thickness varies from 50 to 800 µm. Parameters used in the simulation are given in table 1, case A. The curves correspond with the data in figure 4.

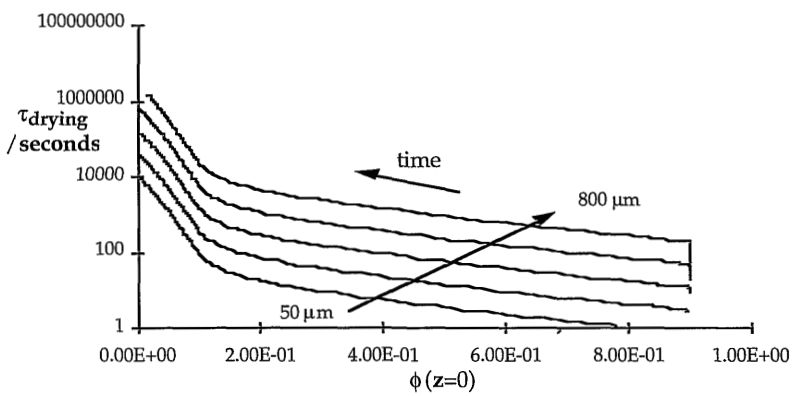

figure 7: The characteristic time τ of the drying process as a function of solvent volume fraction ϕ at the supported side of the film. The initial film thickness varies from 50 to 800 µm. Parameters used in the simulation are given in table 1, case B. The curves correspond with the data in figure 5.

The solvent volume fraction will decrease in time. Therefore, the characteristic time τ_{drying} will increase in time as shown in figures 6 and 7. A bend in the curve of the drying time plotted against $\phi(z=0)$ is seen near the solvent volume fraction at the glass transition. At lower volume fractions, the increase of the characteristic time of drying with decreasing solvent volume fraction is more steep than at volume fractions above ϕ_{Tg}. The characteristic time of drying is about proportional to the reciprocal diffusion coefficient corresponding to the volume fraction $\phi(z=0)$. Comparing the curves with different initial casting thicknesses, the characteristic time at any volume fraction $\phi(z=0)$ is proportional to the square of the film thickness.
When the solvent volume fraction near the supported side approaches zero the characteristic time of drying approaches a value that is smaller than the square of the dry film thickness divided by the diffusion coefficient at zero volume fraction of solvent.

The drying process has been simulated in this paragraph, with realistic data taken from literature. It is possible to get an estimate of the time-scales at which drying proceeds. Knowledge of these drying times is of importance. In the simulations it has been assumed that there is no excess volume of mixing. Furthermore it has been assumed that throughout the simulations the polymer/solvent film remains in its equilibrium state, also in the "vitrified" state. Therefore these calculated characteristic time-scales of the drying process should be compared with the time-scales of volume relaxation of the polymer matrix.

4.5. Time-scale of drying versus time-scale of volume relaxation

The importance of the time-scales involved in sorption and desorption of vapours and liquids in (glassy) polymers has been recognized by Vrentas *et al.* [22-24]. In order to perform accurate measurements of diffusion coefficients they stated that a characteristic time of polymer relaxation should be small compared to a characteristic time of diffusion. Therefore the concept of a Deborah number for diffusion, being the ratio of the two characteristic times, has been introduced. This concept can be applied to the drying of a film. The characteristic time of drying which replaces the characteristic time of diffusion because of the range of diffusion coefficients involved, has been identified already in the foregoing paragraph. The Deborah number for drying or transient diffusion equals:

$$(DEB)_{drying} = \frac{\tau_{material}(\phi)}{\tau_{drying}(\phi)}, \qquad (28)$$

with $(DEB)_{drying}$ the Deborah number for drying, $\tau_{material}$ the characteristic relaxation time of the material and τ_{drying} the characteristic time of drying. Both time-scales depend on the amount of solvent in the polymer matrix.
Thus far the adjective "characteristic" has been used, because one can not give an exact relaxation time of a material. In general the material is characterized by a spectrum of relaxation times. In case of sorption or desorption one can only give the order of magnitude of the time-scale involved in the diffusion process.
A $(DEB)_{drying}$ value (much) smaller than one implies that the material can react fast enough to changes in amount of solvent. The material remains in its equilibrium state. A $(DEB)_{drying}$ value (much) larger than one means that the relaxation of the material is not fast enough in order to remain in the equilibrium state.
There is a difference in the way the characteristic time of drying has been determined compared to literature. In general, given a film with known thickness, the characteristic time of diffusion is considered a material property, or better a film property.

$$\tau_{diffusion}(\phi) = \frac{L^2}{D(\phi)}. \qquad (29)$$

In drying a range of diffusion coefficients is involved and therefore the characteristic time of drying has been evaluated with eq. (27), and this value replaces the characteristic time of diffusion.

The characteristic relaxation time of the (diluted) polymer matrix can be evaluated for example from mechanical experiments. Although these experiments have not been performed here, one can estimate these relaxation times from literature data.
The characteristic times at various temperatures are related to each other by the WLF equation (Williams, Landel and Ferry) [25]:

$$\log a_T = \log \frac{\tau_{material}(T)}{\tau_{material}(T_0)} = - \frac{c_1^0 (T - T_0)}{c_2^0 + T - T_0}, \qquad (30)$$

with a_T the shift factor which is the ratio of the relaxation times at temperature T and the reference temperature T_0, and c_1^0 and c_2^0 two empiric constants.
This equation is based on the empiric Doolittle equation, that relates the viscosity of a low molecular liquid to the fractional free volume of the liquid. Eq. (30) is applicable to polymers as well, even in the glassy state, subject to the condition that the free volume varies linearly with temperature.
For polyvinylacetate (PVAc), c_1^0 = 8.86, c_2^0 = 101.6 (a constant with any unit of temperature), and T_0 = 349 K [25]. The characteristic time at 25 °C is needed, because that temperature corresponds to the diffusion coefficients used in the numerical simulation. From experimental data of Kovacs on the isothermal contraction of PVAc at different temperatures after a temperature quench from above the glass transition temperature [26] a characteristic time at 32.5 °C is found to be 0.02 h. Combination of the shift factors in eq. (29) at 25 °C and 32.5 °C will give the characteristic time at 25 °C, $\tau_{material}(T=25\ °C) = 1.4 \cdot 10^4$ s.

Another equation relates the characteristic time of a material with a certain solvent volume fraction to the characteristic time of the undiluted material [25]. It is also based on the Doolittle equation and on the linear increase of fractional free volume with increase of solvent volume fraction.

$$\log a_\phi = \log \frac{\tau_{material}(\phi)}{\tau_{material}(\phi=0)} = - \frac{B\beta'\phi}{2.303\, f\, (f + \beta'\phi)}, \qquad (31)$$

with a_ϕ the shift factor which is the ratio of the relaxation time at solvent volume fraction ϕ and the relaxation time of the undiluted polymer, f the fractional free volume of the pure polymer, B a constant in the Doolittle equation and β' relates the fractional free volume to the solvent volume fraction. Usually the value of B is set

equal to unity. The parameter β' tells to what extent the fractional free volume $f(\phi)$ of the polymer/solvent system is increased by an increase of the solvent volume fraction.

$$f(\phi) = f + \beta'\phi. \qquad (32)$$

Eq. (32) has been applied only to concentrated solutions, above the glass transition temperature of the polymer [25], although both eqs. (30) and (31) are based on the same free volume concept. Here eq. (31) will be applied to the 'glassy state' too. The time-scale corresponding to the glass transition is rather ambiguous.
Kovacs [26] measured the isothermal contraction of polymers after a quench of the temperature below its glass transition temperature. Kovacs showed that in a plot of the specific volume of the polymer versus temperature a clear point is seen at which the thermal expansion coefficient changes abruptly. This point is usually defined as the glass transition temperature. However, the glass transition temperature defined in this way depends on the elapsed time with respect to the time of the temperature quench at which the specific volume is plotted. The glass transition temperature decreases with increase of elapsed time [26]. One could also look at it in another way. If one decreases the temperature slowly enough the glass transition will not be traversed and the material will remain in its equilibrium state. It justifies then the use of eqs. (30) and (31), because the material is on the verge of the glassy state and can be considered a concentrated polymer solution in the 'transition zone'. The relaxation times depend in the transition zone on the segmental motions of the polymer, which in turn depend on the equilibrium amount of free volume. These cooperative segmental motions are responsible for volume relaxation in case of drying. The corresponding time-scale of volume relaxation should then of course be small compared to the time-scale of drying.

The value of the characteristic time at T = 25 °C in eq. (30) equals the characteristic time at $\phi = 0$ in eq. (31), i.e. $\tau_{material}(T=25\ °C, \phi=0) = 1.4 \cdot 10^4$ s. The fractional free volume f can be calculated, because eqs. (29) and (30) assume that the material is in its equilibrium state. The fractional free volume at 305 K is 0.028 and its thermal expansion coefficient is $5.9 \cdot 10^{-4}\ K^{-1}$ [25]. Therefore, at 25 °C the fractional free volume f is 0.024. The value of the parameter β' depends on the solvent and could be calculated, applying eq. (31), if the solvent volume fraction at the glass transition would be known together with the corresponding time-scale of the glass transition. As both parameters are not known an estimate of β' must be made. According to Ferry [25] β' varies from 0.1 to 0.3, which are reasonable values valid for the fractional free volume of a solvent.
In figure 8 the characteristic relaxation time of (diluted) polyvinylacetate is shown as a function of the solvent volume fraction for three different values of the parameter β'. In the same plot the characteristic time of drying is shown for case A and case B and an initial casting thickness of 50 μm. These plots are taken from figures 6 and 7 respectively.
With increasing solvent volume fraction the relaxation time goes down drastically, showing the capacity of the solvent to plasticize the polymer matrix. The relaxation

time decreases 4 orders of magnitude with a solvent volume fraction of only 0.07, 0.035 and 0.0225, corresponding to β' values of 0.1, 0.2 and 0.3, respectively.

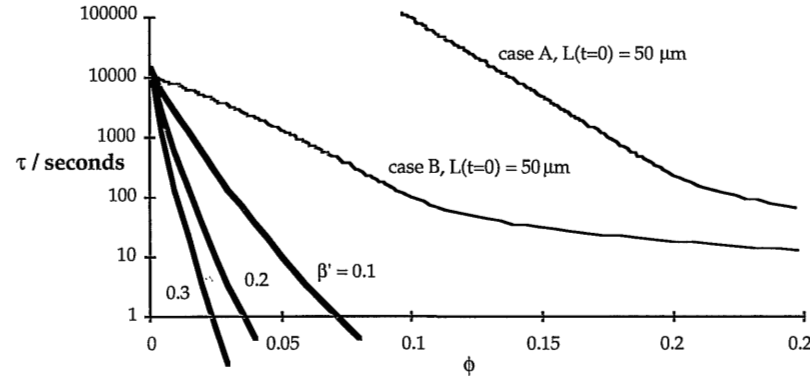

figure 8: The characteristic time of the drying process (thin lines) plotted logarithmically as a function of solvent volume fraction at the supported side of the film, and the relaxation time of the (diluted) polymer matrix (thick lines) as a function of solvent volume fraction. In the simulated drying process an initial film thickness of 50 μm is applied, both for case A and B, and parameters are as in table 1. The change of relaxation time with solvent volume fraction has been calculated for three values of the parameter β', namely 0.1, 0.2 and 0.3.

The characteristic drying time for case B, with a dry film thickness of 5 μm, becomes of the same order of magnitude as the characteristic relaxation time of the polymer when the solvent volume fraction approaches zero. A further decrease of the dry film thickness by decreasing the initial casting thickness would certainly mean that volume contraction of the polymer matrix is not fast enough anymore, resulting in excess free volume frozen into the matrix. The excess free volume enhances diffusion, thereby decreasing the real time-scale of the drying process compared to the calculated time-scale using eq. (27). Applying eq. (1) to drying is then not valid anymore. For case A, the drying process is always slow enough. One can estimate that a conflicting situation between the rates of drying and volume relaxation exists only when the dry film thickness gets of the order of 0.15 μm or thinner in case A. However, turning to faster diffusing solvents, drying proceeds in a material that does not maintain its local equilibrium state, at relatively thick films already. The diffusion coefficient of methanol in polyvinylacetate at zero solvent volume fraction is $4.46 \cdot 10^{-14}$ $m^2 s^{-1}$ [18]. As this value is 44.6 times as much as the corresponding diffusion coefficient in case B, problems are encountered rougly at the square root of 44.6 times 5 μm is 33 μm. These estimates are based on the following empiric relation for the equivalence of the polymer relaxation time and the characteristic time of drying:

$$(DEB)_{drying} \approx 1 : \tau_{material}(\phi=0,T) \approx \frac{L_{dry}^2}{D_0(T)}. \qquad (33)$$

Eq. (33) can be used in drying problems to get an indication whether drying proceeds in an equilibrium state of the polymer/solvent system. In the more general case of transient diffusion processes with only small variations in solvent activities, the

Deborah number of diffusion has to be applied.

$$(DEB)_{diffusion} \approx 1 : \tau_{material}(\phi,T) \approx \frac{L^2}{D(\phi,T)}. \qquad (34)$$

The influence of dry film thickness and diffusion coefficients on the drying process has been discussed, but the polymer relaxation time is an important parameter too. In the simulated drying process the temperature was 25 °C which is equal to or a little bit below reported glass transition temperatures for polyvinylacetate. If the temperature is far below the glass transition temperature of the polymer, the corresponding relaxation time will increase enormously. From the WLF equation it can be seen that, for all polymers in the glassy state, a decrease in temperature of only 3 °C, will theoretically result in about a tenfold increase of the relaxation time [25].

4.6. Discussion and conclusions

The properties of solvent-cast thin films from glassy polymers may be influenced by the kinetics of the drying process. If drying proceeds at a too high rate the glass transition will be traversed and excess free volume is frozen into the polymer matrix. The rate of drying is proportional to the reciprocal film thickness, and proportional to the concentration dependent solvent diffusion coefficient. A film, prepared by evaporating solvent from a cast polymer solution, does not maintain its equilibrium state during drying when the relaxation time of the diluted polymer gets of the same order of magnitude as the characteristic time of drying. This situation arises when the casting thickness of the polymer film is decreased or the solvent diffusion coefficient at zero volume fraction is increased by using another solvent or the temperature of the drying process is decreased. The last mentioned condition is the same as drying a polymer solution at the same temperature, using a polymer with a higher glass transition temperature. The fractional free volume is about the same for all polymers at the glass transition, f = 0.025 ±0.005 [25], when the corresponding time-scale is less than 1 hour.

The excess free volume frozen into the polymer matrix directly influences the gas permeabilities of the polymer because of their sensitivity towards the available free volume. Initially a decrease in the permeability ratio of inert gases has been measured for a polyimide and polycarbonate film [27] and can be attributed to the initially increased excess free volume. The relaxation times in these polymers must be high, but cannot be calculated using the WLF equation because of the too large differences in temperature with respect to the glass transition temperature. The WLF equation is applicable down to temperatures of 50 °C below generally reported glass transition temperatures. The polyimide in ref. [27] has been cast from a solution in methylene chloride which must have a high diffusion coefficient compared to other solvents. Furthermore the dry films are extremely thin with thicknesses below 0.5 μm. All

forementioned conditions that could result in a non-equilibrium state of the polymer have been fulfilled.
The non-equilibrium state of the polymer film is of course an unwanted situation in gas separation applications. On the other hand it cannot be avoided as the membrane thicknesses are decreased to improve fluxes through the membrane. The effects due to excess free volume, however, disappear in time because of the non-equilibrium nature of the glass. In time the glassy polymer tries to attain its equilibrium state. The time-scale of volume relaxation or physical aging is long compared to the time-scale of drying but changes can be seen within experimentation time. Within a few hours or days the forementioned polyimide and polycarbonate membranes reach gas permeation selectivities comparable to the ones for thick films [27].
As long as drying proceeds at a slow enough rate, it can be modelled and numerically simulated. As in general the evaporation step is not the limiting factor when drying a solution of a glassy polymer, the transport equation is of importance. In this chapter a procedure is presented to incorporate concentration dependent diffusion coefficients in the numerical relation of the transport equation. The numerical simulations are performed in an identical way compared to the simulations with a constant diffusion coefficient.

4.7. List of symbols

a	ratio of relaxation times at different temperatures or solvent volume fractions
c_1, c_2	constants in concentration dependent diffusion coefficient
c_1^0, c_2^0	constants in WLF equation
f	fractional free volume
i	index
k	mass transfer coefficient
n	number of layers
t	time
z	place coordinate
β'	parameter relating fractional free volume to volume fraction of solvent
γ	plasticization constant
τ	characteristic time
ϕ	solvent volume fraction
B	constant in Doolittle equation
D	mutual diffusion coefficient
D_m	modified diffusion coefficient
J	volume flux
L	film thickness
T	dimensionless time, or absolute temperature
Z	dimensionless distance
(DEB)	Deborah number for diffusion or drying

4.8. References

1. S.A. Jenehke, Effects of solvent mass transfer on flow of polymer solutions on a flat rotating disk, Industrial & Engineering Chemistry Fundamentals 23 (1984) 425-432.
2. J.S. Vrentas, C.M. Vrentas, Drying of solvent-coated polymer films, Journal of Polymer Science, Part B: Polymer Physics 32 (1994) 187-194.

3. G.M. Sletmoe, The evaporation of nonhydrogen-bonding solvents from resin films, Journal of Paint Technology, 38 (1966) 642-655.
4. A.A. Sarnotsky, Evaporation of solvents from paint films: I. Evaporation of solvent blends, Journal of Paint Technology, 41 (1969) 692-701.
5. A.J. Reuvers, C.A. Smolders, Formation of membranes by means of immersion precipitation. Part II. The mechanism of formation of membranes from the system cellulose acetate-acetone-water, Journal of Membrane Science 34 (1987) 67-86.
6. J.E. Anderson, R. Ullman, Mathematical analysis of factors influencing the skin thickness of asymmetric reverse osmosis membranes, Journal of Applied Physics 44 (1973) 4303-4311.
7. C. Castellari, S. Ottani, Preparation of reverse osmosis membranes. A numerical analysis of asymmetric membrane formation by solvent evaporation from cellulose acetate casting solutions, Journal of Membrane Science 9 (1981) 29-41.
8. L. Yilmaz, A.J. McHugh, Modelling of asymmetric membrane formation. I. Critique of evaporation models and development of a diffusion equation formalism for the quench period, Journal of Membrane Science, 28 (1986) 287-310.
9. W.B. Krantz, R.J. Ray, R.L. Sani, K.J. Gleason, Theoretical study of the transport processes occuring during the evaporation step in asymmetric membrane casting, Journal of Membrane Science, 29 (1986) 11-36.
10. C.A. Tsay, A.J. McHugh, Mass transfer dynamics of the evaporation step in membrane formation by phase inversion, Journal of Membrane Science 64 (1991) 81-92.
11. C.S. Tsay, A.J. McHugh, An improved numerical algorithm for ternary diffusion with a moving interface, Chemical Engineering Science 46 (1991) 1179-1187.
12. C.M. Hansen, Polymer coatings. Concepts of solvent evaporation phenomena, Ind. Eng. Chem. Prod. Res. Develop. 9 (1970) 283-286.
13. S. Birgül Tantekin, W.B. Krantz, A.R. Greenberg, The dynamics of evaporation in polymer/solvent films - importance in asymmetric polymeric membrane formation, Polymer Preprints 30 (1989) 36-37.
14. Y-O Tu, R.L. Drake, Heat and mass transfer during evaporation in coating formation, Journal of Colloid and Interface Science 135 (1990) 562-572.
15. S.R. de Groot, P. Mazur, Non-equilibrium thermodynamics, North-Holland Publishing Company 1962, Ch. XI, § 4.
16. J. Crank, The mathematics of diffusion, Oxford University Press 1975,
- Ch. IX,
- Ch. X.
17. H. Fujita, Diffusion in polymer-diluent systems, Fortschr. Hochpolym.-Forsch. 3 (1961) 1-47.
18. C.M. Hansen, Measurement of concentration-dependent diffusion coefficients, Industrial & Engineering Chemistry Fundamentals 6 (1967) 609-614.
19. C.M. Hansen, A mathematical description of film drying by solvent evaporation, J. Oil Col. Chem. Assoc. 51 (1968) 27-43.
20. J.A. Wesselingh, R. Krishna, Mass transfer, Ellis Horwood 1990, Ch. IV.
21. B. Carnahan, H.A. Luther, J.O. Wilkes, Applied numerical methods, John Wiley & Sons 1969, Ch. VI.
22. J.S. Vrentas, C.M. Jarzebski, J.L. Duda,A Deborah number for diffusion in polymer-solvent systems, AIChE Journal 21 (1975) 894-901.
23. J.S. Vrentas, J.L. Duda, Diffusion in polymer-solvent systems. III. Construction of Deborah number diagrams, Journal of Polymer Science: Polymer Physics ed. 15 (1977) 441-453.
24. J.S. Vrentas, J.L. Duda, W.J. Huang, Regions of Fickian diffusion in polymer-solvent systems, Macromolecules 19 (1986) 1718-1724.
25. J.D. Ferry, Viscoelastic properties of polymers, John Wiley & Sons 1980,
- Ch. XI,
- Ch. XVII.
26. A.J. Kovacs, La contraction isotherme du volume des polymères amorphes, Journal of Polymer Science 30 (1958) 131-147.
27. M.E. Rezac, P.H. Pfromm, L.M. Costello, W.J. Koros, Aging of thin polyimide-ceramic composite membranes, Industrial & Engineering Chemistry Research 32 (1993) 1921-1926.

Chapter 5

Dielectric Properties of a Polymer Film;
measurements with the comb-electrodes

5.1. Introduction

For materials and especially polymers in the glassy state the momentary configuration can strongly depend on its thermal history. If a sample is quenched from a temperature above the glass transition, excess free volume is frozen into the structure. Physical aging, i.e. the relaxation towards the equilibrium free volume, proceeds at a self-decreasing rate [1]. Therefore material properties will depend on the thermal history of the material.
One can also enter the glassy state from a solution, by extracting or evaporating the solvent. Instead of heat transport, mass transfer is involved in the solidification process. The latter process requires in general more time for solidification of the material, compared to the cooling process. But also in this case the properties of the material depend on its history [2-4]. During the drying process the time-scale of volume relaxation may become larger than the time-scale of diffusion [5]. It implies that excess free volume will be frozen into the polymeric matrix when volume relaxation is very slow and this is expected to occur upon drying in thin solvent-cast films. The excess free volume will disappear then by physical aging. It has been found in permeation of inert gases through thin films of glassy polymers in which the accessible free volume is an important parameter that gas fluxes do decrease in time [6].
The material property of interest in this chapter is the complex dielectric constant. Dielectric spectroscopy is a versatile technique to determine the polarization of dipoles in an applied electric field. The permanent or induced dipole moments in a molecule will change their orientations upon the interaction with the electric field. Therefore, a disturbance of the equilibrium configuration of a material is needed to measure an intrinsic property of the material.
The solidification of a drying polymer solution will be investigated. In this case relatively low frequencies are of interest when monitoring the mobility of the dipoles. The solvent molecules will respond faster to changes in the electric field compared to the polymer.
Usually the material of interest is inserted into a condenser or capacitor and its capacitance can be measured from the response in an electric network. In order to follow continuously the change in dielectric properties of a drying polymer solution a special electrode configuration is needed. Hill *et al.* use two metal strips on glass or wood substrates as the electrodes [7-8]. These configurations suffer, however, from the inability to calculate the dielectric constant from the measured capacitance, because the potential distribution between the electrodes is unknown.

With the appearance of interdigitated or comb electrodes [9], fabricated onto an insulating substrate, dielectric permittivities and loss factors could be measured. Each electrode has a comb-like shape and interdigitates the other. Due to its ease of fabrication, and the quantative measurements possible, this configuration has been adopted in our experiments.
The development of the microdielectrometer sensor [9-11] is also based on the electrode configuration of the comb-electrodes and is essentially a field effect transistor (FET).
In paragraph 5.2. an introduction will be given to the theory of dynamic dielectric spectroscopy. In paragraph 5.3. the experimental set-up will be described. In paragraph 5.4 results of experiments on the drying of a cast polymer solution will be shown. The evaporation is modelled and solvent mass transfer coefficients in the glassy polymer film are calculated. A procedure to determine solvent diffusion coefficients with the comb-electrodes will be described. In paragraph 5.5. the experimental results will be discussed.

5.2. Theory

The polarization **P** of a material is defined as the sum of the dipole moment vectors per unit volume. The permanent or induced dipoles try to oppose the applied electric field. Because the alignment of the dipoles is not instantaneous, the polarization lags behind in an alternating electric field. A linear, time-invariant, theory of electric polarization, i.e. the equivalent of linear visco-elasticity, has been developed to describe this phenomenon.
Assuming an isotropic material, the electric displacement **D**(t) can be written, according to the Boltzmann superposition principle [12], as a function of the complete history of the electric field **E**(t).

$$\mathbf{D}(t) = \int_{-\infty}^{t} g(t-t')\mathbf{E}(t')dt', \qquad (1)$$

with g(t) being a retardation memory function, describing the response of the electric displacement in time to a unit pulse in the electric field, and t′ is the time variable of integration.
One can extend the integral in eq. (1) to infinity by stating that future events do not contribute to the present. Then the integral represents a convolution, and with the help of the Fourier transformation a simple relationship is obtained between the Fourier transforms of electric displacement and electric field.

$$\mathbf{D}(i\omega) = \varepsilon_0\varepsilon^*(i\omega)\mathbf{E}(i\omega), \qquad (2)$$

where $\varepsilon_0\varepsilon^*(i\omega)$ is the Fourier transform of g(t). ε_0 is the dielectric permittivity of free space, i.e. $8.8542 \cdot 10^{-12}$ Fm^{-1}, and $\varepsilon^*(i\omega)$ is the relative, complex dielectric constant, defined as

$$\varepsilon^*(i\omega) = \varepsilon'(\omega) - i\varepsilon''(\omega), \tag{3}$$

with $\varepsilon'(\omega)$ being the relative dielectric permittivity, $\varepsilon''(\omega)$ the relative loss factor and i the imaginary unit. Throughout this chapter the adjective 'relative' is usually omitted. The loss factor accounts for the dielectric loss due to the polarization of dipoles and the conductivity due to the presence of free ions.

$$\varepsilon''(\omega) = \varepsilon''_{\text{polarization}}(\omega) + \frac{\sigma_{dc}}{\omega\varepsilon_0}, \tag{4}$$

where $\varepsilon''_{\text{polarization}}(\omega)$ is the dielectric loss due to polarization and σ_{dc} the direct current conductivity.
Performing experiments with harmonic signals, the ratio of amplitudes of the electric displacement and the electric field will give the magnitude of the complex dielectric constant, and the phase difference between the two will give the phase of the complex dielectric constant.
In dielectric experiments often a harmonic voltage or potential ΔV is applied to the electrodes of a capacitor and an electric field is created in the material between the electrodes. The response of the material, the electric displacement, follows from eq. (2) and is related to the current I to the electrode configuration. The complex electric impedance $Z(i\omega)$ of a capacitor with a complex capacitance $C^*(i\omega)$, for example the comb-electrodes, is defined by the complex ratio of applied voltage and current.

$$Z(i\omega) \equiv \frac{\Delta V(i\omega)}{I(i\omega)} = \frac{1}{i\omega C^*(\varepsilon^*(i\omega))}. \tag{5}$$

The relation between the voltage applied to and the current going through the electrode configuration is a measure of the dielectric properties of the material between the electrodes, the configuration of the electrodes and possible resistances in the electrodes.
In the experiments the dielectric properties of a polymer solution that is changing during the experiment in a very thin polymeric layer, will be investigated. The change of dielectric properties with time is monitored at a fixed frequency of the voltage applied to the comb-electrodes.

5.3. The experimental set-up

Because of its ease of fabrication the comb electrode configuration which makes a quantitative measurement of dielectric properties possible, has been chosen for the

experiments. Since the tests should be carried out with very thin polymer films of less than twenty micrometer thickness a restriction is placed onto the inter-electrode spacing. In appendix A the relation between the electrode configuration, the complex dielectric constants of the glass and the polymeric layer and the measured capacitance will be derived. Given the distance between the two electrodes the minimal material thickness needed to cover the electrodes is estimated. The latter value should meet our requirements.
Appendix B shows that the use of the comb-electrodes is restricted to low frequencies and materials with a relatively low dielectric permittivity and loss factor. Finally appendix C will give an error analysis of the experiments.

Comb-electrodes have been made by selectively etching chromium from a chromium mask with a photolithographic technique. The thickness of the chromium layer is about 100 nm. The inter-electrode distance and the width of the electrodes are approximately 5 μm. The surface of the electrode configuration is 1.4 square cm. The minimal thickness of the polymeric layer covering the electrodes with an electrode spacing of 5 μm, should be about 7 μm. This layer of 7 μm contributes to the observed complex capacitance of the comb-electrodes assuming that the charge density in the polymeric layer and glass support is zero and that the finite thickness of the electrodes may be neglected (see appendix A). Commercially available electrodes have a much larger spacing and are of no interest, because the final film thicknesses should be of the order of 20 μm and preferably thinner. In figure 1 part of the comb-electrodes is shown, as observed with a light microscope.

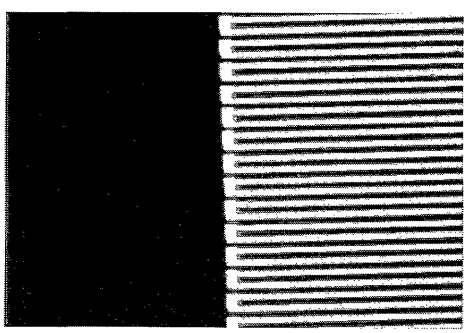

figure 1: *Top view of the comb electrode configuration as seen with a light microscope. The inter-electrode distance and the width of the electrodes is 5 μm.*

The comb electrode configuration is prepared on a glass surface. This means that not only the polymer solution or polymer film will contribute to the measured capacitance, but also the glass support. The respective contributions to the capacitance are acting parallel and may therefore be added. Neglecting the resistances in the electrodes and assuming the same proportion of the dielectric properties to their respective capacitances, based on the small thickness of the comb-electrodes compared to the electrode spacing, one may write:

$$C^*(i\omega) = k\varepsilon_0\{\varepsilon^*_{glass}(i\omega) + \varepsilon^*_{polymer}(i\omega)\}, \quad (6)$$

with k being a geometry factor, with unit length. In appendix A an analytical expression is derived relating the geometry factor k to the electrode configuration. In this configuration the numerically determined value of k is 7.5 m. This value holds when the charge density in the polymer and glass support are zero.

In figure 2 the electric network, in which the comb electrode configuration is incorporated, is drawn.

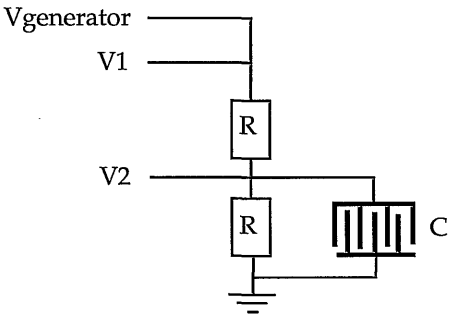

figure 2: Schematic diagram illustrating the electric network which was used in this study. The network consists of two resistors R and a non-ideal capacitor C, the comb-electrodes. V_1 and V_2 are the two measured voltages.

The complex ratio of the two measured voltages V_1 and V_2 is called a transfer function and is given by:

$$\frac{V_1(i\omega)}{V_2(i\omega)} = 2 + i\omega RC^*(i\omega). \quad (7)$$

Here i is the imaginary unit, ω the angular frequency of the sinusoidal voltage applied by the generator, R the known resistance of the two resistors in the electric network and C* the complex capacitance of the comb-electrodes.
The contribution of the glass substrate to the measured capacitance can be eliminated, when the resistance in the electrodes may be neglected, by measuring first the transfer function with the polymeric material of interest, indicated by subscript p, and then measuring the same transfer function of the bare comb-electrodes in a nitrogen atmosphere, indicated by subscript N_2, and subtracting these two values at corresponding frequencies. This will give relation (8).

$$\left(\frac{V_1}{V_2}\right)_p - \left(\frac{V_1}{V_2}\right)_{N_2} = \omega Rk\varepsilon_0\varepsilon''_p + i\omega Rk\varepsilon_0(\varepsilon'_p - \varepsilon'_{N_2}). \quad (8)$$

Calibration of the comb-electrodes according to eq. (8) has been performed with the Baysilon M350 polydimethylsiloxane oil from Bayer, supplied by Necarbo. The numerical geometry factor k of 7.5 m is not precisely the value of the geometry factor

found by calibration, which is 10.0 ± 0.4 m, because the thickness of the chromium is neglected and the distance between the electrodes is not exactly 5 μm. In the experiments the value found by calibration will be used. The relatively large error in the calibration factor results from limited accuracy of the electronic equipment.

In figure 3 an atomic force microscope picture is given of the bottom surface of a polymer film that has been cast onto one of the comb-electrodes. The scale of the height has been enlarged significantly to show the depth of the profiles in the polymer film. Because of the thin chromium layer the resistance in this layer can be of the same order as the impedance of the glass and the polymer solution between the two electrodes. Application of eq. (8) to the measured transfer functions of dry polymer films at frequencies near 1 MHz gave calculated dielectric permittivities smaller than 1. Therefore the effect of the resistances in the electrodes has been analysed. In appendix B a deviation function for the complex capacitance will be derived that tells to what extent the resistance in the chromium layer will influence the ideal capacitance as given in eq. (6). For evaluation of this deviation function one has to know the geometry of the comb, the thickness of the chromium layer and the specific resistance of chromium. The thickness is estimated from AFM-pictures like in figure 3, and is about 100 nm.
Evaluation of the deviation function shows that eqs. (6) and (8) is valid only at relatively low frequencies (< 10,000 Hz) and using materials with a relatively low complex dielectric constant.

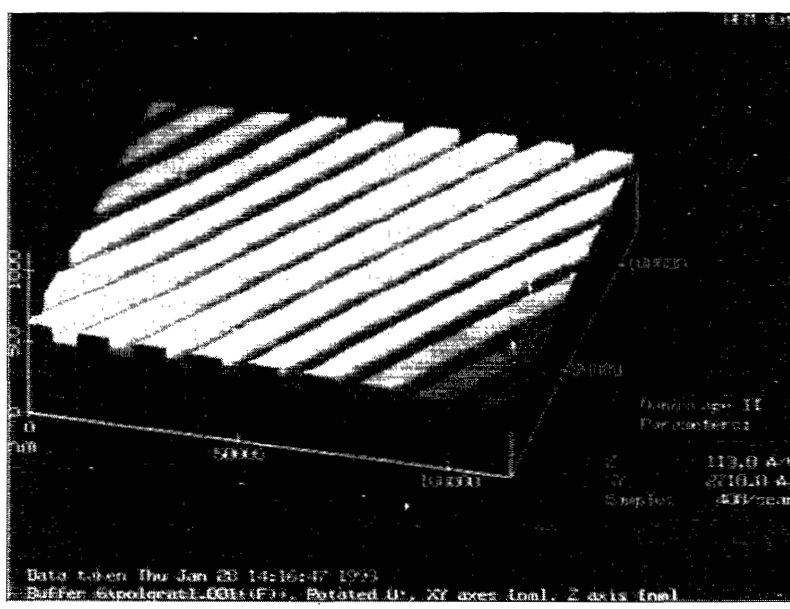

figure 3: An atomic force microscope picture of that surface of a polymer film that has been in direct contact with the comb-electrodes.

There are two limitations to the magnitude of the voltage that can be applied to the comb electrodes. First of all, the electric field should be far below the dielectric strength of the material, which is in the order of 10^6 - 10^7 Vm^{-1} for ceramics and waxes [13]. Secondly, the presence of the solvent may inhibit reduction/oxidation reactions at the electrodes.
The latter effect will directly influence the measured complex dielectric permittivity, because of the chromium ions present in the solution. The maximum voltage that can be applied has been determined by polarography [14]. The Metrohm Herisau E505 electrode compartment consisted of two chromium electrodes, dipped into a solvent in which a suitable salt has been dissolved and a Ag/AgCl reference electrode in a KCl buffer solution. The direct current through the reference electrode has been recorded as a function of the applied voltage across the chromium electrodes with a Metrohm Herisau E506 polarograph. Above a certain voltage level, the current is increasing more than proportionally, indicating the generation of additional free ions in the solution. Solvents used are water, N,N-dimethylacetamide, dimethylsulfoxide, 1-methyl-2-pyrrolidinone, N,N-dimethylformamide, acetone and dichloroethane. Tetraethylammoniumperchlorate has been used with all solvents as the dissolved salt. The minimum voltage required to see the forementioned effect is 0.3, 0.42, 0.54, 0.66, 0.6, 0.72 and 0.54 V, respectively for the aforementioned solvents.
Setting the generator voltage in our electric network to 0.6 V ensures that the voltage applied to the comb-electrodes never exceeds 0.3 V. The resulting electric field is always lower than or equal to $6 \cdot 10^4$ Vm^{-1}.

An automated experimental set-up has been designed for generating the input signal of the electric network in figure 2, measuring the transfer function and collecting the data (see figure 4). A personal computer controls via an IEEE-bus the Solartron 1255 Frequency Response Analyzer (FRA). Two low frequency, high impedance, buffers have been constructed to match the high impedances of the electric network and the relatively low input impedances of the FRA (10^6 Ω in parallel with 35 pF).

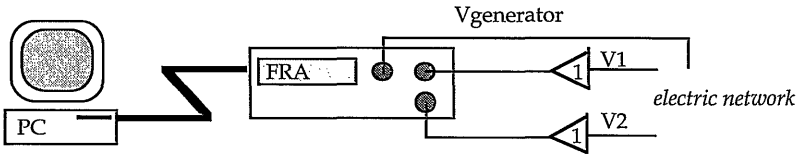

figure 4: Automated experimental set-up for the determination of the complex dielectric constant.

The accuracy of the measurements with the FRA will be discussed in appendix C.
The input buffers are taken from literature [15], with a small adaptation. A 47 Ω resistor has been added to avoid the destruction of the output operational amplifier by spurious voltage steps on the buffer-output. Each buffer consists of two, low output impedance (3Ω), voltage followers (Harris HA 5002) and one high input impedance differential amplifier (LF 356). The closed loop ensures that the output and the shield of the coax cable are driven at the same potential as the input or core of the coax cable. Although there is a certain capacitance between core and shield of the coax cable, no

leaking currents will exist. The input impedance of the LF 356 is 10^{12} Ω in parallel with 3 pF.

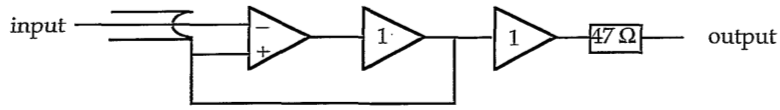

figure 5: High input-impedance, voltage follower with low output-impedance.

The comb-electrodes are placed in a box in which the atmosphere is controlled by a continuous flow of nitrogen. This flow can be mixed with a nitrogen stream satured with the vapour of any solvent.

5.4.1. Evaporation of solvent from a polymer solution.

With the comb-electrodes one can monitor the drying of a polymer solution in a non-invasive way. In the experiments amorphous polymers have been dissolved in a suitable solvent which is evaporating into a nitrogen atmosphere upon casting the solution on the comb-electrodes.
The polymers chosen are polyacrylonitrile (Aldrich), polyethersulfone E1000 (BASF), and polyimide XU 218 (Ciba-Geigy). Dielectric data are given in table 1.

table 1: Dielectric properties, as supplied by the manufacturers, of polymers used in the dielectric experiments.

frequency Hz	temperature °C	dielectric permittivity	dielectric loss
polyethersulfone E1000[1]			
50	23	3.6	$1.7 \cdot 10^{-3}$
$1 \cdot 10^{6}$	23	3.5	$11 \cdot 10^{-3}$
polyimide Matrimid 5218[1,2]			
$1 \cdot 10^{2}$	25	3.4	-
$1 \cdot 10^{3}$	25	3.3	$8.5 \cdot 10^{-3}$
$1 \cdot 10^{6}$	25	3.0	-
$1 \cdot 10^{3}$	60	3.0	$11.7 \cdot 10^{-3}$
$1 \cdot 10^{3}$	100	3.0	-
$1 \cdot 10^{3}$	150	3.0	-

[1] moisture might be present in the polymer sample due to the humidity of air
[2] XU 218 is the experimental version of Matrimid 5218

For the polyimide dielectric permittivities are given at four different temperatures. The measured permittivity at 25 °C is high compared to the permittivities at 60, 100 and 150 °C. This is not expected, and probably stems from moisture absorbed from the

air. The effect of humidity on the dielectric permittivity of the polyimide will be clear from the experiments in paragraph 5.4.3.

The solvents used are dimethylformamide (Aldrich, analytical grade), 1-methyl-2-pyrrolidinone (Janssen Chimica) and dimethylacetamide (Merck, synthesis grade). At 30 °C which is the temperature of the thermostated box with the comb-electrodes these solvents evaporate rather slowly. This slow evaporation is needed, because the final thicknesses obtained are often below 50 μm. With the slowly evaporating solvents, not only the time needed to solidify the complete polymer solution is delayed, but also significant changes can be observed in the glassy state when the solvents have a relatively large dipole moment or dielectric constant compared to the polymer. Dimethylformamide and dimethylacetamide have a dipole moment of 3.82 D and 3.81 D respectively [13]. The dipole moment of 1-methyl-2-pyrrolidinone is 4.09 D [16]. All solvents used have a dipole moment larger than the dipole moment of water, which is 1.85 D [13]. The dielectric constants of dimethylformamide, dimethylacetamide and water are 36.7, 37.8 and 78.5 respectively [17].

In figures 6 and 7 the drying of a solution of 10 wt.% polyacrylonitrile (PAN) in dimethylformamide (DMF) is shown. Figure 6 is the double-logarithmic plot of the measured dielectric permittivity versus time, whereas figure 7 gives the corresponding loss factor. A difference in final film thickness is obtained by varying the initial casting thickness, using the same polymer solution. From bottom to top these final thicknesses are respectively 7.5, 13 and 20 μm. The applied frequency is 1 Hz.
Measurements are started within one or two minutes after casting the polymer solution and last for 22 hours. The first part of the measurement is not shown because there the impedance of the comb-electrodes is not only determined by the impedance of the polymer solution but also by the resistance within the electrodes (see appendix B). After a certain time the dielectric permittivity and loss factor, calculated with eq. (8), can be plotted. A sharp decrease in time is seen in both the dielectric permittivity and loss factor. The high dielectric permittivity, > 100, is probably due to electrode polarization and the corresponding loss factor due to conduction.

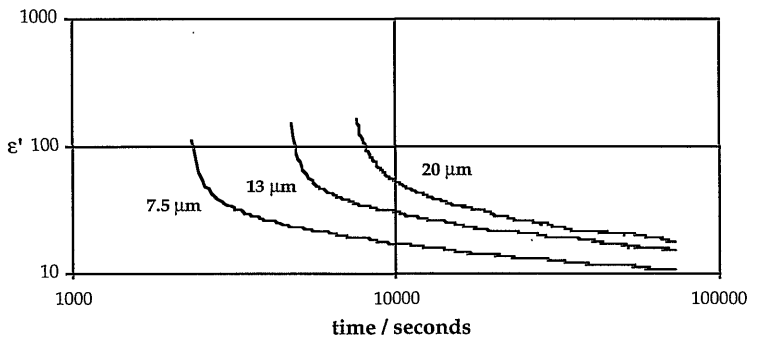

figure 6: Dielectric permittivity of a polyacrylonitrile/dimethylformamide solution as a function of time. Three measurements with dry film thicknesses as indicated are presented. Drying is carried out in a nitrogen atmosphere. The applied frequency is 1 Hz.

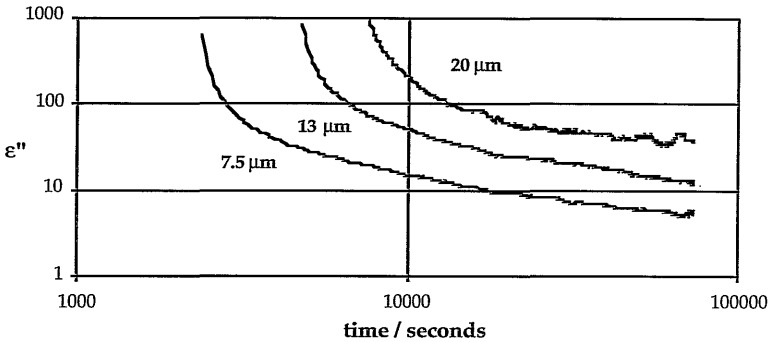

figure 7: Loss factor of a polyacrylonitrile/dimethylformamide solution as a function of time. Three measurements with dry film thicknesses as indicated are presented. Drying is carried out in a nitrogen atmosphere. The applied frequency is 1 Hz.

From the frequency dependence of the complex dielectric constant, measured after the presented experiments had stopped, it is concluded that there is no contribution of the conduction of free ions to the measured loss factor. In the final phase of drying the loss factor is equal to the dielectric loss due to the polarization of dipoles.
A region is seen in figures 6 and 7 where the curves bend strongly. This 'bending point' is attributed to the vitrification of the polymer solution or better the vitrification of the solution near the electrodes. Any time after the bending point a polymer film may be lifted from the comb-electrodes and although the films are still plasticized by the solvent they exhibit sufficiently mechanical strength corresponding to the glassy state. The vitrification has been verified by coagulating a cast polymer solution in water, a non-solvent for the polymer. The time between casting the 10 wt.% PAN/DMF solution and coagulating the remaining film in water has been varied. The underlying idea is that a vitrified but still plasticized polymer solution cannot be phase-separated into a polymer-rich and a polymer-poor phase [18]. If the drying time before coagulation is too short the polymer solution can demix and a solid polymer matrix with a porous structure is obtained. The porous structure gives the film an opaque appearance when the pore sizes have a radius comparable to the wavelength of visible light. In case the polymer solution has vitrified, no phase separation will occur upon coagulation in water. The polymer film then remains transparent.
In table 2 the results of the coagulation experiment are compared to the corresponding times at the bending points in figure 6. The bending point is determined by the intersection of the tangents to the left and the right of a curve. For the coagulation experiments several samples with initial casting thicknesses of 100 and 200 μm have been prepared. The polymer films are coagulated in water at various times after casting the polymer solution.
The vitrification times from the demixing experiments are denoted with reserve. Although several drying times are employed at each casting thickness, one can not exactly give the vitrification time, because the change from opaque to transparent appearance after coagulation is gradual. A film that is hazy after coagulation can become transparent after lifting the polymer film from the water bath.

table 2: Time needed to vitrify a polymer solution; comparison of dielectric measurements with coagulation of polymer solutions/films in a nonsolvent bath. The initial casting thickness is given between brackets.

film thickness μm	temperature °C	time to vitrify s (dielectric experiments)	time to vitrify s (coagulation)
10 wt.% PAN/DMF solution			
7.5 (100)	30	$2.5 \pm 0.1 \cdot 10^3$	
13 (200)	30	$5.2 \pm 0.2 \cdot 10^3$	
20 (300)	30	$8.8 \pm 1.0 \cdot 10^3$	
10 wt.% PAN/DMF solution			
9 ± 1 (100)	23 ± 1		$< 3.9 \cdot 10^3$
22 ± 2 (200)	24^+		$> 6.7 \cdot 10^3$
14 ± 1 (200)	24^+		$< 12.4 \cdot 10^3$

From table 2 it is concluded that the bending points in figures 6 and 7 represent the vitrification of the polymer solution near the electrodes. The larger the initial casting thickness of the polymer solution, the more time it takes to vitrify the entire polymer solution. This is seen by a shift to the right of the drying curves with increasing casting thickness.

From figures 6 and 7 one can conclude that there must be a relevant amount of solvent left in the glassy state. Both the dielectric permittivity and the dielectric loss are decreasing further in time. The decrease in solvent is due to diffusion through the vitrified polymer film followed by the evaporation in the nitrogen atmosphere. In the glassy state the diffusion process is the rate limiting step. The tangent of the curves in figures 6 and 7, in the glassy state is almost constant which means that the change in time of the dielectric permittivity and dielectric loss near the comb-electrodes can be approximated by the following relation:

$$\varepsilon', \varepsilon'' \propto t^{-n}, \qquad (9)$$

with n the absolute value of the slope in the double-logarithmic plots given.
From eq. (10) it is clear that drying proceeds in a self-decreasing rate.

Both the dielectric permittivity and the dielectric loss show the same trend during drying. In the following experiments only the dielectric permittivity will be shown. After vitrification of the polymer solution the ratio of dielectric loss and permittivity becomes smaller than 0.1 and the accuracy of the dielectric loss is being lost.
In figure 8 the dielectric permittivity is given as a function of time, for the drying of a solution of 25 wt.% polyethersulfone (PES) E1000 in DMF.

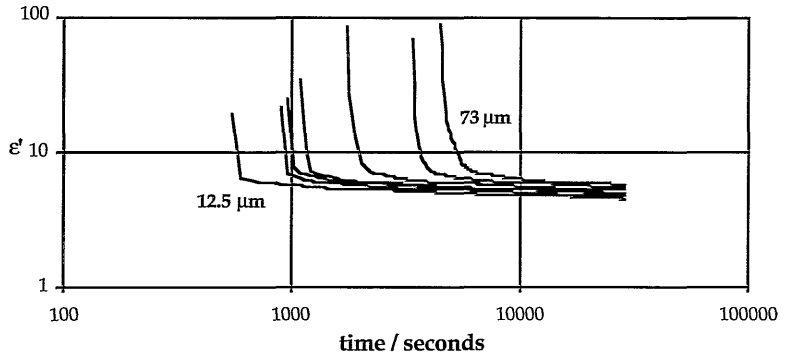

figure 8: Dielectric permittivity of a polyethersulfone/dimethylformamide solution as a function of time. Drying proceeds in a nitrogen atmosphere. The applied frequency is 100 Hz.

The final film thicknesses are, from the left to the right, 12.5, 13.5, 16, 19, 31, 51 and 73 µm. The applied frequency is 100 Hz. Measurements at other frequencies will show the same trend. Every measurement takes about 8 hours.
In figure 9 the drying curve is given for a solution of 30 wt.% PES in 1-methyl-2-pyrrolidinone (NMP). The same frequency of 100 Hz has been applied.

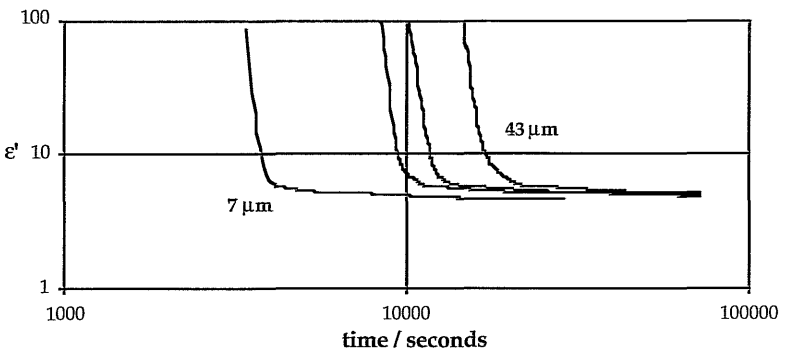

figure 9: Dielectric permittivity of a polyethersulfone/1-methyl-2-pyrrolidinone solution as a function of time. Drying proceeds in a nitrogen atmosphere. The applied frequency is 100 Hz.

The final film thicknesses in figure 9 are 7, 20, 29 and 43 µm. Comparing the time scales of this figure with the former one, it is noticed that a longer time is needed for the vitrification of a solution with NMP as the solvent, than with DMF.

In figures 10 and 11 the drying of a solution with the polyimide XU 218 is shown. In one case the solvent is DMF and in the other dimethylacetamide (DMAc). The molecular difference between the two solvents is that the latter solvent has one more methyl group, instead of a hydrogen atom, connected to the carbonyl group.
The final film thicknesses in figure 10 are, from left to right, 8.0, 13.5, 12.6 and 17.5 µm. The frequency is 1 Hz.

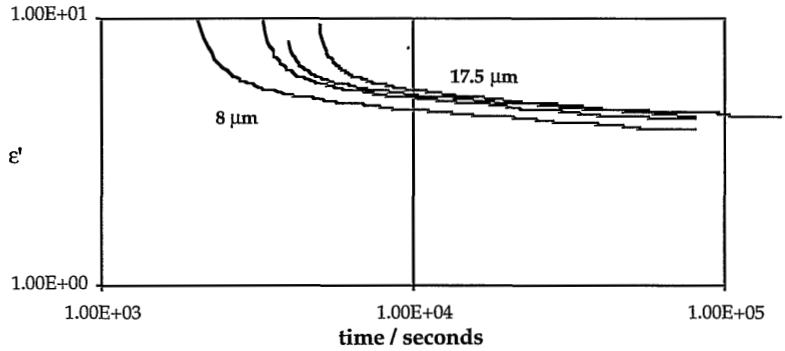

figure 10: Dielectric permittivity of a polyimide/dimethylformamide solution as a function of time. Drying proceeds in a nitrogen atmosphere. The applied frequency is 1 Hz.

The applied frequency in figure 11 is the same as in figure 10. Final film thicknesses are ranging from 8.6, 14.2, 14.8 to 25.8 µm. Although there is only a small difference between DMF and DMAc, considerably more time is needed to obtain a glassy film, with the same thickness, from a solution with DMAc. The differences are not that obvious compared to the drying of PES dissolved in DMF or NMP.

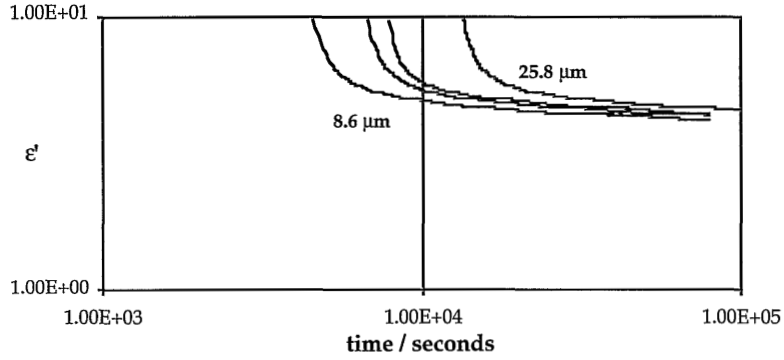

figure 11: Dielectric permittivity of a polyimide/dimethylacetamide solution as a function of time. Drying proceeds in a nitrogen atmosphere. The applied frequency is 1 Hz.

From the experiments shown in this paragraph a clear point that is attributed to the vitrification of the polymer solution can be identified. After vitrification loss of residual solvent is controlled by diffusion of the solvent through the plasticized polymer matrix towards the free surface where evaporation can take place. In the next paragraph this diffusion process will be modelled.

5.4.2. A model for the evaporation step

In paragraph 5.4.1. experiments are shown on the drying of a polymer solution in a nitrogen atmosphere. The removal of solvent is controlled by evaporation, diffusion in the gas phase above the cast polymer solution, and diffusion in the polymer solution towards the solution/nitrogen interface where evaporation takes place.

Interest is directed to the final phase of the drying process, i.e. when the glassy state of the polymer is reached. Drying is controlled by diffusion to the nitrogen exposed side of the polymer film. In order to know the absolute solvent flux through the boundary the solvent diffusion coefficient has to be known as a function of volume fraction, concentration or activity. The dependence of the solvent diffusion coefficient on composition is not known and therefore the concentration profile during drying cannot be calculated.
In literature diffusion coefficients measured with a variety of experimental techniques are presented. Usually stepwise changes of solvent activity are applied to a sample that is at thermodynamic equilibrium. The system under investigation adapts a new equilibrium state with every change of solvent activity in its environment. The process is not instantaneous but kinetically determined.
Determination of the diffusion coefficient in the glassy state can be tedious due to the relatively slow diffusion processes and sometimes it is made impossible by the strong dependence on solvent concentration. The strong solvent dependence is noticed in the case of polymer-solvent systems. Swelling of the polymer matrix will significantly increase the diffusion coefficient. This is in contrast with polymer-penetrant systems, i.e. in which no or negligible swelling is involved and in which diffusion does not depend on solvent activity [19].
In polymer-solvent systems, the diffusion coefficient can even vary over decades within the glassy state [19-20]. Often the logarithm of measured diffusion coefficients is plotted as a function of solvent concentration. This strong dependence on the amount of solvent has certain drawbacks. Very often 'paired' sorption and desorption curves do not match, indicating that Fick's second law does not hold. Furthermore polymer relaxation may interfere to a certain extent with sorption and desorption experiments [5].
On the basis of the strong dependence of diffusion coefficient D on solvent concentration c, one may assume the following solvent concentration profile in the glassy state.

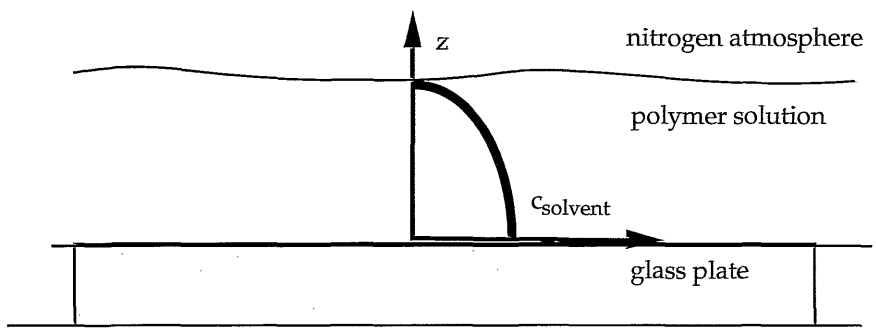

figure 12: Schematic drawing illustrating concentration profile of solvent in the glassy polymer.

In figure 12 the solvent concentration is zero at the nitrogen exposed side of the polymer film, and has a non-zero value at the glass plate side. At the latter interface the derivative of the concentration with respect to the direction z is zero: i.e. no flux

occurs through this boundary. The concentration profile must have a steeper gradient near the interface where evaporation takes place compared to steady-state permeation with the same solvent concentrations at both interfaces because in steady-state permeation there is a non-zero gradient for z=0 and fluxes are independent of the distance in the film.
For comparison the concentration profile in steady-state transport is calculated assuming an exponential dependence of the diffusion coefficient on solvent concentration.

$$D = D_0 \exp(\gamma c), \tag{10a}$$
$$z = 0: \quad c = c_0, \tag{10b}$$
$$z = L: \quad c = 0, \tag{10c}$$

where γ is a so-called plasticization constant and L the total film thickness.

One can readily derive the concentration as a function of distance in the film using Fick's first law.

$$c(z) = \frac{1}{\gamma} \ln\left(\frac{z}{L} + \exp(\gamma c_0)\cdot\left(1 - \frac{z}{L}\right)\right), \qquad \gamma > 0. \tag{11a}$$

$$c(z) = c_0 \left(1 - \frac{z}{L}\right), \qquad \gamma = 0. \tag{11b}$$

The ratio of the gradients at z=L and z=0 is equal to:

$$\frac{\partial c}{\partial z}_{z=L} \Big/ \frac{\partial c}{\partial z}_{z=0} = \exp(\gamma c_0) = \frac{D(c_0)}{D_0}. \tag{12}$$

The result of eq. (12) is always larger than one if the plasticization constant is not zero. The ratio of the diffusion coefficients at concentration c_0 and at concentration c=0 may even vary over decades for a polymer solution in the glassy state. When eq. (10) is valid during the drying of a polymer film and there is a zero concentration gradient at z=0, then the concentration gradient near the nitrogen exposed side of the film is steeper than the corresponding concentration gradient in steady-state permeation.

For a polymer-solvent system it is likely that the diffusion coefficient strongly depends on the solvent concentration and that during drying of a polymer film in the glassy state the concentration gradient is steep near the nitrogen exposed side of the film. Therefore figure 12 is simplified into the following picture.

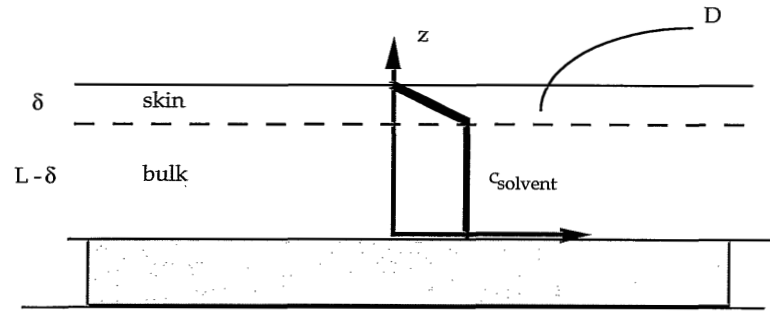

figure 13: Simplified schematic drawing showing a solvent concentration profile in the glassy polymer.

In figure 13 the polymer film is divided into two regions, i.e. a bulk and a skin layer, with thicknesses of L-δ and δ respectively. The concentration gradient is completely situated in the skin layer. The gradient in the bulk layer is neglected, although it must be there for else no further drying will happen.
With the assumptions made it is implicitly stated that

$$\delta << L. \tag{13}$$

Drying proceeds due to the solvent diffusing through the skin layer with an apparent diffusion coefficient D followed by evaporation of the solvent into the nitrogen atmosphere. The solvent flux results in a depletion of solvent, which has to be realised in the bulk layer. These two conditions lead to the following time-dependence of the bulk solvent concentration, in which swelling has been neglected.

$$c(t\text{-}t_{ref}) = c(t=t_{ref})\cdot\exp\left(-\frac{D}{\delta(L-\delta)}(t\text{-}t_{ref})\right). \tag{14}$$

From a certain reference time t_{ref} on, drying proceeds in such a way that the concentration depends only on the concentration, the apparent diffusion coefficient D and thicknesses δ and L at the reference time. The reference time may be any time, subsequent to the conditions that the polymer film is in the glassy state and inequality (13) is true. During drying the apparent diffusion coefficient and the skin and bulk layer thicknesses will vary, and therefore also the time-dependence of the decrease in solvent concentration varies. Both D and L will decrease with time, or better, with the decrease in bulk solvent concentration. In deriving eq. (14), however, it is assumed that the film thickness is constant.

The solvent concentration and solvent volume fraction are a measure of the amount of solvent per unit volume of polymer film. The concentration c can be related to the dielectric permittivity, i.e. the parameter ε'-1 is a measure of the number of dipoles, multiplied with respective dipole moments, per unit volume. A plot of the ratio of dielectric loss and the measured dielectric permittivity subtracted with the permittivity of the pure polymer versus time is constant in the glassy polymer. It confirms the idea

that the decrease of dielectric permittivity and dielectric loss in time is directly related to the amount of solvent. Neglecting both swelling of the polymer film and enhanced mobility of the polymer chains, due to the presence of solvent, the following relation between solvent concentration and dielectric permittivity of the plasticized and dry polymer film is established.

$$c(t) \propto \varepsilon'(t) - \varepsilon'_{polymer}. \tag{15}$$

The same relation is used by Day [20] in the determination of water diffusion coefficients in polyimides and is based on the large dielectric constant of water, i.e. 78.5 [13,16], compared to the permittivity of the polymer. Although the dielectric constants of the solvents used are not as large as the dielectric constant of water, they are still large compared to the polymers. Combining eqs. (14) and (15) gives:

$$\varepsilon'(t-t_{ref}) - \varepsilon'_p = (\varepsilon'(t=t_{ref}) - \varepsilon'_p)\cdot\exp(-\frac{D}{\delta(L-\delta)}(t-t_{ref})). \tag{16}$$

Plotting the measured dielectric permittivity minus the dielectric permittivity of the pure film, as a function of time, one can evaluate eq. (16). One may take any reference time t_{ref}, and draw a tangent to the curve at t_{ref}. The tangent line will intersect the time axis, and the reciprocal of the time-span θ between the intersection point and t_{ref} equals:

$$\frac{1}{\theta} = \frac{D}{\delta(L-\delta)}. \tag{17}$$

Multiplying the reciprocal of time θ with the thickness of the dry polymer film one gets the solvent mass transfer coefficient k if inequality (13) holds and swelling may be neglected.

$$\frac{L}{\theta} = \frac{DL}{\delta(L-\delta)} \cong k. \tag{18}$$

Multiplying the reciprocal of time θ with the square of thickness L, gives eq. (19).

$$\frac{L^2}{\theta} = \frac{DL^2}{\delta(L-\delta)} = \frac{D}{x(1-x)} \cong \frac{D}{x}, \tag{19}$$

with $x=\delta L^{-1}$.

The analysis of dielectric data with the proposed bulk-skin model is performed only when the polymer film is in the glassy state. The conduction of free ions does not contribute then to the loss factor and the dielectric permittivity is not influenced by electrode polarization. Furthermore, inequality (13) is expected to be true for polymer-solvent combinations. The effective layer thickness in which the dielectric properties

are measured is 7 μm and when film thicknesses exceed ≈ 8 μm the concentration gradient in the layer of 7 μm covering the electrodes can safely be neglected. The measured dielectric properties are then a measure of solvent concentration.

In the glassy state drying is controlled by the diffusion of solvent through the polymer film towards the nitrogen atmosphere. Therefore it is expected that the solvent concentration profiles in the glassy state are the same for all film thicknesses and can be drawn relative to the nitrogen exposed side and the glass plate side of the film. It is expected that solvent mass transfer coefficients in the glassy state increase with decreasing film thickness due to the decrease in the skin layer thickness.

In figures 14 and 15, the mass transfer coefficients of DMF and NMP respectively, are given as a function of the measured dielectric permittivity minus the permittivity of the pure polymer. The latter value has been taken from table 1. The x-axis is a measure for the bulk solvent concentration or volume fraction. The data has been obtained by application of the forementioned procedure on figures 8 and 9.

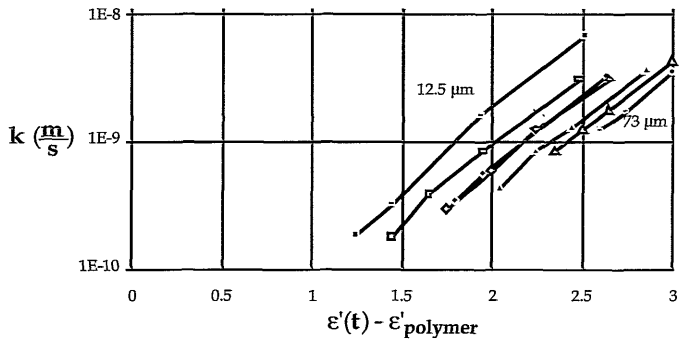

figure 14: Mass transfer coefficient of dimethylformamide in a polyethersulfone film as a function of the measured dielectric permittivity minus the permittivity of the polymer.

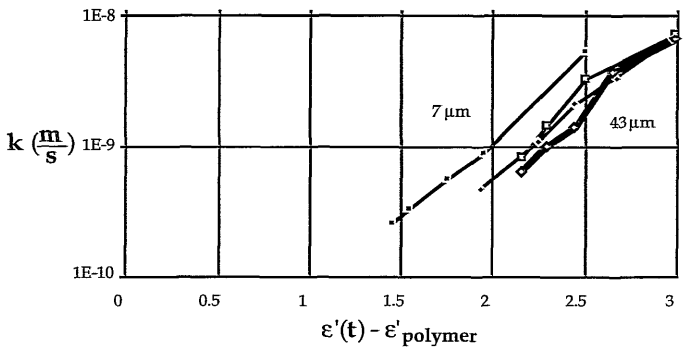

figure 15: Mass transfer coefficient of 1-methyl-2-pyrrolidinone in a polyethersulfone film as a function of the measured dielectric permittivity minus the permittivity of the polymer.

The mass transfer coefficient is decreasing with decreasing concentration. The reason is twofold due to the composite nature of the mass transfer coefficient incorporating an

apparent diffusion coefficient and a thickness. First the ratio of the diffusion coefficients at the nitrogen exposed side and glass plate side will decrease during drying. The transition from skin to bulk layer will become less distinct, resulting in a thicker skin layer. Second the diffusion coefficient will decrease throughout the whole film, and therefore also the apparent diffusion coefficient of the skin layer decreases. The expected thickness dependence of the mass transfer coefficient is shown. A thinner film has a higher solvent mass transfer coefficient at the same concentration or dielectric permittivity at the glass plate side. This is seen most prominently in the experiments with DMF. For NMP the mass transfer coefficient seems to be relatively independent of the film thickness.

The drying process of the polyimide films has been analyzed in the same way. Figures 16 and 17 give the mass transfer coefficients in XU 218 for dimethylformamide and dimethylacetamide respectively. The dielectric permittivity of the pure polymer is assumed to be 3.0. The deviating values in table 1 are probably the result of moisture uptake. Figure 16 represents the mass transfer coefficient of DMF in the polyimide XU 218 as a function of the 'concentration'. The same trend is seen: the smaller the final film thickness the higher is the mass transfer coefficient.

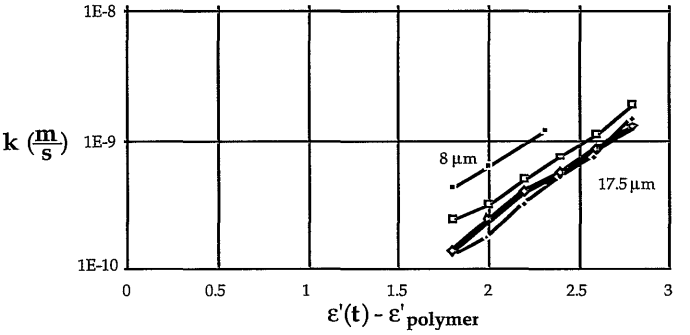

figure 16: Mass transfer coefficient of dimethylformamide in a polyimide XU 218 film as a function of the measured dielectric permittivity minus the permittivity of the polymer.

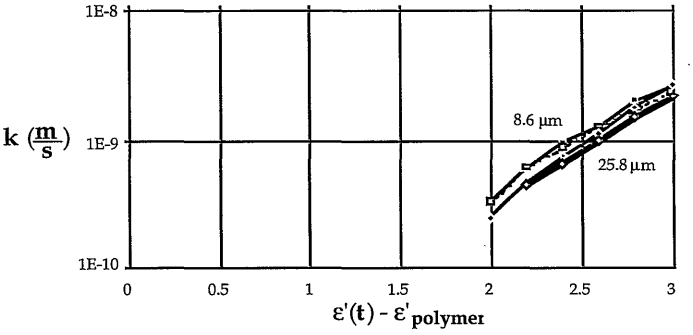

figure 17: Mass transfer coefficient of dimethylacetamide in a polyimide XU 218 film as a function of the measured dielectric permittivity minus the permittivity of the polymer.

In figure 17 the DMAc mass transfer coefficient in XU 218 is given, for the

measurement data presented in figure 11. No strong dependence of the mass transfer coefficient on the polyimide film thickness is noticed.

From figures 14 to 17 it is clear that the solvent mass transfer coefficient is a function of the film thickness. With DMF as a solvent, the increase of the mass transfer coefficient with decreasing film thickness is more pronounced than with NMP and DMAc, the more slowly evaporating solvents. If the solvent concentration profile in the polymer film could be drawn relative to the nitrogen exposed side and the glass plate side, then the parameter $Dx^{-1}(1-x)^{-1}$ in eq. (19) would not be a function of the film thickness. The dimensionless number $x=\delta L^{-1}$ would then be the same for all film thicknesses, and the same apparent diffusion coefficient D could be assigned to the skin layer. For the solvents NMP and DMAc the parameter $Dx^{-1}(1-x)^{-1}$ is slightly decreasing with decreasing film thickness. With the solvent DMF a slight decrease is noticed when decreasing the film thickness down to 15 μm, followed by a rather sharp increase in $Dx^{-1}(1-x)^{-1}$ when further decreasing the film thickness. This is seen with both polyethersulfone and polyimide. In figure 18 the variation of $Dx^{-1}(1-x)^{-1}$ with film thickness is shown for PES/DMF, at a fixed concentration.

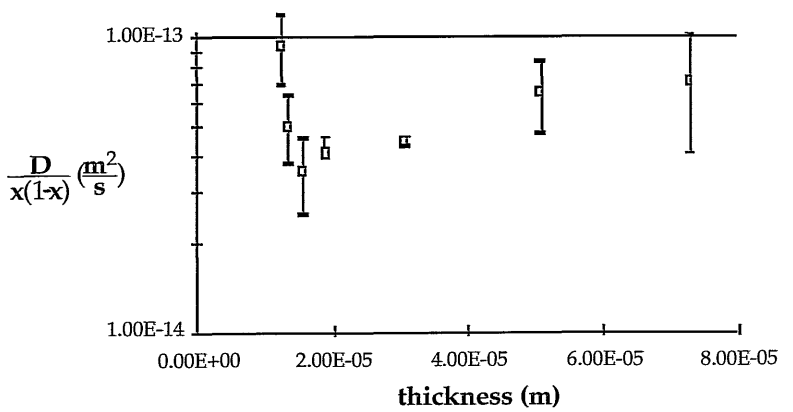

figure 18: $Dx^{-1}(1-x)^{-1}$ versus film thickness for dimethylformamide evaporating from polyethersulfone. Values are taken at a fixed concentration, i.e. measured dielectric permittivity minus permittivity of the pure polymer is 2.5. The errors in $Dx^{-1}(1-x)^{-1}$ result from the error in the film thickness.

As the parameter $Dx^{-1}(1-x)^{-1}$ is not a constant value for all film thicknesses, one might conclude that during the evaporation of residual DMF from thin films the polymer film is not in its equilibrium state. The evaporation is too fast compared to the volume relaxation that has to be realized because of the evaporation.
The ratio x of skin layer thickness and total film thickness is (much) smaller than 1. The apparent diffusion coefficient D in the skin layer is therefore (much) smaller than the depicted values of $Dx^{-1}(1-x)^{-1}$, which in the experiments presented range from 10^{-15} to 10^{-12} m^2s^{-1}.

5.4.3. Determination of diffusion coefficients

In paragraph 5.4.2. the drying of a polymer film has been modelled, and mass transfer coefficients could be calculated from experimental curves of the dielectric permittivity measured as a function of time.

Apart from the mass transfer coefficient, one can also determine diffusion coefficients with dielectric experiments. The mathematics of the diffusion process are known in case a polymer film, initially in an equilibrium state, is exposed to an environment in which the solvent vapour activity is changed stepwise. Assuming a constant diffusion coefficient in the activity range of interest and neglecting swelling effects the corresponding increase/decrease of solvent concentration c(z,t) from the initial concentration c_0 to the final concentration c_1 is given by Crank [22]:

$$\frac{c(z,t)-c_0}{c_1-c_0} = 1 - \frac{4}{\pi}\sum_{n=0}^{\infty}\frac{(-1)^n}{2n+1}\cdot\exp\{\frac{-D(2n+1)^2\pi^2 t}{4L^2}\}\cdot\cos\{\frac{(2n+1)\pi z}{2L}\}, \qquad (20)$$

with $-L \le z \le L$.

Eq. (20) applies to a film of thickness of 2L, and concentration steps are applied at the interfaces z=-L and z=L. There is no concentration gradient at z=0. The agreement with the comb electrode configuration is clear when the electrodes are placed at z=0 and the z-coordinate is limited to $0 \le z \le L$.

For z=0 the cosine term is one. Furthermore, the introduction of a dimensionless time T

$$T = \frac{Dt}{L^2} \qquad (21)$$

will give the following equation:

$$\frac{c(z=0,t)-c_0}{c_1-c_0} = 1 - \frac{4}{\pi}\sum_{n=0}^{\infty}\frac{(-1)^n}{2n+1}\cdot\exp\{-\frac{(2n+1)^2\pi^2}{4}T\}. \qquad (22)$$

Due to the summation of n up to infinity, this equation seems complicated. For large values of T, however, it is accurately described by:

$$\frac{c(z=0,t)-c_0}{c_1-c_0} = 1 - \frac{4}{\pi}\cdot\exp\{-\frac{\pi^2}{4}T\}, \qquad \text{for } T > 0.2. \qquad (23)$$

Rewriting eq. (23) gives:

$$-\frac{4}{\pi^2}\ln\{\frac{\pi}{4}\cdot\frac{c_1-c(z=0,t)}{c_1-c_0}\} = T\ (\equiv\frac{D}{L^2}t), \qquad \text{for } T > 0.2. \qquad (24)$$

In dielectric measurements the concentration is replaced by the measured dielectric

permittivity [21]. Subtracting the dielectric permittivity of the pure polymer like in eq. (16) should be done, but is superfluous.
Plotting the left-hand side of eq. (24) against the experimental time t, a constant slope DL^{-2} is reached after a time $0.2 \cdot L^2 D^{-1}$. From the slope the diffusion coefficient can be calculated when the film thickness L is known.

The sensor layer thickness of the comb-electrodes, i.e. the 7 μm thick layer where the electrode configuration is sensitive to changes in dielectric properties, has been omitted thus far. For z=0.2 L and large T, eq. (23) should be multiplied with $\cos(0.1\pi)$, i.e. 0.951. Putting the sensor layer thickness equal to 0.2 L, the error in using eq. (23) or eq. (24) is smaller than 5%. Film thicknesses should then exceed 35 μm.

In figure 20 an example is given of a measurement in which stepwise changes in solvent activity are applied to a polymer film. Due to the high dipole moment of water and its high diffusion coefficient, changes in activity as small as 0.2 can be applied, without loosing accuracy.

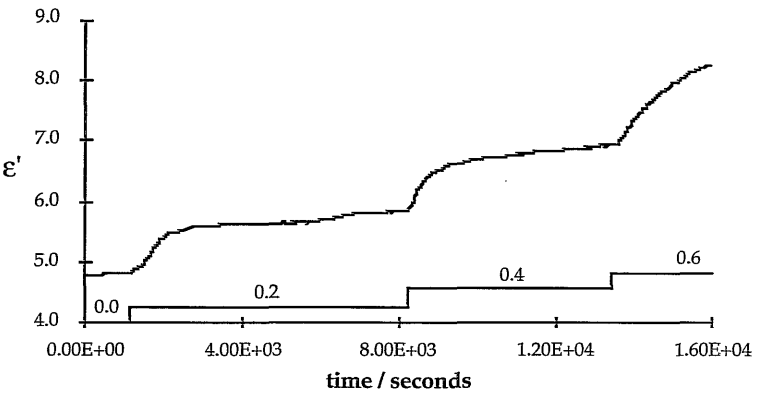

figure 20: Dielectric permittivity of polyimide XU 218 as a function of time, after applying stepwise changes in water vapour activity as indicated. The applied frequency is 1 Hz.

The water activity in figure 20 has been changed from 0.0, to 0.2, 0.4 and 0.6. The frequency of the measurement is 1 Hz, and the film thickness is 46 ± 2 μm. The variation in measured dielectric permittivity with water activity is large, and is due to the high dipole moment of water, and due to the relatively large water solubility in XU 218. This might well confirm the assumption made in table 1 that the unexpected values of the dielectric permittivity of Matrimid 5218, are due to moisture uptake. Due to the high water diffusion coefficient the increase or decrease of dielectric permittivity is also very fast with changes in water activity in the environment. Experimental determination of dielectric properties at laboratory temperature and low frequencies is easily influenced by the relative humidity in the laboratory.
From the data in figure 20 and from other experiments, diffusion coefficients have been calculated using eq. (24), see table 3. The activity has been increased to 0.8 and then decreased again. Near activity 0.8 it is not possible to calculate the diffusion

coefficient. The difference between the reference resistances in the network and the decreased impedance of the comb-electrodes at high water activity has probably become too large for accurate measurements.

table 3:Diffusion coefficients of water in polyimide XU 218 at 30 °C.

activity	diffusion coefficient m^2s^{-1}
$0.0 \rightarrow 0.2$	$2.2\text{-}2.5\ 10^{-12}$
$0.2 \rightarrow 0.4$	$1.7\text{-}2.0\ 10^{-12}$
$0.6 \rightarrow 0.4$	$2.5\ 10^{-12}$
$0.4 \rightarrow 0.2$	$2.0\text{-}2.5\ 10^{-12}$
$0.2 \rightarrow 0.0$	$2.0\ 10^{-12}$

From table 3 one can conclude that the diffusion coefficient of water in XU 218 is not a function of the water activity.
Experiments with stepwise changes in ethanol activity failed. Due to the low diffusion coefficient, variations in lab temperature are interfering with the experiment (see appendix C). In changing the ethanol activity from 0.0 to 0.8 it takes about 8 hours to reach the new stationary state. Calculated diffusion coefficients for ethanol are about ten times lower than the diffusion coefficients for water, and they are not very accurate ($D_{ethanol} \approx 2\text{-}4\ 10^{-13}\ m^2s^{-1}$).

5.5. Discussion

With the comb-electrodes a technique has been found that can monitor the drying of a polymer solution without disturbing the drying process. Due to the internal resistance of the comb-electrodes it is only the final stage of drying that can be followed. A clear transition is noticed on a double-logarithmic plot of dielectric permittivity or loss, versus time. The transition is attributed to the vitrification of the polymer solution near the comb-electrodes. After vitrification drying proceeds at a self-decreasing rate. The rate at which the solvent concentration decreases depends on the diffusion coefficient of the solvent, which in turn depends on the solvent concentration. This circular argument applies, at any time, in the glassy state of a polymer. The power-law coefficient n in eq. (10), determined from the dielectric loss, varies for the polyacrylonitrile/DMF film from 0.5 to 0.7. For the polyethersulfone films with DMF and NMP n varies from 0.4 to 0.7.
The kinetics of the drying process have been modelled in a simple way. Although no information is obtained about the diffusion coefficients involved one can estimate the mass transfer coefficients. In the model swelling is neglected and the concentration gradient needed for evaporation is situated in a relatively thin layer near the

evaporation surface. The mass transfer coefficients are decreasing with bulk solvent concentration. Calculated mass transfer coefficients range from 10^{-10} to 10^{-8} ms^{-1}. These values are lower, as expected, than mass transfer coefficients for liquids in porous media, which roughly vary between 10^{-7} to 10^{-4} ms^{-1} [23].
Due to the large resistance to diffusion at the evaporation interface, one might expect that the concentration profile can be drawn relative to the nitrogen exposed side and the glass plate side, i.e. as a function of the relative height in the polymer film. This idea is rejected by the observation that for the polymer films with DMF the parameter $Dx^{-1}(1-x)^{-1}$ of eq. (19) goes through a minimum. With thin films it is very likely that excess free volume is frozen into the glassy state. Vrentas *et al.* [5] compare the characteristic relaxation time of a material, which is in the glassy state of the order of one hour or more, with a characteristic time of diffusion. When the latter time is small compared to the time of volume relaxation excess free volume is frozen into the polymer material. A global estimate of the characteristic time of diffusion or drying would be given by the ratio of the film thickness and the calculated solvent mass transfer coefficient. The mass transfer coefficient is a measure of the rate of drying and the film thickness is a measure of the volume in which drying has to be realized. With film thicknesses of the order 10 μm and calculated solvent mass transfer coefficients of the order 10^{-9} ms^{-1}, the characteristic time of drying is about 10,000 seconds. This value might well be smaller than the characteristic time of volume relaxation.
The comb electrode configuration can in principle be used to determine diffusion coefficients in the glassy state. In paragraph 5.4.3. a mathematical procedure is given to calculate the diffusion coefficient from the measured dielectric permittivity, neglecting swelling effects and concentration dependence of the diffusion coefficient, within the range of the applied step in solvent activity. The mathematical procedure outlined circumvents the problem of fitting the measured dielectric permittivities to the full summation [21] reproduced in eq. (22). The minimum polymer film thickness required is related to the inter-electrode distance of the comb electrode configuration. A too thin polymer film will give too high diffusion coefficients. This is found in water sorption experiments with a micro-dielectric sensor [21] varying the polyimide film thickness from 20 μm to 90 μm. Material properties are detected with the sensor in the bottom 10 μm [21], so that at least a film of 50 μm was required. The water diffusion coefficient in the aromatic polyimide benzophenone tetracarboxylic dianhydride / oxydianiline (BTDA/ODA), is 2.2 - 4.8 10^{-13} m^2s^{-1}, going in one step from 0 to 90 % relative humidity and back to 0 % relative humidity [21]. This is a factor 5 to 10 lower than the diffusion coefficient of water in polyimide XU 218, presented in this work. The polyimide XU 218 is also a BTDA based polymer but instead of the ODA it contains a diaminophenylindane (DAPI) group. Incorporation of a different group may significantly change polymer densities and glass transition temperatures within one class of polyimides. For 6FDA based polyimides CO2 diffusion coefficients are found to change more than one decade depending on the repeat unit [24]. Comparing the structures of the 6FDA based polyimides with BTDA/ODA and BTDA/DAPI it is expected that the latter has a significantly higher water diffusion coefficient because of the bulky DAPI group decreasing the polymer packing-ability.

5.6. Acknowledgement

A. Kooy of the MESA-institute of the University of Twente is acknowledged for making the comb-electrodes.

5.7. List of symbols

a	surface
c	solvent concentration in polymer film
g	response of dielectric displacement to unit step in electric field
i	imaginary unit
k	geometry factor, or solvent mass transfer coefficient
n	slope in double-logarithmic plot of dielectric permittivity or loss versus time
t	time
x,y,z	directional coordinates
w	weight fraction
e	basic vector of Carthesian system
n	outward normal on surface
α	selectivity
γ	plasticization constant of the diffusion coefficient
δ	skin layer thickness
ε_0	dielectric permittivity of free space
ε^*	complex dielectric constant
ε'	dielectric permittivity
ε''	(total) dielectric loss
θ	time-span
ρ	resistivity
σ	conductivity
ϕ	potential, voltage
ω	angular frequency
A	area of cross-section comb-electrodes
C^*	complex capacitance
I	current
L	length of the needle of an electrode, or total film thickness
N	number of needles of an electrode
Q	charge
R	resistance
S	surface
T	dimensionless time
V	potential, voltage
Z	impedance
D	electric displacement
E	electric field
P	polarization

5.8. References

1. L.C.E. Struik, Physical aging in amorphous polymers and other materials, Elsevier 1978.
2. G.S. Park, The glassy state and slow process anomalies, Diffusion in polymers, ed. by J. Crank, G.S. Park, Academic Press 1968.
3. W.R. Vieth, Diffusion in and through polymers, Principles and Applications, Hanser Publishers 1991.
4. J.W.F. Spitzen, G.H. Koops, M.H.V. Mulder, C.A. Smolders, The influence of membrane thickness on pervaporation performance, Proceedings of third international conference on pervaporation processes in the chemical industry, ed. by R. Bakish, Nancy, France, 1988.
5. J.S. Vrentas, C.M. Jarzebski, J.L. Duda, A Deborah number for diffusion in polymer-solvent systems, AIChE Journal 21 (1975) 894-901.

6. M.E. Rezac, P.H. Pfromm, L.M. Costello, W.J. Koros, Aging of thin polyimide-ceramic and polycarbonate-ceramic composite membranes, Industrial & Engineering Chemistry Research 32 (1993) 1921-1926.
7. L.A. Dissado, R.M. Hill, T.A. Strivens, Power-law decay of conductance during drying of latex paints,J. Phys. D: Appl. Phys. 22 (1989) 713-716.
8. R.M. Hill, L.A. Dissado, T.A. Strivens, Applications of dielectric measurements to studies of latex film formation, Fifteenth International Conference In Organic Coatings Science And Technology, 71-86.
9. S.D. Senturia, N.F. Sheppard Jr., Dielectric analysis of thermoset cure, Adv. Polym. Sci. 80 (1986) 1-47.
10. S.D. Senturia, S.L. Garverick, Methods and apparatus for microdielectrometry, United States Patent, 4423371 (1983).
11. N.F. Sheppard, D.R. Day, H.L. Lee, S.D. Senturia, Microdielectrometry, Sensors and Actuators 2 (1982) 263-274.
12. H. Markovitz, Boltzmann and his superposition principle: centenary observance, Proc. of the VIIth Int. Congress on Rheology, (1976) 37-39.
13. Handbook of Chemistry and Physics, CRC Press, Inc., Cleveland, Ohio.
14. I.M. Kolthoff, J.J. Lingane, Polarography, Interscience Publishers 1952.
15. G. Chiodelli, P. Lupotto, Experimental approach to the impedance spectroscopy technique, J. Electrochem. Soc. 138 (1991) 2703-2710.
16. T.E. Daubert, R.P. Danner, Physical and thermodynamic properties of pure chemicals, Data compilation, Taylor & Francis 1993.
17. Bruker Almanac 1993.
18. S.-G. Li, Preparation of hollow fiber membranes for gas separation, PhD-thesis, University of Twente, Enschede, the Netherlands, 1988.
19. H. Fujita, Diffusion in polymer-diluent systems, Fortschr. Hochpolym.-Forsch. 3 (1961) 1-47.
20. C.M. Hansen, A mathematical description of film drying by solvent evaporation, J. Oil Col. Chem. Assoc. 51 (1968) 27-43.
21. D.R. Day, Moisture monitoring at the PI-SiO2 interface using microdielectric sensors, Polyimides: materials, chemistry and characterization, ed. by C. Feger, M.M. Khojasteh, J.E. McGrath, Elsevier 1989.
22. J. Crank, The mathematics of diffusion, Oxford University Press 1975, Ch. IV, §3.
23. J.A. Wesselingh, R. Krishna, Mass Transfer, Ellis Horwood 1990, Ch. IV.
24. I. Blume, E. Smit, M. Wessling, C.A. Smolders, Diffusion through rubbery and glassy polymer membranes, Makromol. Chem., Macromol. Symp. 45 (1991) 237-257.

Appendix A

The Relation between the Configuration of the Comb-Electrodes and the Measured Capacitance

In figure 1 the cross-section of the comb-electrodes is given. From its geometry it is clear that both the glass and the polymer (solution), will contribute to the measured capacitance.

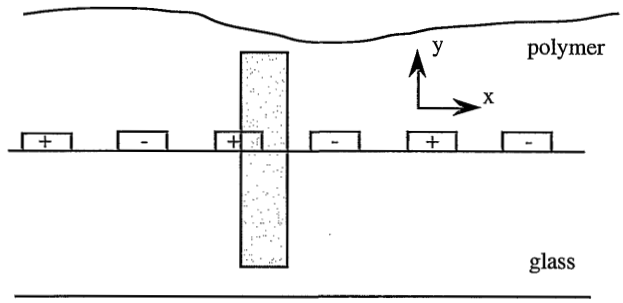

figure 1: Schematically drawn cross-section of the comb-electrodes. The shaded part is the area of interest for the calculation of the geometry factor k.

The relation between the configuration of the comb-electrodes and the capacitance can be derived straightforwardly.
The voltage difference over the electrodes results in an electric field. In vectorial notation omitting the subscript glass or polymer, the following relation is obtained:

$$\mathbf{E}(t) = -\,\mathrm{grad}\,\phi(t), \qquad (1)$$

with $\mathbf{E}(t)$ the electric field and $\phi(t)$ the potential.
The surface integral of the electric displacement $\mathbf{D}(t)$ over one electrode is equal to the time-integral of the current I(t).

$$\int_S \mathbf{D}(t)\cdot\mathbf{n}\,da = \int I(t)dt, \qquad (2)$$

with $\mathbf{n}$ the outward normal on surface S, and area a the variable of integration.
When applying a sinusoidal potential difference to the electrodes the electric field will also be sinusoidal. But in the comb-electrodes configuration the electric field is not only a function of time, but also of the place. Thus:

$$\phi(x,y,t) = \phi(x,y)\cos\omega t. \qquad (3)$$

Application of eq. (3) to eq. (1) will give the components of the electric field in x and y direction.

$$E_x(x,y,t)\mathbf{e}_x + E_y(x,y,t)\mathbf{e}_y = \{-\frac{\partial\phi(x,y)}{\partial x}\mathbf{e}_x - \frac{\partial\phi(x,y)}{\partial y}\mathbf{e}_y\}\cos\omega t. \qquad (4)$$

Here $\mathbf{e}_x$ and $\mathbf{e}_y$ are unit vectors in the x and y direction respectively and ω is the angular frequency of the potential difference applied to the electrodes.
When the Boltzmann superposition principle applies and an isotropic medium is assumed, then the following relation between the Fourier transforms of the electric displacement and electric field holds.

$$\mathbf{D}(i\omega) = \varepsilon_0\varepsilon^*(i\omega)\mathbf{E}(i\omega). \qquad (5)$$

Here i is the imaginary unit, ε_0 the dielectric permittivity of free space and $\varepsilon^*(i\omega)$ the complex dielectric constant.
The amplitude of the Fourier transform of electric displacement in x and y direction respectively, is given by:

$$D_x(x,y) = -\varepsilon_0\varepsilon^*(i\omega)\frac{\partial\phi(x,y)}{\partial x}, \qquad (6)$$

and

$$D_y(x,y) = -\varepsilon_0\varepsilon^*(i\omega)\frac{\partial\phi(x,y)}{\partial y}. \qquad (7)$$

The complex capacity $C^*(i\omega)$ is defined as:

$$C^*(i\omega) = \frac{I(i\omega)}{i\omega V(i\omega)}, \qquad (8)$$

with $V(i\omega)$ the complex potential difference applied to the electrodes and $I(i\omega)$ the complex current to the electrodes.
Application of the Fourier transform to eq. (2), using eqs. (6) and (7), and putting the result in eq. (8), gives:

$$C^*(i\omega) = \frac{2NL\varepsilon_0}{\Delta V}\{-\varepsilon^*_{polymer}(i\omega)\int\frac{\partial\phi_{polymer}(x,y)}{\partial y}dx$$
$$-\varepsilon^*_{polymer}(i\omega)\int\frac{\partial\phi_{polymer}(x,y)}{\partial x}dy+\varepsilon^*_{glass}(i\omega)\int\frac{\partial\phi_{glass}(x,y)}{\partial y}dx\}, \qquad (9)$$

with N the number of needles on one of the two interdigitating combs, L the length of

such a needle, and ΔV the amplitude of the applied potential difference. All three integrals are with respect to the electrode-polymer and electrode-glass interface drawn within the shaded area of figure 1. When the height of the electrodes is neglected the relation between the complex capacitance and the complex dielectric constants is evident.

$$C^*(i\omega) = k\varepsilon_0\{\varepsilon^*_{glass}(i\omega) + \varepsilon^*_{polymer}(i\omega)\}. \tag{10}$$

Here k is a geometry factor with unit length, and equal to:

$$k = \left| \frac{2NL}{\Delta V} \int \frac{\partial \phi_{polymer\ or\ glass}(x,y)}{\partial y} dx \right|. \tag{11}$$

With a computer simulation of the potential distribution in the upper or lower part of the shaded area in figure 1, one can estimate the value of the geometry factor k with the help of eq. (11). For the computer simulation a square grid has been constructed in which every point representing a potential value only depends on the potential of close neighbours according to the Laplace equation thereby neglecting the existence of space charges.

$$\phi(i,j) = \frac{1}{4}\{\phi(i+1,j) + \phi(i-1,j) + \phi(i,j+1) + \phi(i,j-1)\}. \tag{12}$$

The square grid consists of 50 points in the horizontal direction and a variable number of points in the vertical direction. All points have the same distance with respect to their nearest neighbours. The boundary values of this grid together with the direction of the electric field are given schematically in figure 2.

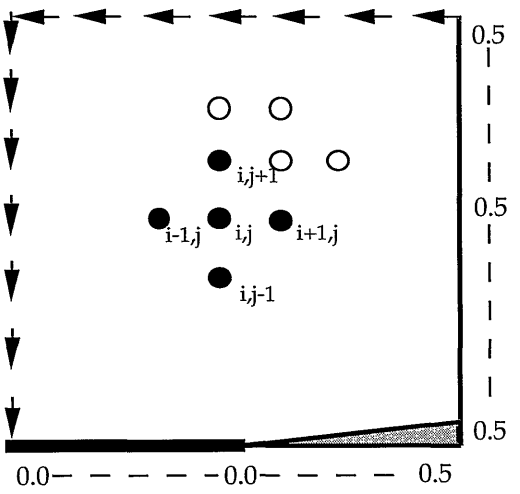

figure 2: The grid used in numerical simulations to estimate the geometry factor k. The numbers denote fixed values for the potential at the boundary and the arrows indicate the direction of the electric field at the remaining boundary.

Because of symmetry arguments the lower boundary covers only half the width of one electrode and half the width of the gap in between the electrodes. The potential at the electrode shown is set equal to 0 and the potential at the other electrode is equal to 1. The potential is 0.5 in the plane that is perpendicular to the x-axis and in the middle of the gap between the electrodes, because of symmetry arguments. The electric field is in the vertical direction in the plane that is perpendicular to the x-axis and in the middle of an electrode. In the plane parallel to, but at a large distance from the plane of the electrodes the electric field is assumed to be horizontal.
The outcome of the numerical simulation is given in figure 3. The geometry factor k has almost approached a final value when 70 data points in the vertical direction are used. This means that with an electrode spacing of 5 μm the minimal layer thickness covering the comb-electrodes, should be 7 μm.

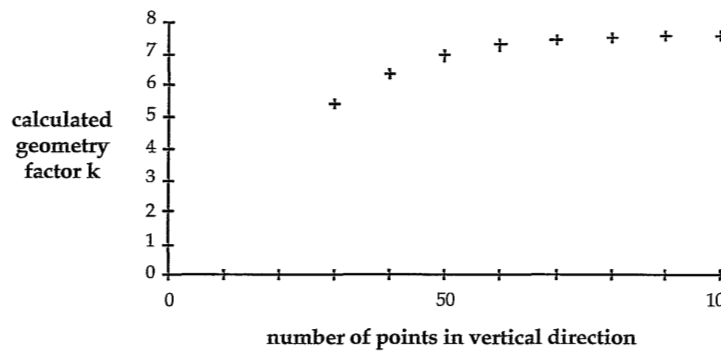

figure 3: Numerically determined geometry factor k as a function of the dimension perpendicular to the plane with the comb-electrodes.

In the figure 4 the potential distribution is shown in a three dimensional plot. The calculation is performed with a grid consisting of 50 points in both x and y direction, using eq. (12) and the boundary conditions as represented in figure 2.

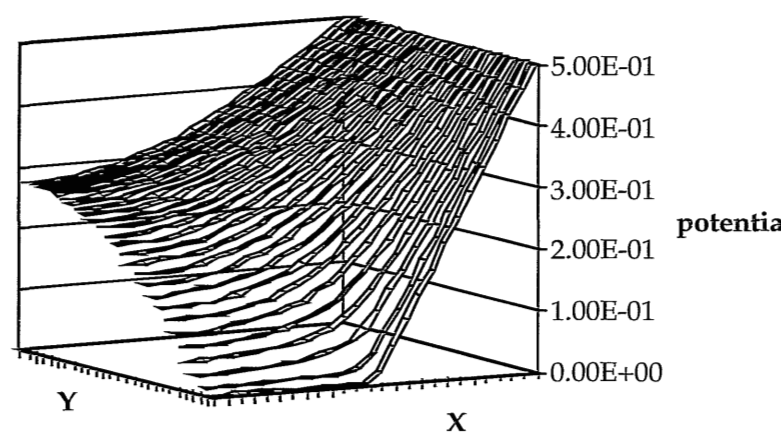

figure 4: The calculated potential distribution in a 50 50 grid. The x-direction is in the plane of the electrodes, the y-direction is out of this plane.*

Appendix B

The Influence of the Resistance in the Comb-Electrodes on the Measured Capacitance

Because of the small thickness of the chromium layer, the impedance of the comb-electrodes is not solely determined by the complex capacitance of the material in between the electrodes but also by the resistance in the electrodes.
The potential is now a function of the distance z along the needle of a comb.

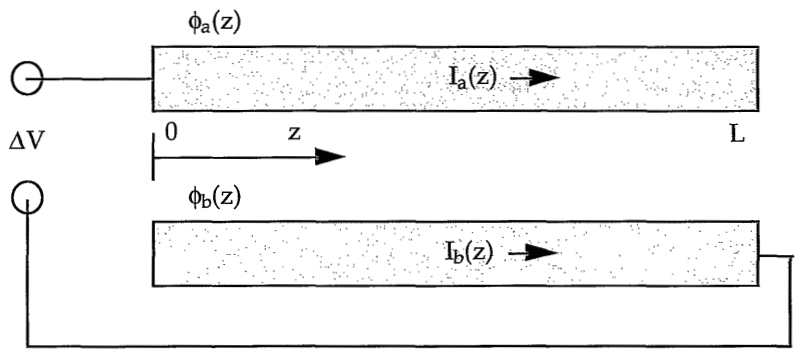

figure 1: Schematically drawn comb-electrodes, defining the potential ϕ and current I as a function of the distance z along the electrode. ΔV is the potential applied to the comb electrode configuration.

The current in the electrode stems from Ohm's law:

$$I_a(z) = -\frac{A}{\rho}\frac{d\phi_a(z)}{dz}, \qquad (1a)$$

$$I_b(z) = -\frac{A}{\rho}\frac{d\phi_b(z)}{dz}, \qquad (1b)$$

with I the current, ϕ the potential, A the total cross-section of one comb in the plane perpendicular to the z-direction and ρ the resistivity of the electrode material. The subscripts a and b indicate which electrode is considered.
The differentiation of eq. (1) with respect to the directional coordinate z gives the change with distance of the current through an electrode and this change is being balanced by the current from one electrode to the other.

$$\frac{dI_a(z)}{dz} = -\frac{A}{\rho}\frac{d^2\phi_a(z)}{dz^2} = -\left(\frac{i\omega C^*}{L}\right)\cdot\left(\phi_a(z)-\phi_b(z)\right). \qquad (2a)$$

$$\frac{dI_b(z)}{dz} = -\frac{A}{\rho}\frac{d^2\phi_b(z)}{dz^2} = -\left(\frac{i\omega C^*}{L}\right)\cdot\left(\phi_b(z)-\phi_a(z)\right). \qquad (2b)$$

Here i is the imaginary unit, ω the angular frequency of the voltage ΔV applied to the electrodes and C^*L^{-1} the complex capacitance of the material in between the electrodes (i.e. both glass and polymer), per unit length.
Combining eqs. (2a) and (2b) gives:

$$\frac{d^2\phi_a(z)}{dz^2} = -\frac{d^2\phi_b(z)}{dz^2}. \tag{3}$$

The solution of eq. (3) contains two constants, k_1 and k_2.

$$\phi_b(z) = -\phi_a(z) + k_1 z + k_2. \tag{4}$$

Owing to the symmetrical structure of the comb-electrodes one can state that

$$\phi_b(z) = \phi_a(0) - \phi_a(L-z), \tag{5}$$

with L the length of the needles that make up the comb electrode configuration. Implicitly $\phi_b(L)$ is defined to be zero.
Eqs. (4) and (5) should be equal for all z-values, therefore:

$$k_1 = \frac{2}{L}(\phi_a(L) - \phi_a(0)), \tag{6a}$$

$$k_2 = 2\phi_a(0) - \phi_a(L). \tag{6b}$$

One can put eq. (4) into eq. (2a).

$$\frac{d^2\phi_a(z)}{dz^2} = \left(\frac{i\omega\rho C^*}{AL}\right)\cdot\left(2\phi_a(z) - k_1 z - k_2\right). \tag{7}$$

For simplicity the term $\sqrt{2i\omega\frac{\rho C^*}{AL}}$ will be called K.
Twice differentiating eq. (7) with respect to z and introducing K, gives:

$$\frac{d^4\phi_a(z)}{dz^4} - K^2\cdot\frac{d^2\phi_a(z)}{dz^2} = 0. \tag{8}$$

The solution for the second derivative of $\phi_a(z)$ then reads:

$$\frac{d^2\phi_a(z)}{dz^2} = k_3\exp(-Kz) + k_4\exp(Kz), \tag{9}$$

with k_3 and k_4 are two integration constants.
Twice integrating eq. (9) and applying eqs. (4) through (6) gives $\phi_a(z)$.

$$\phi_a(z) = \frac{k_3}{K^2}\exp(-Kz) + \frac{k_4}{K^2}\exp(Kz) + \frac{1}{2}k_1 z + \frac{1}{2}k_2. \qquad (10)$$

The constants k_3 and k_4 are found by applying to eq. (10) the following boundary conditions.

$$\phi_a(0) = \Delta V, \qquad (11a)$$

$$\left(\frac{d\phi_a(z)}{dz}\right)_{z=L} = 0. \qquad (11b)$$

The constants k_3 and k_4 are:

$$k_3 = \frac{K}{L}\cdot\frac{(\Delta V - \phi_a(L))}{1-\exp(-KL)}, \qquad (12a)$$

$$k_4 = \frac{K}{L}\cdot\frac{(\Delta V - \phi_a(L))}{\exp(KL)-1}, \qquad (12b)$$

with

$$\phi_a(L) = \Delta V\frac{\exp(KL)-\exp(-KL)}{\frac{1}{2}KL(1-\exp(-KL))(\exp(KL)-1)+\exp(KL)-\exp(-KL)}. \qquad (13)$$

All four integration constants in eq. (10), k1, k2, k3 and k4, are known now. They depend only on the amplitude ΔV and the angular frequency ω of the applied voltage, and on parameters related to the comb-electrodes, which are the area A, length L and resistivity ρ.
In order to determine the impedance of the comb-electrodes the current going from one electrode to the other, due to the applied potential ΔV, is needed.

$$I = \int_0^L -\frac{dI_a}{dz}\,dz = \frac{i\omega C^*}{L}\int_0^L (\phi_a(z) - \phi_b(z))dz =$$

$$i\omega C^*\Delta V\left\{\frac{2(1-\exp(-KL))(\exp(KL)-1)}{KL(\frac{1}{2}KL(1-\exp(-KL))(\exp(KL)-1)+\exp(KL)-\exp(-KL))}\right\}. \qquad (14)$$

The impedance Z is obtained by rewriting eq. (14).

$$Z \equiv \frac{\Delta V}{I} = \frac{1}{i\omega C^*\left\{\frac{2(1-\exp(-KL))(\exp(KL)-1)}{KL(\frac{1}{2}KL(1-\exp(-KL))(\exp(KL)-1)+\exp(KL)-\exp(-KL))}\right\}}. \qquad (15)$$

The term in brackets in eq. (15) is a deviation function and it tells to what extent the resistance of the conducting electrodes influences the measured capacitance. The amplitude and phase of the deviation function have been calculated with:

$\rho_{chromium} = 13 \cdot 10^{-8}\ \Omega m$,
$A = 3.5 \cdot 10^{-10}\ m^2$,
$L = 1.4 \cdot 10^{-2}\ m$.

Instead of a complex capacitance a real capacitance has been taken and its value has been varied from 0.1 nF to 100 nF. In figure 2 the amplitude of the deviation function is given as a function of the frequency and in figure 3 the phase of the deviation function is given as a function of the frequency. The larger the capacitance gets the more the impedance of the pure capacitor approaches the impedance of the resistance in the electrodes.

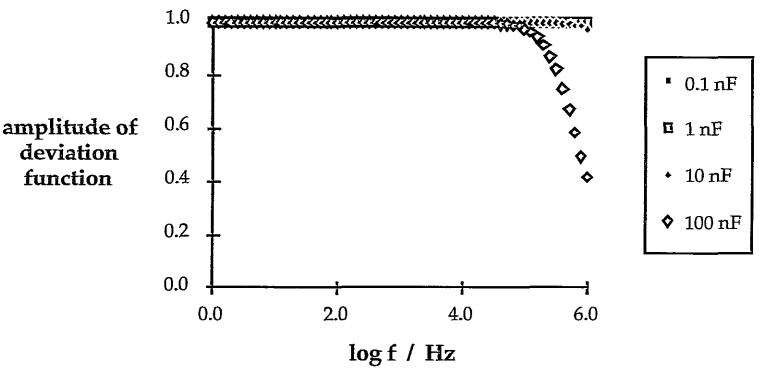

figure 2: Amplitude of the deviation function as a function of the frequency, for various capacitances.

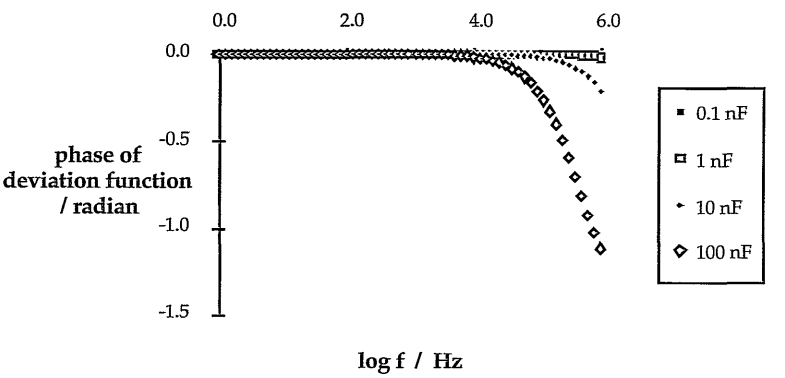

figure 3: Phase of the deviation function as a function of the frequency, for various capacitances.

It is allowed to neglect the resistance of the electrodes only if:

$$2\frac{\rho}{A}L << \left|\frac{1}{\omega C^*}\right|. \qquad (16)$$

With the help of appendix A of this chapter the capacitance of the comb-electrodes is estimated to be 0.5 to 1.0 nF. Investigating materials with a capacitive nature frequencies up to 10000 Hz may be used.

Appendix C

Accuracy of the Measurements with the Frequency Response Analyzer and the Low Frequency Buffers

The dielectric properties of the material under investigation are calculated straightforward from eq. (9) in chapter 4.

$$\varepsilon'_p = \frac{\mathrm{im}\left(\frac{V_1}{V_2}\right)_p - \mathrm{im}\left(\frac{V_1}{V_2}\right)_{N_2}}{\omega R k \varepsilon_0} + \varepsilon'_{N_2}, \qquad (1)$$

and

$$\varepsilon''_p = \frac{\mathrm{re}\left(\frac{V_1}{V_2}\right)_p - \mathrm{re}\left(\frac{V_1}{V_2}\right)_{N_2}}{\omega R k \varepsilon_0}. \qquad (2)$$

Here ε' and ε'' are the dielectric permittivity and loss factor respectively, ε_0 the dielectric permittivity of free space, ω the angular frequency, R the resistance and k the geometry factor of the comb-electrodes. The abbreviations "re" and "im" stand for the real and imaginary parts of the transferfunction defined in eq. (8) in chapter 4. The subscripts p and N_2 indicate polymer and nitrogen respectively. The dielectric loss of nitrogen is assumed to be zero.
One can calculate from eqs. (1) and (2) the maximum error in the dielectric properties if the errors in all the variables appearing in these equations are known.

$$\Delta\varepsilon'_p = \frac{1}{\omega R k \varepsilon_0}\left\{\Delta\mathrm{im}\left(\frac{V_1}{V_2}\right)_p + \Delta\mathrm{im}\left(\frac{V_1}{V_2}\right)_{N_2} + \left|\mathrm{im}\left(\frac{V_1}{V_2}\right)_p - \mathrm{im}\left(\frac{V_1}{V_2}\right)_{N_2}\right| \cdot \left(\frac{\Delta k}{k} + \frac{\Delta R}{R} + \frac{\Delta\omega}{\omega}\right)\right\} + \Delta\varepsilon'_{N_2}, \qquad (3)$$

and

$$\Delta\varepsilon''_p = \frac{1}{\omega R k \varepsilon_0}\left\{\Delta\mathrm{re}\left(\frac{V_1}{V_2}\right)_p + \Delta\mathrm{re}\left(\frac{V_1}{V_2}\right)_{N_2} + \left|\mathrm{re}\left(\frac{V_1}{V_2}\right)_p - \mathrm{re}\left(\frac{V_1}{V_2}\right)_{N_2}\right| \cdot \left(\frac{\Delta k}{k} + \frac{\Delta R}{R} + \frac{\Delta\omega}{\omega}\right)\right\}. \qquad (4)$$

The symbol Δ represents the absolute value of the error in the variable that follows this symbol. In the above analysis the influence of the low frequency buffers on the measurement of the transferfunction $V_1 \cdot V_2^{-1}$ has been omitted.

The dielectric permittivity of nitrogen is taken from literature. The error in its value is

not significant compared to any of the other errors.
The relative error in the geometry factor k, determined from calibration with the Baysilon oil M350 from Bayer is 0.04.
The relative error in the resistance R depends on the resistance used in a specific measurement. The value of R is chosen in such a way that R is of the order of the impedance of the comb-electrodes. A 1GΩ resistor with an accuracy of 0.5% and 22MΩ resistor with an accuracy of 1% have been used.

Errors in the measurement of the transferfunction $V_1 \cdot V_2^{-1}$ and of the frequency are taken from the datasheets of the frequency response analyzer. The frequency error is ±100 ppm. At an ambient temperature of 20 °C ± 10 °C the limit of error in the magnitude of the transferfunction is 0.02 dB and the limit of error in the phase 0.2°.

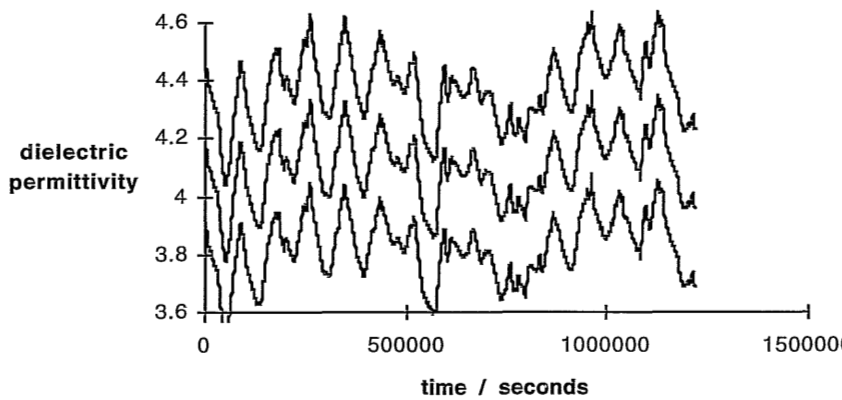

figure 1: The calculated dielectric permittivity of a dry cellulose acetate film.

In order to investigate the influence of the ambient temperature on our experiments the dielectric permittivity has been measured during two weeks at a frequency of 1 Hz. A film of cellulose acetate has been prepared by casting the polymer from a solution with acetone. As no traces of the solvent acetone can be detected the dielectric permittivity should remain constant. In figure 1 the influence of the day-night rhythm of the temperature on the measurements with the frequency response analyzer is clear. The ambient temperature during the experiment varied between 15 °C and 28 °C.
In eqs. (3) and (4) errors in the low frequency buffers have not been taken into account. The equality of the two buffers has been checked by measuring the same potential in an electric network. For frequencies below 10000 Hz the error in the amplitude ratio of V1 and V2 is smaller than 0.5 %, and the phase difference between the two signals smaller than 1 degree.

Chapter 6

Mechanical Properties of a Drying Polymer Film;
measurements with the drying-film torsion-pendulum

6.1. Introduction

In the glassy state material properties depend on the history of the material. If excess free volume is frozen into the structure, for example by quenching the material to a temperature below the glass transition temperature, so-called free volume relaxation or physical aging will take place. The relaxation of excess free volume proceeds at a rate that depends on the amount of free volume [1].
The presence of solvent molecules in the glassy state makes the relaxation processes even more complex. In the preparation of dense membranes of glassy polymers from a polymer solution, changes in the drying process are shown to give different permeation and separation properties [2]. Diffusion of a solvent in a glassy polymer depends on the thermal and/or dissolution history.
In this work the solidification of a drying polymer solution will be investigated. The material property of interest in this chapter is the complex shear modulus. This quantity describes the visco-elastic behaviour of a material, in complex notation. During the evaporation of solvent from a polymer solution, the solution will change from a predominantly viscous state into a glassy state.
Most of the (dynamic) mechanical analyzing techniques available today suited for this purpose, were constructed to follow the curing process of a resin. Techniques as torsional braid analysis and dynamic spring analysis, could not be applied directly in this study, due to the irregular shape of the deposited polymer solution or resin. In torsional braid analysis a braid or fiber is impregnated with the material of interest [3-4]. This apparatus is operated around its resonance frequency. Dynamic spring analysis [5] or dynamic flat-spring analysis [6] is a variant where a spring supports the material. The spring is extended harmonically in forced oscillation. In both torsional braid analysis and dynamic spring analysis, the braid or spring should have a negligible effect on the elastic moduli.
The filmviscometer is based on the rolling ball method [7]. The ball is rolling, due to the gravity, on a tilted, rotating plane on which a film is deposited. One can analyze the effects of temperature and solvent evaporation of films in flat form.
With the impedometer [8] one can monitor the changes during the drying process in a non-destructive way. Shear waves propagate through a quartz crystal to the interface between the crystal and the deposited film. The reflection of the shear wave depends on the mechanical properties of the quartz and the deposited film. Because quartz crystal resonators are used, the frequency of operation is in the megahertz region.
The apparatus that has been used in this work is the drying-film torsion-pendulum. It

has been constructed in the Rheology Group of the Applied Physics Department of the University of Twente, based on their experience with an electromagnetic drive and detection system, developed for a torsion pendulum that can measure the complex shear modulus of liquids [9-10].
In this chapter the mechanical properties of a drying polymer film are discussed. In paragraph 6.2. an introduction will be given to the theory of dynamic mechanical spectroscopy. In paragraph 6.3. the operation mechanism of the drying-film torsion-pendulum will be clarified, and in paragraph 6.4. experiments will be shown on the drying of a cast polymer film. In paragraph 6.5. the results will be discussed.

6.2. Theory of dynamic mechanical spectroscopy

In the first half of the nineteenth century time-dependent mechanical behaviour was determined which could not be explained by the theories of a Hookean solid or a Newtonian fluid. The effect was referred to as "Nachwirkung" or "after-effect". Maxwell introduced the concept of a relaxation time, but it was Boltzmann who proposed that the stresses in a material at a given time depend on the momentary deformation and on the previous deformations. The influence of previous deformations on the momentary stress fades out with time [11].
The time-dependent mechanical behaviour refers to the relaxation behaviour of a material and does not refer to transient diffusion processes or physical aging, in which the material itself is changing with time. Vrentas *et al.* [12] showed that transient diffusion processes and time-dependent mechanical behaviour may interfere.
In case the material does not change in time, the Boltzmann superposition-principle may be applied if the contributions to the momentary stress, of deformations at various times t' can be superposed, i.e. when the material behaves linearly. The shear stress $\tau(t)$ can be written as a convolution, up to time t, of the shear strain $\gamma(t)$ and the time derivative of the relaxation function g(t). The function $\dot{g}(t) \equiv \frac{dg(t)}{dt}$ tells to what extent a previous shear strain contributes to the momentary shear stress.

$$\tau(t) = \int_{-\infty}^{t} \dot{g}(t-t')\gamma(t')dt'. \qquad (1)$$

The relaxation function g(t) is the response of the shear stress to a unit step in shear strain. The time interval of integration in eq. (1) may be extended to infinity, because of the principle of causality. Eq. (1) is brought into the frequency domain with the help of the Fourier transformation.

$$\tau(i\omega) = G^*(i\omega)\gamma(i\omega), \qquad (2)$$

with

$$\tau(i\omega) = \mathbb{F}\{\tau(t)\} = \int_{t=-\infty}^{\infty} \tau(t)\exp(-i\omega t)\, dt, \qquad (3a)$$

$$\gamma(i\omega) = \mathbb{F}\{\gamma(t)\}, \qquad (3b)$$

and

$$G^*(i\omega) = \mathbb{F}\{\dot{g}(t)\} = G'(\omega) + iG''(\omega). \qquad (3c)$$

Here is $\mathbb{F}$ the Fourier transformation operator, i the imaginary unit and ω the angular frequency. $G^*(i\omega)$ is the complex shear modulus, which is the Fourier transform of the relaxation memory function $\dot{g}(t)$. One representation of the complex shear modulus has been obtained by splitting the complex number into a real and an imaginary part with $G'(\omega)$ the storage modulus and $G''(\omega)$ the loss modulus.
Both the storage modulus and the loss modulus, as a function of ω, contain the same information as the relaxation memory function does, i.e. the mechanical relaxation behaviour of the material under investigation. This information can be obtained, for example, by imposing a sinusoidal strain, with angular frequency ω, and measuring the sinusoidal stress in steady-state and by calculating then the complex shear modulus from the phase difference between the two sinusoidal waves, and the ratio of their amplitudes. The determination of the complex shear modulus should be performed as a function of the (angular) frequency of the sinusoidal strain.

6.3. The drying-film torsion-pendulum

Aim of the work described in this chapter is to determine the dynamic mechanical properties of a drying polymer solution, without disturbing the drying process. Both the impedometer and the drying-film torsion-pendulum, furtheron abbreviated as DFTP, are good candidates for this purpose. The former operates at relatively high frequencies, and therefore vitrification of the polymer solution will be noticed in an early stage in the drying process. The inverse of the frequency gives the time-scale of the experiment in which the response of the material will be detected. Increasing the frequency results in a time-scale that may become smaller than the relaxation time of the polymer (solution). The DFTP is designed to operate at lower frequencies. Changes in the glassy state of polymers, if they are present, are possibly seen more pronouncedly.
In this paragraph the construction of the DFTP is described, and the equation of motion for the oscillation of the pendulum is given. When the DFTP is loaded with a film, this affects the equation of motion of the torsion pendulum.

6.3.1. Construction of the drying-film torsion-pendulum

The Rheology Group at the University of Twente developed an electromagnetic drive and detection system for an apparatus that can measure the complex shear moduli of

liquids in the frequency range 80-2500 Hz [9-10]. Based on this drive and detection system the DFTP is constructed. Instead of a liquid it is the drying polymer solution and its substrate that exerts a 'mechanical impedance' onto the motion of the torsion pendulum. In figure 1 the cross-section of the drying-film torsion-pendulum is given schematically.
The apparatus has to be operated near its resonance frequency. When there is no load exposed to the pendulum the resonance curve has a very narrow bandwidth. Due to the presence of the polymer solution, brought into contact with the pendulum with a rubber film acting as intermediate, the resonance frequency will shift away from its original value, and the bandwidth gets larger.

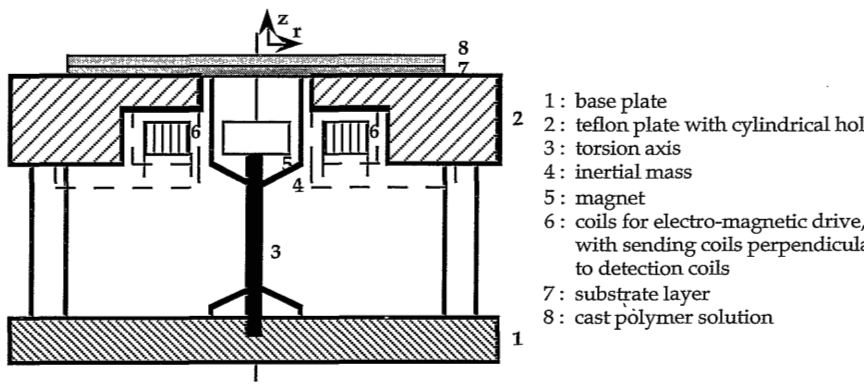

figure 1: Schematic figure of the drying-film torsion-pendulum.

The torsion pendulum essentially exists of an axis, fixed to the base plate. The upper part of the axis is bearing an inertial mass. By oscillations of the inertial mass the axis is twisted between the inertial mass and the non-moving base plate. If the pendulum can oscillate freely, the equation of motion is completely characterized by the values of the stiffness and the damping of the torsion axis, and of the mass inertia of the torsion pendulum. The equation of motion is affected by imposing a load to the pendulum. In paragraph 6.3.2. the definition of the so-called mechanical impedance, will be given. This parameter accounts for the influence of the applied load on the equation of motion.
In figure 2 the electromagnetic drive and detection system is given schematically. The magnet sealed into the inertial mass is set into motion by the electromagnetic drive consisting of two sending coils. When a sinusoidal current is going through the coils a sinusoidal magnetic field will be induced. The magnet in the pendulum will try to oppose this magnetic field. The motion of the pendulum has a high amplitude when the frequency of the magnetic field is near the resonance frequency of the pendulum. Oscillations of the magnet are noticed with two detection coils, placed perpendicular to the sending coils in order to minimize the "cross-talk" between excitation and measuring coils.
The applied torque to the pendulum is proportional to the magnetic field in the sending coils, and thus proportional to the excitation current. The current is measured

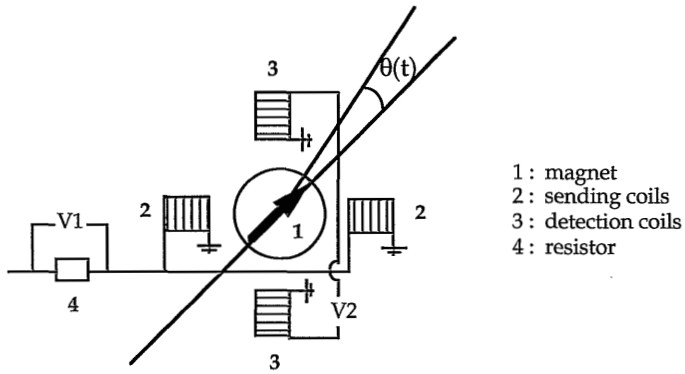

figure 2: Schematic figure of the electromagnetic drive and detection system, and top-view of the drying-film torsion-pendulum. The input signal, a current, is measured by the voltage difference V_1 across a resistor. The output signal V_2 is the induced voltage in the detection coils.

as a voltage drop across a known resistance, placed in series with the sending coils. The induction voltage of the detection coils is proportional to the angular velocity of the inertial mass.

In order to establish a good contact between the pendulum and the rubber film, a vacuum is applied to the upper surface of both the teflon plate and the pendulum. For this purpose the torsion axis is hollow and the upper surface of the inertial mass is porous. In a previous version of the DFTP the upper surface consisted of a metal disk with machine-drilled holes. The new DFTP has an aluminium oxide membrane with a porosity of 50 % and a pore diameter of 0.2 μm. The improved upper surface ensures that the rubber film in contact with the pendulum is perfectly flat. Therefore the drying process can be studied in flat form.

6.3.2. The resonance curve and the mechanical impedance

The equation of motion of the pendulum determines the shape of the resonance curve. This equation is derived from the torque balance of the pendulum, which means that the sum of all torques M(t) equals:

$$\sum M(t) \equiv I\frac{d^2\theta(t)}{dt^2} = M_a(t) - D\frac{d\theta(t)}{dt} - K\theta(t) + M_{load}(t) = 0, \qquad (4)$$

with $M_a(t)$ being the applied torque, I the mass inertia of the pendulum, D the damping and K the spring constant of the axis, and $\theta(t)$ the angle of rotation. $M_{load}(t)$ is the torque imposed by a rubber film onto the torsion pendulum. When the pendulum is not loaded $M_{load}(t)$ is zero.

Eq. (4) is a second order differential equation, which means that there can be a resonance frequency. Due to the low damping of the torsion axis, the resonance curve has a very narrow resonance peak, when the torsion pendulum is not loaded and can

oscillate freely.
It is convenient to write the torque balance as a function of the (angular) frequency instead of the time. The resonance curve described by eq. (4) is obtained then by varying the frequency of the applied torque and monitoring the induced oscillation of the torsion pendulum. Application of the Fourier transform to the equation of motion, eq. (4), is allowed if the mass inertia I, the damping D and the spring constant K are constants.

$$-I\omega^2\theta(i\omega) = M_a(i\omega) - Di\omega\theta(i\omega) - K\theta(i\omega) + M_{load}(i\omega), \qquad (5)$$

with i the imaginary unit, and ω the angular frequency.
The mechanical impedance $Z(i\omega)$ is defined as the negative complex ratio of the torque and the rotational velocity [9,12]. The mechanical impedance is a complex number and can be split into a real and an imaginary part, $R(\omega)$ and $X(\omega)$ respectively.

$$Z(i\omega) \equiv \frac{-M_{load}(i\omega)}{\dot{\theta}(i\omega)} = \frac{-M_{load}(i\omega)}{i\omega\theta(i\omega)} = R(\omega) + iX(\omega), \qquad (6)$$

where $\theta(i\omega)$ is the Fourier transform of $\frac{d\theta(t)}{dt}$, the rotational velocity.
Combination of eqs. (5) and (6) gives:

$$M_a(i\omega) + I\omega^2\theta(i\omega) - (D+R(\omega)+iX(\omega))i\omega\theta(i\omega) - K\theta(i\omega) = 0. \qquad (7)$$

The relation between the mechanical impedance and propagation of shear waves in the geometry of the DFTP will be discussed in the next paragraph and in appendix A. During the drying process of a polymer solution its mechanical properties will change. Therefore the mechanical impedance will change in time. The changing mechanical impedance is noticed as changes in both the resonance frequency and resonance bandwidth.

It is not possible to measure directly the applied torque and the angle of rotation. The applied torque $M_a(t)$ is proportional to the excitation current and therefore proportional to the voltage drop $V_1(t)$ across a small resistance, put in series with the excitation coils (see figure 2).

$$V_1(i\omega) \propto M_a(i\omega). \qquad (8)$$

The induced voltage $V_2(t)$ of the detection coils is proportional to the rotational velocity.

$$V_2(i\omega) \propto i\omega\theta(i\omega). \qquad (9)$$

By the measurement of the transfer function $H(i\omega)$, here defined as the complex ratio of V_2 and V_1, as a function of the angular frequency, the resonance curve is known. The transfer function $H(i\omega)$ is found by combining eqs. (7) through (9).

$$H(i\omega) \equiv \frac{V_2(i\omega)}{V_1(i\omega)} \propto \frac{i\omega}{-I\omega^2 - X(\omega)\omega + K + i\omega(D + R(\omega))}. \qquad (10)$$

The complex transfer function can be split into a real and an imaginary part. For simplicity two real numbers $\chi(\omega)$ and $H_0(\omega)$ [10], which are explained in eqs. (12a) and (12b), are introduced in eq. (11).

$$H(i\omega) \equiv \mathrm{Re}\{H(i\omega)\} + i\,\mathrm{Im}\{H(i\omega)\} = H_0(\omega)\frac{1 - i\chi(\omega)}{1 + \chi^2(\omega)}, \qquad (11)$$

with

$$\chi(\omega) = \frac{I\omega^2 + X(\omega)\omega - K}{\omega(R(\omega) + D)}, \qquad (12a)$$

and

$$H_0(\omega) = \frac{C}{R(\omega) + D}. \qquad (12b)$$

C is a constant depending on the experimental set-up.
Both the real and imaginary part of the transfer function contain, as a function of ω, the same information as the equation of motion, eq. (4).

The resonance frequency of the resonance curve is defined as the frequency where the amplitude of the transfer function $H(i\omega)$ has a maximum value. The real part of the transfer function has the same maximum value at the resonance frequency. The resonance bandwidth is defined as the difference between the two angular frequencies where the amplitude of the transfer function has decreased to a value $\frac{1}{2}\sqrt{2}$ times the amplitude at the resonance frequency. The real part of the transfer function has decreased then to a value $\frac{1}{2}$ times the amplitude at the resonance frequency. When the frequency dependence of the mechanical impedance is negligible near resonance and can be considered a constant, the resonance frequency ω_0 and resonance bandwidth $\Delta\omega$ are given by respectively:

$$\omega_0 = \frac{-X}{2I} + \sqrt{\frac{X^2}{4I^2} + \frac{K}{I}}, \qquad (13a)$$

and

$$\Delta\omega = \frac{R + D}{I} + \sqrt{\frac{(R + D - X)^2}{4I^2} + \frac{K}{I}} - \sqrt{\frac{(R + D + X)^2}{4I^2} + \frac{K}{I}}, \qquad (13b)$$

under the assumption that $R(\omega)$ and $X(\omega)$ are constant.
When no load is imposed to the pendulum, i.e. $R(\omega)$ and $X(\omega)$ are equal to zero, the resonance curve in vacuum or air, is described by the mass inertia I, and the damping D and spring constant K of the torsion axis. The resonance frequency $\omega_{0,\mathrm{vacuum}}$ and resonance bandwidth $\Delta\omega_{\mathrm{vacuum}}$, of the resonance curve, are given by respectively:

$$\omega_{0,vacuum} = \sqrt{\frac{K}{I}}, \tag{14a}$$

and

$$\Delta\omega_{vacuum} = \frac{D}{I}. \tag{14b}$$

The shift of the resonancy frequency ω_0 with the imaginary part of the mechanical impedance X is linear only when the condition $|\omega_0-\omega_{0,vacuum}| << \omega_{0,vacuum}$ is true. The increase of the resonance bandwidth $\Delta\omega$ with the increase of the real part of mechanical impedance R is linear only when the condition $\Delta\omega << \omega_{0,vacuum}$ is true. The real part of the resonance curve is symmetric around the resonance frequency when the latter condition holds.

Ganzevles [14] and Van den Ende *et al.* [10] show that the symmetry of the amplitude of the transfer function round the resonance frequency can get lost if there is "cross-talk" between sending and detection coils. The effect of this cross-talk shows up as an offset in the real and imaginary parts of the transfer function when the frequency dependence of the cross-talk is negligible near resonance. Therefore it is convenient to measure directly the real and the imaginary part of the transfer function instead of its amplitude and phase. The effect of cross-talk between sending coils and detection coils is taken into account by adding two parameters $A_1(\omega)$ and $A_2(\omega)$ to the real and the imaginary part of the transfer function $H(i\omega)$ respectively.

$$Re\{H(i\omega)\} = H_0(\omega)\frac{1}{1+\chi^2(\omega)} + A_1(\omega), \tag{15a}$$

and

$$Im\{H(i\omega)\} = H_0(\omega)\frac{-\chi(\omega)}{1+\chi^2(\omega)} + A_2(\omega). \tag{15b}$$

The cross-talk is a function of frequency, but if the frequency span in an experiment to record the resonance curve is small enough, their variation is negligible within that frequency-span. In the experiments the real part of the resonance curve, Re{H}, is measured and fitted to eq. (15a). Imposing no load to the pendulum, i.e. $R(\omega)$ and $X(\omega)$ equal zero, four parameters are needed to describe the complete resonance curve, $\omega_{0,vacuum}$, $\Delta\omega_{vacuum}$, C and A_1. Knowing these parameters and the mass inertia I of the pendulum the resonance curve of the loaded pendulum is described by R, X and A_1. In a fit the latter three parameters are considered to be constant near resonance.

The resonance frequency of the unloaded pendulum will shift to a lower value by placing a known mass inertia on top of the pendulum, because the total mass inertia of the pendulum is increased. From the shift of the resonance frequency the mass inertia of the pendulum itself has been calculated using eq. (14a). This has been done for two values of added mass inertia.

$$I = (9.7 \pm 0.3)\cdot 10^{-6}\ kgm^2. \tag{16}$$

The resonance frequency appears to depend slightly on the temperature. The torsion axis has been made of Therm-elast 4290 obtained from Vacuumschmelze. Therm-elast 4290 has a shear modulus that is almost temperature independent. The resonance curve has been measured for various temperatures. In figure 3 the real part of the measured resonance curve is given. The full lines are obtained by fitting the measured data to eq. (15a).

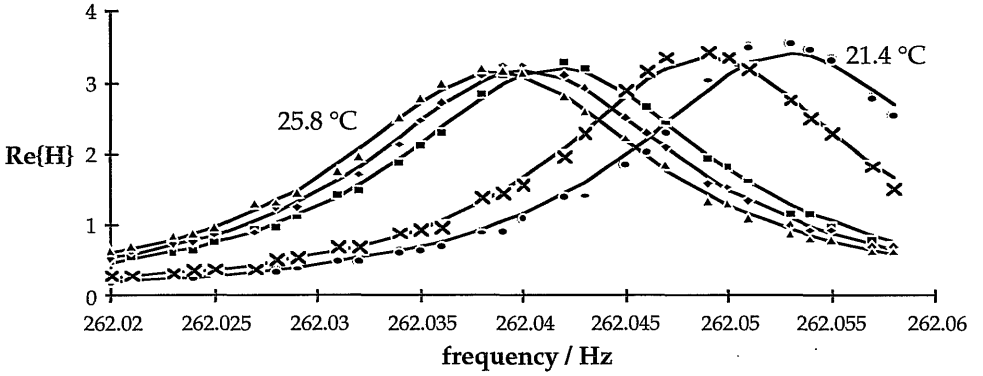

figure 3: The temperature dependence of the real part of the resonance curve. Temperatures from left to right 25.8, 25.0, 24.6, 22.6, 21.4 ^{0}C. Full lines represent fitted curves.

The resonance frequency decreases from 262.053 Hz at 21.4 ^{0}C to 262.039 Hz at 25.6 ^{0}C. In this temperature range the spring constant K of the torsion axis is obtained by combining eq. (12a), with the already obtained mass inertia of the pendulum, result (16), which gives:

$$K = 26.3 \pm 0.8 \text{ kgm}^2\text{s}^{-2}. \qquad (17)$$

The bandwidth of the resonance curve is very small, ranging from 0.018 to 0.020 Hz. The damping D of the torsion axis is calculated by combining eq. (12b) with result (16), and using the experimentally determined resonance bandwidths.

$$D = (1.16 \pm 0.08)\cdot 10^{-6} \text{ kgm}^2\text{s}^{-1}. \qquad (18)$$

6.3.3. The propagation of shear waves

In the previous section the relation between the mechanical impedance and the resonance curve of the torsion pendulum has been established. In this section the relation between mechanical impedance and the viscoelastic properties of the rubber film and the polymer (solution) will be derived. Starting point will be the deformation of a layer at the interface with the pendulum. One can calculate the torque that the pendulum will exert on an infinitesimal small ring of the layer when the latter is being deformed (see figure 4). The ring has a radius r and a thickness dr.

The Fourier transform of the shear stress τ is given by multiplying the complex shear modulus with the Fourier transform of the deformation in the vertical direction, see

eq. (2).

$$\tau(i\omega) = G^*_r(i\omega)\frac{\partial S(i\omega)}{\partial z}, \tag{19}$$

with $S=r\theta$ the linear displacement in θ-direction and G^*_r the complex shear modulus of the rubber film that is in contact with the pendulum. The displacement S is a function of the position, i.e. radius and height, in the rubber film.

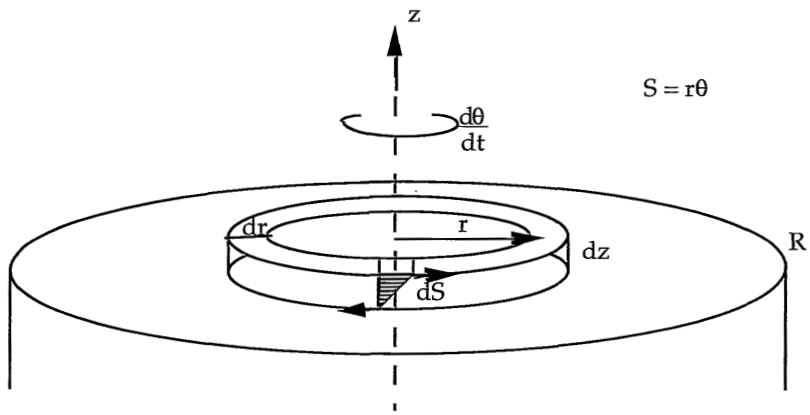

figure 4: Deformation of a small ring of a layer on top of the pendulum, due to the motion of the pendulum.

The shear force is the shear stress, multiplied with the area $2\pi r dr$ on which it is working. The total torque exerted by the pendulum onto the ring, is obtained by multiplying the radius with the negative value of the shear force. Integrating all these contributions from r=0 to r=R, the radius of the pendulum, and dividing the result by the rotational velocity gives the mechanical impedance as defined in eq. (6).

$$Z(i\omega) = -\frac{\int_0^R 2\pi r dr\, r\, G^*_r(i\omega)\frac{\partial S(i\omega)}{\partial z}}{i\omega\,\theta(i\omega)}. \tag{20}$$

In order to know the deformation in the z-direction at the interface of the pendulum and the rubber film, one has to know how the oscillation of the pendulum propagates into the complete rubber film.
In order to find a solution of the displacement as a function of r and z, an approach is used that will take into account the viscoelastic behaviour of a material (see for example ref [15]). The law of conservation of momentum, Cauchy's first law, is applied. The radial velocity v_r and the vertical velocity v_z are zero, because there is only rotation or oscillation around the axis of symmetry. The conservation of momentum is evaluated for the linear velocity v_θ in θ-direction.

$$\rho\frac{\partial v_\theta(r,z,t)}{\partial t}=\frac{1}{r^2}\frac{\partial(r^2\tau_{\theta r}(r,z,t))}{\partial r}+\frac{\partial\tau_{\theta z}(r,z,t)}{\partial z}, \qquad (21)$$

with ρ the density, v_θ the velocity, i.e. the time derivative of the linear displacement $S = r\theta$, τ the shear stress, and r and z the radius and height in the film. In eq. (21) the effect of hydrostatic pressure differences is neglected, and an incompressible fluid or solid is assumed. The explicit dependence of v_θ and τ on r and z will not be indicated for simplicity. The shear stress depends on the history of the deformation rate, analogous to eq. (1). When the relaxation function g(t) is no function of r and z, then eq. (21) becomes:

$$\rho\frac{\partial v_\theta(t)}{\partial t}=\int_{-\infty}^{t} g(t-t')\left\{\frac{1}{r^2}\frac{\partial(r^2\dot{\gamma}_{\theta r}(t'))}{\partial r}+\frac{\partial\dot{\gamma}_{\theta z}(t')}{\partial z}\right\}dt', \qquad (22)$$

where t′ is the time variable of integration. The deformation or strain rates in radial and vertical direction are given by respectively [14]:

$$\dot{\gamma}_{\theta r}(t)=r\frac{\partial(\frac{v_\theta(t)}{r})}{\partial r}, \qquad (23a)$$

and

$$\dot{\gamma}_{\theta z}(t)=\frac{\partial v_\theta(t)}{\partial z}. \qquad (23b)$$

Combination of eqs. (22) and (23) gives:

$$\rho\frac{\partial v_\theta(t)}{\partial t}=\int_{-\infty}^{t} g(t-t')\left\{\frac{\partial^2 v_\theta(t')}{\partial r^2}+\frac{1}{r}\frac{\partial v_\theta(t')}{\partial r}-\frac{v_\theta(t')}{r^2}+\frac{\partial^2 v_\theta(t')}{\partial z^2}\right\}dt'. \qquad (24)$$

The momentary accelaration around the axis of symmetry is known, when the complete history of the angular velocity, as a function of r and z, is known. Eq. (24) has the appearance of a Navier-Stokes equation, but it differs in the history dependence at the right-hand side of the equation.
The time interval of integration may be extended to infinity because of the principle of causality. Eq. (24) can be brought into the frequency domain with help of the Fourier transform.

$$-\omega^2 \frac{\rho}{G^*(i\omega)} = \frac{1}{S(i\omega)} \frac{\partial^2 S(i\omega)}{\partial z^2} + \frac{1}{S(i\omega)} \frac{\partial^2 S(i\omega)}{\partial r^2} + \frac{1}{rS(i\omega)} \frac{\partial S(i\omega)}{\partial r} - \frac{1}{r^2}. \qquad (25)$$

The following two relations have been applied in obtaining eq. (25).

$$\mathbb{F}\{\dot{g}(t)\} = G^*(i\omega) = i\omega\eta^*(i\omega) = i\omega\mathbb{F}\{g(t)\}, \qquad (26)$$

and

$$\mathbb{F}\{v_\theta(t)\} = v_\theta(i\omega) = i\omega S(i\omega) = i\omega\mathbb{F}\{S(t)\}, \qquad (27)$$

where $\mathbb{F}$ represents the Fourier transformation and $\eta^*(i\omega)$ the complex shear viscosity. Eq. (25) contains the solution to the propagation of shear waves in the rubber film on top of the torsion pendulum. The angular displacement, as a function of ω, depends on the complex shear modulus and density of the rubber film, and it depends on the geometry of the DFTP. There does exist an analytical solution for the angular displacement as a function of radius r and height z, if appropriate boundary conditions are known.
The rubber film that is in direct contact with the torsion pendulum is only an intermediate with the purpose to support the cast polymer solution. Shear waves do not propagate only into the rubber substrate, but also into the polymer solution or polymer film on top of the substrate. Therefore two Fourier transformed "Navier-Stokes" equations are encountered. Both take the form of eq. (25). There are two additional boundary conditions for the propagation of shear waves at the interface between substrate and polymer solution. A further discussion is given in appendix A.

If one assumes a radial propagation of shear waves, and gap-loading of these shear waves (shear waves are not damped before reaching the teflon plate), then it is found in appendix A that the mechanical impedance is directly proportional to the height of a layer, and almost proportional to the complex shear modulus and the reciprocal angular frequency. The ratio of the loss modulus and the storage modulus is almost proportional to the ratio of the real and the imaginary part of the mechanical impedance. The density will have hardly any effect.

6.4. Experiments with the drying-film torsion-pendulum

The Solartron 1255 Frequency Response Analyzer (FRA) supplies the input current to induce a sinusoidal magnetic field in the sending coils of the DFTP. The FRA measures the input current by the voltage drop across a resistance in the input circuit, and measures the output voltage of the detection coils. A computer program controls the FRA via an IEEE-488 interface bus, and keeps track of the position of the resonance curve in time. This has been accomplished by continuously sweeping back and forth the frequency signal through the resonance curve, instead of using a random

frequency excitation source [16]. It takes two to three minutes to record one resonance curve. Each resonance curve has a frequency span twice the apparent resonance bandwidth, and consists of 21 equidistant frequencies. The position of the maximum, the apparent resonance frequency, can be determined with an accuracy equal to the frequency step in measuring the transfer function $H(i\omega)$. The apparent resonance bandwidth is determined by the two frequencies where the real part of the transfer function has decreased to half the value corresponding to the apparent resonance frequency. Both the apparent resonance frequency and the apparent bandwidth are determined without fitting the measured transfer function to eq. (15) by assuming that the real part of the resonance curve is symmetric around the measured maximum and by assuming that the mechanical impedance and the offset are constant within the recorded resonance curve. In a mathematically simple way the computer program can calculate then the position of the resonance curve. All resonance curves are recorded for later analysis.
An experiment is started after casting a polymer solution on a suitable substrate. Drying proceeds at lab temperature and in a nitrogen atmosphere.

6.4.1. Preparation of rubber substrates

In the experiments a substrate is needed to support the cast polymer solution. This substrate should meet three criteria.
- The substrate may not swell, neither dissolve, in the solvent of the polymer solution.
- The polymer solution has to wet the substrate.
- The contribution of the substrate to the mechanical impedance has to be negligible, and the propagating shear waves in the substrate should not be damped before reaching the polymer solution.

The combination of the three constraints is hard to fulfil, and this is the main reason why it is difficult to operate the DFTP. The most important constraint is the negligible contribution of the substrate to the mechanical impedance and its low damping, because otherwise the presence of a polymer solution or film on top of the substrate is not noticed at all.
A rubber film has a relatively low shear modulus and therefore its contribution to the mechanical impedance is small. Two substrates have been made, one is a polydimethylsiloxane and the other one a polyurethane. Both substrates are crosslinked.
A polydimethylsiloxane (PDMS) substrate is prepared by mixing the RTV 615A silicone rubber compound and the RTV 615B silicone curing agent obtained from General Electric in a ratio of 10 to 1 by weight. The mixture is cast on a perspex plate using a casting knive with a 200 μm slit. The perspex plate is placed in an oven at 80 °C for at least three hours. The fully crosslinked PDMS film is lifted from the perspex plate using the capillary force of ethanol.
The thickness of the cured film has been measured by examination of gold-sputtered cross-sections with a JEOL T220A electron microscope. The thickness varies from 120 and 125 μm.

The shear modulus G' of the PDMS film described above is calculated applying the following equation:

$$G' = \frac{\rho RT}{M_e}, \qquad (28)$$

with ρ the density, R the gas constant, T the absolute temperature and M_e the molecular weight between entanglements or crosslinks.
The density of PDMS hardly depends on the crosslink density and is approximately $0.98 \cdot 10^3$ kgm^{-3}. The molecular weight between the crosslinks has been determined by Blume *et al.* using swelling experiments [17]. The value of 1200 $gmol^{-1}$ has been compared with the results obtained by Van den Brule [18], correlating the shear modulus and the molecular weight between the crosslinks. The calculated shear modulus is $2 \cdot 10^6$ Nm^{-2}.
A polyurethane (PUR) substrate is made by dissolving 7.5 gram urethane compound in 30 ml dimethylformamide. The Estane 5722 urethane compound, from BF Goodrich, is based on a polyester. After dissolving the polymer, 0.75 gram toluene di-isocyanate is added. The solution is cast, with an intial thickness of 300 μm, onto a glass plate. After evaporation of the solvent, the PUR film is cured overnight. The PUR substrate has a final thickness of 31.7 ± 1.3 μm, as measured with a Mitutoyo screw micrometer. A typical value for the tensile strength, as given by the manufacturer, is 60.7 N mm^{-2}.

6.4.2. Mechanical experiments

The DFTP has been designed to induce shear waves in the radial direction. Due to its design, there must be a deformation in the vertical direction. Mathematically the mechanical impedance is calculated from the deformation in vertical direction, although it results from the propagation of shear waves in both radial and vertical direction. In order to know the extent of the deformation of the rubber substrate between the torsion pendulum and a film with a high modulus on top of the substrate, the following experiments have been performed.
The resonance curve of the DFTP loaded directly with only a polyethylene film, has been compared with the resonance curve of the DFTP loaded with a PDMS substrate and the same polyethylene film on top of the PDMS. The same procedure has been performed with a polyester film. The thickness of the polyethylene film, given by the manufacturer, is 15 μm, and the thickness of the polyester film, measured with a screw micrometer, is 20 μm. Polyethylene is a partially crystalline polymer. The amorphous part has a glass transition temperature well below room temperature. The amorphous polyester is in the glassy state. The shear modulus of polyethylene will therefore be much smaller than the shear modulus of the polyester. Results of the comparison between PDMS-supported and non-supported polyethylene and polyester films are shown in table 1. The resonance frequency and bandwidth of the unloaded pendulum and the pendulum loaded with a PDMS film only, are given as well. The values corresponding to the PDMS film are determined for various films prepared by the procedure outlined before.

table 1: Comparison of the resonance curves of a polyethylene and polyester film, supported by a PDMS substrate, or directly placed on top of the drying-film torsion-pendulum. The resonane frequency and bandwidth of the unloaded pendulum and the pendulum loaded with a PDMS film are given as reference.

	resonance frequency Hz	resonance bandwidth Hz
PDMS + polyethylene	294.0	6.5
polyethylene	295.3	6.5
PDMS + polyester	447	23
polyester	608	12
PDMS	263.9 ± 0.4	0.7 ± 0.1
no load	262.045 ± 0.010	0.019 ± 0.001

If one compares the resonance frequencies of a film with and without the PDMS substrate, then the resonance frequency is higher when there is no PDMS layer. This is not expected in case there is a purely radial deformation, because any added layer will increase the mechanical impedance, and must therefore result in an increase of the resonance frequency.

The polyester film imposes a higher mechanical impedance onto the pendulum compared to the polyethylene film, as expected from its larger shear modulus and larger film thickness. Experimentally this is noticed as a shift from the resonance curve to higher frequencies. Placing then the polyester film on top of the PDMS is almost like placing a fixed wall close to the pendulum. This apparently fixed wall is closer to the pendulum than the teflon plate, being a real, fixed wall; the distances are respectively 120 - 125 μm and 0.3 cm. There must be a deformation in the vertical direction, between the pendulum and the polyester, followed by the radial deformation of the polyester in the gap between the pendulum and the teflon plate. The maximum amplitude of rotation in the polyester has decreased substantially compared to the corresponding amplitude of the pendulum, as seen from the large discrepancy in the resonance frequencies of the unsupported and supported polyester film. A purely vertical deformation results in a lower resonance frequency, because that situation is comparable to placing films only on top of the pendulum, thereby increasing the mass inertia of the pendulum.

The same argument applies to the experiments with the polyethylene film. The deformation in the vertical direction is not so large, because the difference in shear modulus of PDMS and polyethylene is small compared to the difference in shear modulus of the same PDMS and polyester.

Comparing the respective bandwidths of polyester in table 1 makes no sense, because at these high frequencies and with the large resonance bandwidths, the offset A_1 in eq. (15a) cannot be considered a constant anymore. Within the frequency span needed to record the resonance curve, i.e. twice the apparent resonance bandwidth, the offset A_1 is a function of the frequency. The same applies to the mechanical impedance.

Although it is a function of the frequency, it has been assumed to be a constant in deriving the resonance frequency and resonance bandwidth, eqs. (13a) and (13b). The latter assumption only holds when a small frequency span is needed to record the resonance curve and therefore the frequency dependencies of A1, R and X become noticable with a larger bandwidth of the resonance curve.
Both the offset due to "crosstalk" between sending and detection coils, and the real and the imaginary part of the mechanical impedance, depend on the (angular) frequency. Therefore no good fit of the resonance curve can be obtained using eq. (15a), when the frequency span needed to record the resonance curve is too large. It is not even correct to perform a fit, because in deriving this equation both the offset due to "crosstalk" and the mechanical impedance were assumed to be constant!

When the frequency dependence of the mechanical impedance and the offset is not present, i.e. when the bandwidth of the resonance curve is small enough, one can calculate the mechanical impedance from the apparent resonance frequency and apparent bandwidth determined by the computer program that keeps track of the position of the resonance curve. This calculation is done straightforwardly by fitting the measured resonance frequencies and bandwidths to the following equations that are found by combining eqs. (13) and (14).

$$\omega_0 = \frac{-X}{2I} + \sqrt{\frac{X^2}{4I^2} + \omega_{0,\text{vacuum}}^2}, \tag{29a}$$

and

$$\Delta\omega = \Delta\omega_{\text{vacuum}} + \frac{R}{I} + \sqrt{\frac{(R+I\Delta\omega_{\text{vacuum}}-X)^2}{4I^2} + \omega_{0,\text{vacuum}}^2} - \sqrt{\frac{(R+I\Delta\omega_{\text{vacuum}}+X)^2}{4I^2} + \omega_{0,\text{vacuum}}^2}. \tag{29b}$$

Here $\omega_{0,\text{vacuum}}$ and $\Delta\omega_{\text{vacuum}}$ are the measured resonance frequency and resonance bandwidth of the unloaded pendulum and I is the mass inertia of the pendulum which is given in eq. (16).
Due to the geometry of the DFTP it is expected that shear waves are propagating in the radial direction when the pendulum is loaded with one film only. The mechanical impedance calculated from measured resonance curves can be compared to the derived analytical solution, eqs. (14) and (15) in appendix A of this chapter. The comparison is allowed when the above equations are corrected for the additional inertial mass due to that part of the film that is directly on top of the pendulum.

$$I_{\text{rad}} = I + \frac{1}{2}mR_i^2 = I + \frac{\pi}{2}\rho_{\text{film}}h_{\text{film}}R_i^4. \tag{30}$$

The subscript "rad" means that a radial deformation in the gap between torsion pendulum and teflon plate is assumed. I is the mass inertia of the bare pendulum, m

the mass of the film on top of the pendulum that contributes to the additional mass inertia of the pendulum, ρ_{film} and h_{film} the density and thickness of the film respectively and R_i the radius of the pendulum.
Assuming radial deformation the real part R_{rad} and the imaginary part X_{rad} of the mechanical impedance are determined by fitting the measured data in table 1 to the following equations that account for the additional mass inertia.

$$\omega_0 = \frac{-X_{rad}}{2I_{rad}} + \sqrt{\frac{X_{rad}^2}{4I_{rad}^2} + \frac{I}{I_{rad}}\omega_{0,vacuum}^2}, \qquad (31a)$$

and

$$\Delta\omega = \frac{R_{rad} + I\Delta\omega_{vacuum}}{I_{rad}} + \sqrt{\frac{(R_{rad}+I\Delta\omega_{vacuum}-X_{rad})^2}{4I_{rad}^2} + \frac{I}{I_{rad}}\omega_{0,vacuum}^2}$$

$$- \sqrt{\frac{(R_{rad}+I\Delta\omega_{vacuum}+X_{rad})^2}{4I_{rad}^2} + \frac{I}{I_{rad}}\omega_{0,vacuum}^2}. \qquad (31b)$$

In table to 2 the real and imaginary part of the PDMS and polyethylene film are calculated applying both eq. (29) and eq. (31) to the data presented in table 1. The densities of PDMS and polyethylene used in the calculations are $0.98 \cdot 10^3$ kgm^{-3} and $0.93 \cdot 10^3$ kgm^{-3} respectively. The corresponding thicknesses are 122.5 μm and 15 μm.

table 2: Calculation of real and imaginary part of the mechanical impedance of a typical PDMS film and a polyethylene film. The impedance is calculated applying eq. (29) or eq. (31). For explanation see text.

	mechanical impedance (eq. (29))		mechanical impedance (eq. (31))	
film	R kgm^{2}s^{-1}	X kgm^{2}s^{-1}	R_{rad} kgm^{2}s^{-1}	X_{rad} kgm^{2}s^{-1}
PDMS	$4.1 \cdot 10^{-5}$	$-2.3 \cdot 10^{-4}$	$4.1 \cdot 10^{-5}$	$-2.4 \cdot 10^{-4}$
polyethylene	$3.5 \cdot 10^{-4}$	$-3.8 \cdot 10^{-3}$	$3.5 \cdot 10^{-4}$	$-3.8 \cdot 10^{-3}$

There is a discrepancy between the mechanical impedance determined from eq. (29) and the mechanical impedance determined from eq. (31) when the deformation in the gap is not so large, as in the case with PDMS. The values of R_{rad} and X_{rad} in table 2 may be fitted to eqs. (14) and (15) in appendix A of this chapter which represent the analytical solution to the propagation of shear waves in the radial direction.
For PDMS the calculated storage modulus G' is $4.3 \cdot 10^5$ Nm^{-2} and the loss modulus G'' is $7.4 \cdot 10^4$ Nm^{-2}. The storage modulus is almost a factor 5 too low compared to the

estimated value of $2 \cdot 10^6$ Nm^{-2}. This might be due to the fact that there is deformation in the vertical direction, of the PDMS that covers the pendulum and the teflon plate. The loss modulus of PDMS is certainly overestimated because in ref. [18] the measured shear moduli of crosslinked PDMS vary only 1% or even less when the frequency of the measurement is changed from 1 rad/s to 100 rad/s. This means that the ratio of the loss modulus and storage modulus must be much smaller than 1 in that frequency range. This is certainly not the case in our analysis.
For polyethylene a storage modulus G' of $6.2 \cdot 10^7$ Nm^{-2} and a loss modulus G'' of $5.7 \cdot 10^6$ Nm^{-2} is calculated. The value of G' seems reasonable and compares to tensile moduli of medium density polyethylenes reported in ref. [19]. Again a relatively large and propably overestimated loss modulus is calculated which indicates that the analysis of the resonance bandwidth of the DFTP does not give reliable information.

Drying polymer films

Describing experiments with polymer solutions, the resonance frequency will be recorded as a function of drying time. As a rule of thumb one can state that as the resonance frequency shifts to higher frequencies, the impedance imposed to the pendulum increases.

Due to problems with the wettability of the PDMS and PUR films, only a limited number of experiments have been carried out. Three systems have been investigated. The first system is a polyvinylalcohol solution in water. Polyvinylalcohol is a good film-forming polymer. The second system is a solution of polyacrylic acid in water. This polymer cannot be used to obtain a thin film with sufficient strength to handle. Both polymers have a tendency to form a gel, thereby reducing a fast recession of the polymer solution from the rubbery substrate. The third system is a water-thinnable paint of unknown composition.
The experiments with polyvinylalcohol and polyacrylic acid have been performed using the PUR film as a substrate. This film has a more hydrophilic character compared to the PDMS film. The same PUR film is used for all the experiments. The dry polyvinylalcohol film can be peeled off the PUR film and the polyacrylic acid layer is removed by rinsing the composite with warm water. The paint has been cast onto a PDMS film.

A solution of 2 wt.% polyvinylalcohol in demineralized water has been prepared. The polyvinylalcohol, with a 88 % degree of hydrolysis, has been obtained from Aldrich. The molecular weight is $96 \cdot 10^3$ $gmol^{-1}$. The solution does not have a high viscosity and has the tendency to retract into a drop. After casting the solution a glass ring is placed on top of the solution to prevent flow in the plane of the solution. Three different casting knives have been used. The slit heights are 50, 100 and 200 μm.
In figure 4 the drying of the polymer solution is followed by monitoring the change in the apparent resonance frequency of the DFTP. The resonance frequency increases with increasing mechanical impedance. The resonance frequency shown represents the raw

data as obtained by the computer program. It gives the point of the maximum in the real part of the transfer function. The position of this maximum can only be determined with an accuracy equal to the frequency step in recording the resonance curve. With increasing apparent bandwidth of the resonance curve, the accuracy of the resonance frequency becomes less. In the lowest curve of figure 4 the bandwidth of the resonance curve is much smaller compared to the bandwidth of the upper two curves, and therefore the lowest curve looks much smoother.
The resonance curves start at 310 ± 15 Hz, because in the first moments the mechanical impedance is governed by the impedance of the PUR film. After a relatively short time the resonance frequency increases sharply, and this can be attributed to the solidification of the polyvinylalcohol/water solution. From this time on one can peel a coherent polyvinylalcohol film off the substrate. In the solidified state the resonance frequency is not increasing significantly.

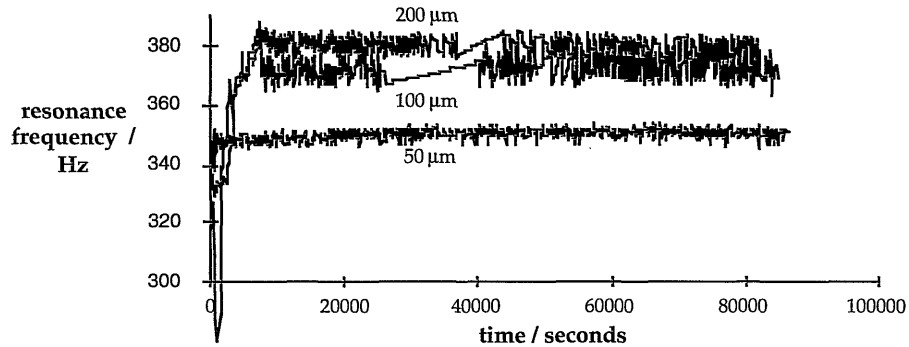

figure 4: Change of resonance frequency in time during the evaporation of water from a solution with polyvinylalcohol. Casting thicknesses from bottom to top 50, 100, and 200 micron.

In table 3 both the resonance frequency and the resonance bandwidth are given for the curves in figure 4. A comparison is made at 10.000 and 80.000 seconds after casting the polymer solution. The values of the apparent resonance frequency are given in a range of 2000 seconds around the times mentioned, because the resonance frequency is determined with a limited accuracy. No distinct changes are seen between the resonance frequencies at 10.000 seconds and the corresponding resonance frequencies at 80.000 seconds.
The resonance frequency in the solidified state increases with an increasing casting thickness of the polymer solution, due to the higher mechanical impedance. For the casting thickness of 50 µm, no final film thickness could be determined. For the casting thicknesses of 100 and 200 µm, the final film thicknesses are 3.6 ± 2.6 µm and 5.3 ± 3.3 µm respectively.

table 3: Resonance frequency and bandwidth at two different times after casting polyvinylalcohol/water solutions with various casting thicknesses.

casting thickness µm	time seconds	resonance frequency Hz	resonance bandwidth Hz
50	10000	346 - 350	29 - 36
	80000	349 - 352	27 - 36
100	10000	365 - 377	126 - 142
	80000	367 - 380	137
200	10000	377 - 386	72 - 89
	80000	376 - 384	77 - 100

The DFTP is already sensitive to relatively thin films of a glassy polymer. An increase in the mechanical impedance by increasing the final film thickness would even further increase the resonance frequency. This in turn would make the experiments less accurate because of the lower amplitude of the torsion pendulum and a correspondingly lower signal to noise ratio. The broader bandwidth implies a stronger dependence of both the mechanical impedance and the offset on the frequency within the frequency span of the experiment.

For the following experiments, a solution of 2 wt.% polyacrylic acid in demineralized water has been prepared. Polyacrylic acid has been obtained from Aldrich, and has a molecular weight of $3 \cdot 10^6$ $gmol^{-1}$ and a Tg of 106 °C. The solution as prepared has already formed a gel. Upon casting this solution on the PUR substrate, hardly any recession will take place. The cast solution has a smooth appearance.
In figures 5 and 6 the change in resonance frequency is given as a function of the drying time. Casting knives with various slits have been used. Slit heights larger than 200 µm resulted, after vitrification, in the curling of the PUR - polyacrylic acid composite, thereby reducing the mechanical impedance to the pendulum. Therefore only experiments with relatively small casting thicknesses can be shown. In figure 5 the casting thickness of the polyacrylic acid/water solution has been varied from 100, 150 to 200 µm.
Like in the experiments with polyvinylalcohol, a sharp increase in the resonance curve depicts the solidification of the polymer solution. However, with polyacrylic acid a small but significant increase in resonance frequency can be seen in time, after the vitrification of the solution. The increase of the resonance frequency implies that the mechanical impedance is increasing in the glassy state. When a radial propagation of shear waves is assumed in the polyacrylic acid film, this can be due to an increase of the complex shear modulus of the vitrified film, and/or an increase of the film thickness (see appendix A). The latter condition is rejected, and therefore the complex shear modulus is still increasing.

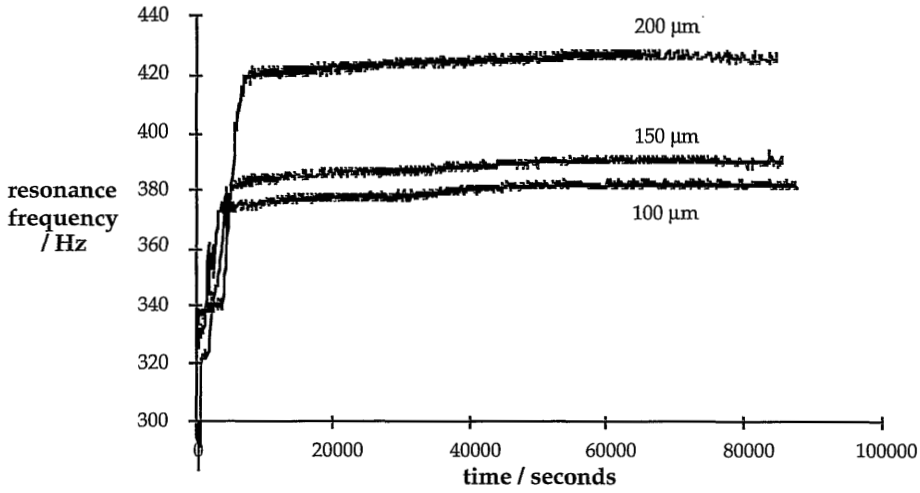

figure 5: Change of resonance frequency in time during the evaporation of water from a solution with polyacrylic acid. Casting thicknesses from bottom to top 100, 150 and 200 µm.

The measured resonance curves indicate that not the macroscopic strength of the deposited 'film' determines the imposed mechanical impedance, since polyacrylic acid is not a film-forming polymer, but the complex shear modulus, being an intrinsic material property.
Unfortunately the final film thicknesses of polyacrylic acid could not be determined.

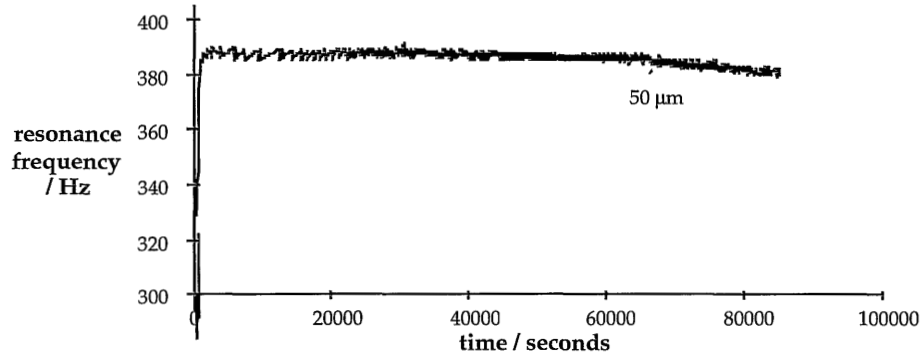

figure 6: Change of resonance frequency in time during the evaporation of water from a solution with polyacrylic acid. Casting thickness 50 µm.

In figure 6 the casting thickness of the polyacrylic acid/water solution has been lowered to 50 µm. In this figure another trend is seen, compared to figures 4 and 5. In the glassy state the resonance frequency is decreasing in time. The trend is shown in table 4, together with the increasing resonance frequencies observed in figure 5.
The decrease in resonance frequency of the polyacrylic acid film cast with an initial thickness of 50 µm, can never be attributed to a lowering of the complex modulus, since residual water can only be removed from the polymer film. The only explanation is a decrease in the height of the vitrified polyacrylic acid/water film. The

table 4: Resonance frequency and bandwidth at two different times after casting polyacrylic acid/water solutions with various casting thicknesses.

casting thickness µm	time seconds	resonance frequency Hz	resonance bandwidth Hz
50	10000	385 - 389	23 - 42
	80000	380 - 383	29 - 35
100	10000	374 - 377	26 - 29
	80000	381 - 384	26 - 30
150	10000	383 - 385	28 - 30
	80000	389 - 392	26 - 31
200	10000	418 - 422	31 - 37
	80000	424 - 427	26 - 32

effect of this shrinkage should overrule the effect of the increase in complex shear modulus, if present. The latter effect is shown in figure 5.

In order to obtain more information concerning the behaviour of the DFTP one experiment is shown on the drying of a water-thinnable paint. Instead of the PUR film a PDMS film has been used as substrate. After casting the paint, it did recede from the rubber film so that only part of the gap between pendulum and teflon plate is covered. About 50° out of 360° of the gap is covered with the paint, with a thickness of $4.7 \pm 0.5 \cdot 10^2$ µm. This would correspond, if only the paint determines the mechanical impedance, to a homogeneous film with a thickness of 65 µm.
In figure 7 only the first part of the drying curve is shown, after 15.000 seconds the bandwidth is continuously increasing, the experimental procedure to keep track of the resonance curve is getting instable, although the apparent resonance frequency is being constant in time then. The unstable bandwidth of the resonance curve is probably due to a film with a non-uniform thickness, like in the experiments with the polyvinylalcohol/water solutions.

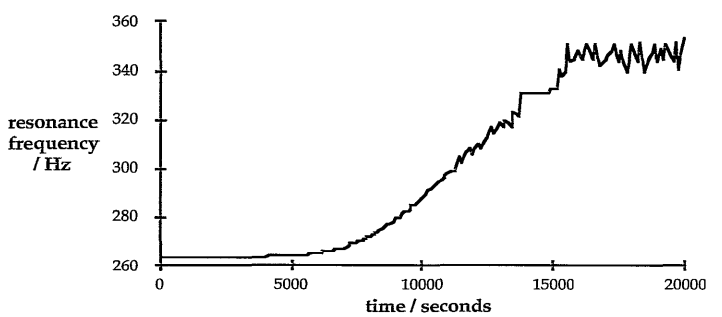

figure 7: Change of resonance frequency in time during the evaporation of water from paint.

A smooth increase in time is seen in the resonance frequency, compared to the drying of the polyvinylalcohol/water and polyacrylic acid/water solutions. However, the support is different, having a much lower shear modulus compared to the PUR support. The lower shear modulus of the PDMS support is the plausible cause of the smooth increase in the resonance frequency, because when the complex shear modulus of the paint is of the order of the shear modulus of the PDMS, the influence of the paint is already noticed.

6.5. Discussion

In this concluding paragraph both the drying-film torsion-pendulum and the experiments with this apparatus are discussed.
The DFTP is a completely new apparatus, designed to monitor the drying of a paint or a polymer solution. The operating principle is based on the change in the resonance curve due to the loading of the pendulum. The polymer solution is brought into contact with the pendulum with a rubber film acting as an intermediate.
The necessity to use a rubber film is a weak point of the DFTP. Several conflicting conditions have to be met. The rubber film may not swell and certainly not dissolve in the solvent of the polymer solution to be investigated. On the other hand the polymer solution should wet the rubber film. Furthermore the shear modulus of this film should be small compared to the modulus of the dry polymer film.
A cross-linked polydimethylsiloxane film has a high solvent resistance and a low shear modulus, but is very hydrophobic. The hydrophobic nature of this rubber film turns out to be a disadvantage. It is not possible to prevent the polymer solution from movement in the plane of casting, thereby dewetting the substrate. Another, more hydrophylic film of polyurethane can solve this problem, but then the solvent resistance is worse and the shear modulus is appreciably higher. Due to these problems only a limited number of experiments has been performed.
The observed phenomena with the DFTP are distinct. The resonance frequency shifts noticably to higher frequencies upon loading of the torsion pendulum. The corresponding change in bandwidth of the resonance curve is even more pronounced. The large bandwidths involved have several drawbacks. A larger frequency span is needed to record the resonance curve. Therefore one can not assume that the mechanical impedance is a constant within the frequency range used. Also the offset in the resonance curve due to cross-talk between sending and detection coils is not constant. The frequency dependence of the offset becomes prominent at higher frequencies. Although this is not shown, it has been verified by measuring the resonance curve of the unloaded pendulum, far away from resonance.
Fitting the measured transfer function to the equations governing the resonance curve, is not allowed because of the forementioned reasons. Therefore only the changes in resonance frequency during drying have been represented.

Water is the evaporating solvent in all the experiments described.
After drying a polyvinylalcohol/water solution, a film could be peeled of the PUR substrate. This film is certainly no gel, although both the solutions of polyvinylalcohol and polyacrylic acid can form a gel. Therefore the sharp increase in the resonance frequency in the first 10.000 seconds is attributed to the glass transition of the polymer solution.
Although polyacrylic acid does not form a coherent film, water will evaporate in a time comparable to the time to dry a polyvinylalcohol/water solution with the same casting thickness and the same initial concentration of the polymer solution. Taking into account the relatively high modulus of the PUR substrate, the sharp increase in the resonance frequency during the drying of a polyacrylic acid/water solution can safely be attributed to the glass transition.
A nice advantage of the DFTP is that, although polyacrylic acid is not a so-called film-forming polymer, the vitrification of a solution containing this polymer can be determined with a dynamic-mechanical technique.

The drying curves of polyacrylic acid/water solutions are not similar to the corresponding curves with polyvinylalcohol. With the latter polymer no distinct changes can be seen in the glassy state. With polyacrylic acid both an increase and a decrease of the resonance frequency, can be seen in the glassy state. The casting knife with the 50 μm slit height shows in time a decrease, whereas the other casting knives with larger slit heights, show an increase of the resonance frequency. The difference between the curves shown results from the absolute time needed to vitrify the complete polyacrylic acid/water solution, this time is less for the smaller slit heights.
The decrease in time cannot be due to evaporation of residual solvent, because in a thicker film more residual solvent is expected. Furthermore, there is no reason why the complex shear modulus of the 'dry' polyacrylic acid should decrease upon removal of water. The decrease in resonance frequency must be a result of a decrease in thickness, due to a compaction of the polyacrylic acid film. Polymer relaxation is taking place.
An increase of the resonance frequency in time implies that the shear modulus is increasing in time. This can be due to the evaporation of residual solvent and/or a structural relaxation of the polymer matrix.

6.6. Acknowledgement

E. Altena and G. Beukema are acknowledged for their support in constructing the drying-film torsion-pendulum. H.T.M. van den Ende is acknowledged for the discussions about the work presented in this chapter and in the appendix.

6.7. List of symbols

g	relaxation function, the response of the shear stress to a unit step in shear strain
h	height
i	imaginary unit
k	wave vector

m	mass
r	radius
t, t'	time
v_θ	velocity in θ-direction
z	place coordinate
α	angle
γ	shear deformation
η^*	complex viscosity
Θ	angle of rotation
ρ	density
τ	shear stress
χ	parameter in transfer function, depending on R, X, I, D, K and ω
ω	angular frequency
ω_0	resonance frequency
$\Delta\omega$	bandwidth
C	constant
D	damping of torsion axis
G^*	complex shear modulus
G'	storage modulus
G''	loss modulus
H	transfer function
H_0	parameter in transfer function, depending on R and D
I	moment of inertia
K	spring constant of torsion axis
M	torque
M_e	molecular weight between entanglements or crosslinks
R	real part of mechanical impedance *or* gas constant *or* radius
S	linear displacement in θ-direction
T	temperature
V_1,V_2	voltage, potential
X	imaginary part of mechanical impedance
Z	mechanical impedance

6.8. References

1. L.C.E. Struik, Physical aging in amorphous polymers and other materials, Elsevier 1978.
2. J.W.F. Spitzen, G.H. Koops, M.H.V. Mulder, C.A. Smolders, The influence of membrane thickness on membrane performance, Proceedings of third international conference on pervaporation processes in the chemical industry, ed. by R, Bakish, Nancy, France 1988.
3. R.R. Meyers, Relaxations during the formation of films, J. Polym. Sci., Part C 35 (1971) 3-21.
4. C.J. Knauss, Molecular relaxation processes during film formation, Surface Coatings 1 (1987) 233-265.
5. D.S. Tjin A-Lim, Crosslinking of poly(meth)acrylates with bisketeenimine, verbal communication, SON-meeting on Macromolecules, Lunteren, 1991.
6. Jianfu Ding, Gi Xue, Rongshi Cheng, Dynamic analysis of flat-spring supported polymers,J. Appl. Polym. Sci. 45 (1992) 987-991.
7. J. van den Berg, H.J. de Vries, Fatipec 1984, Lugano, Vol II, 343.
8. W.P. Mason, W.O. Baker, H.J. McSkimin, J.H. Heiss, Measurement of shear elasticity and viscosity of liquids at ultrasonic frequencies, Physical Review 75 (1949) 936-946.
9 C. Blom, J. Mellema, Torsion pendula with electromagnetic drive and detection system for measuring the complex shear modulus of liquids in the frequency range 80-2500 Hz, Rheologica Acta 23 (1984) 98-105.
10. D. van den Ende, J. Mellema, C. Blom, Driven torsion pendulum for measuring the complex shear modulus in a steady shear flow, Rheologica Acta 31 (1992) 194-205.
11. H. Markovitz, Boltzmann and his superposition principle: centenary observance, Proc. of the VIIth Int. Congress on Rheology, (1976) 37-39.
12. J.S. Vrentas, C.M. Jarzebski, J.L. Duda, A Deborah number for diffusion in polymer-solvent systems, AIChE Journal 21 (1975) 894-901.
13. J.D. Ferry, Viscoelastic properties of polymers, John Wiley & Sons 1980, Ch. V.

14. F. Ganzevles, Calibratie en uittesten van een superponerende oscillator, master thesis, University of Twente, August 1990.
15. R.B. Bird, R.C. Armstrong, O. Hassager, Dynamics of polymeric liquids, Volume 1 Fluid Mechanics, John Wiley & Sons 1987,
- Ch. V,
- Table A.7-2 and B.3.
16. B.Z. Jang, H.B. Hsieh, M.D. Shelby, Real time cure monitoring of composite structures using the technique of mechanical impedance analysis, Polymer Composites 12 (1991) 66-74.
17. I. Blume, A. Bos, P.J.F. Schwering, M.H.V. Mulder, C.A. Smolders, Transport phenomena of vapour and liquid permeants in elastomeric membranes, Proceedings of Fifth International Conference on Pervaporation Processes in the Chemical Industry (1991) 190-199.
18. B.H.A.A. van den Brule, A contribution to the micro-rheological modeling of transport properties, PhD-thesis, University of Twente, Enschede, the Netherlands, 1991.
19. Polymer Handbook, ed. by J. Brandrup and E.H. Immergut, John Wiley & Sons 1989.

Appendix A

The Navier-Stokes Equation applied to the Geometry of the Drying-Film Torsion-Pendulum

In this appendix it is attempted to solve the Fourier transforms of two partial differential equations which resemble the Navier-Stokes equation, in order to calculate the mechanical impedance experienced by the torsion-pendulum.
Shear waves are propagating vertically from the pendulum interface into the rubber film, and are spreading out radially at the same time. First the combined radial and the vertical propagation of shear waves is analyzed. As this problem is hard to solve mathematically, the propagation of shear waves is assumed to be radial in a second, simplifying attempt. In the figure below a cross-section is given of the area of interest where propagation of shear waves is involved.

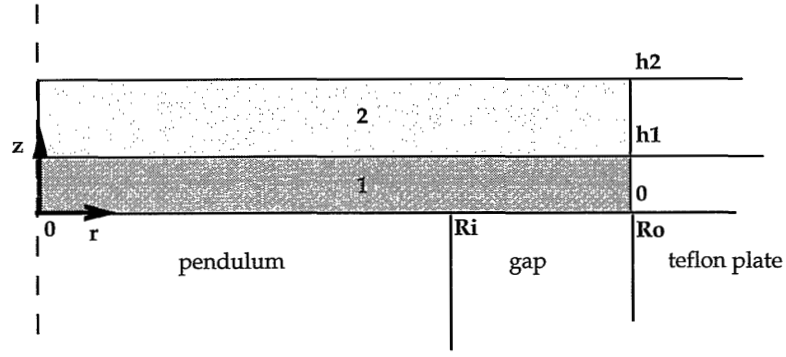

figure 1: Cross-section of the layers on the drying-film torsion-pendulum, defining the radii and the heights of the layers. Layer 1 is the rubber substrate, and layer 2 is a polymer film or a deposited polymer solution.

In figure 1 the heights of layer 1 and layer 2 are defined, as well as the radii of the pendulum geometry, the inner radius R_i and the outer radius R_o.

Combined radial and vertical propagation of shear waves:
Because of the oscillation of the torsion pendulum shear waves are propagating into the rubber film on top of the pendulum. In case this film is covered by another layer, a polymer solution or a glassy film, shear waves will propagate into the latter medium too. Two partial differential equations are encountered.

$$-\omega^2 \frac{\rho_1}{G_1^*(i\omega)} = \frac{1}{S_1(r,z)} \frac{\partial^2 S_1(r,z)}{\partial z^2} + \frac{1}{S_1(r,z)} \frac{\partial^2 S_1(r,z)}{\partial r^2} + \frac{1}{rS_1(r,z)} \frac{\partial S_1(r,z)}{\partial r} - \frac{1}{r^2}, \qquad (1a)$$

The only unknown parameter left, a_{m1}, can be determined if the motion is known for z=0 and r is in [0, R_o], see eq. (8.3.2.) from ref. [2].

$$a_{m1} = \frac{2}{R_o^2 (J_2(k_{1r}R_o))^2} \int_0^{R_o} r\, S_1(r,0)\, J_1(k_{1r}r)\, dr. \qquad (8f)$$

Eqs. (5, 6, 8a-8f) give the analytical solution to the problem if $S_1(r,0)$ is known.
At the interface of the torsion-pendulum with the rubber film, there can be no deformation in the radial direction. The rubber film moves with the pendulum.

$$S_1(r,z=0) = r\theta, \quad 0 \le r \le R_i, \qquad (9)$$

with θ the angle of rotation of the torsion pendulum.
Due to the geometry one may expect a radial deformation in the gap between the pendulum and teflon plate. The solution to the radial propagation of shear waves is given in eq. (12). An analytical solution to the propagation of shear waves exists. This solution is given by the combination of eqs. (5, 6, 8, 9 and 12). The analytical solution does not converge however, for the first twenty values of radial wave vector k_{1r} that correspond to eq. (8b).

One may also try to solve numerically eqs. (1a) and (1b) but then the numerical grid representing the discrete values of radius r and height z needs a very fine mesh near $r=R_i$ and z=0. There the deformation rapidly changes from vertical deformation to radial deformation. This problem is represented in eqs. (10a) and (10b).

$$r \uparrow R_i : k_{1r} = 0, k_{1z} = \omega \sqrt{\frac{\rho_1}{G_1^*(i\omega)}}. \qquad (10a)$$

$$r \downarrow R_i : k_{1r} = \omega \sqrt{\frac{\rho_1}{G_1^*(i\omega)}}, k_{1z} = 0. \qquad (10b)$$

It has not been possible to solve the partial differential equations that apply to the propagation of shear waves in the geometry of the drying-film torsion-pendulum analytically or numerically.

Radial propagation of shear waves:
In a simplifying attempt one can assume there is no or neglible deformation in the vertical direction. This is the same as stating that S(r,z) is no or hardly any function of z. To make the picture clear; the deformation is in between two coaxial cylinders, the inner one, with radius R_i, is oscillating with amplitude $R_i\theta$, and the outer one, with radius R_o, is not oscillating.
The Navier-Stokes equation reduces to:

$$-\omega^2 \frac{\rho}{G^*(i\omega)} = \frac{1}{S(r)} \frac{\partial^2 S(r)}{\partial r^2} + \frac{1}{S(r)} \frac{\partial S(r)}{\partial r} - \frac{1}{r^2}. \qquad (11)$$

The solution of eq. (11) is standard.

$$S(r) = R_i\theta \left\{ \frac{J_1(kr)\, Y_1(kR_o) - J_1(kR_o)\, Y_1(kr)}{J_1(kR_i)\, Y_1(kR_o) - J_1(kR_o)\, Y_1(kR_i)} \right\}. \qquad (12)$$

The shear deformation at R_i is given by

$$\gamma(R_i) = \left(\frac{dS(r)}{dr} \right)_{R_i} - \frac{S(R_i)}{R_i}. \qquad (13)$$

Analogous to the derivation of eq. (21) in chapter 6, the mechanical impedance for radial deformation is obtained.

$$Z(i\omega) = -i\, 2\pi R_i^2 h \frac{G^*(i\omega)}{\omega} f(k,R_i,R_o), \qquad (14)$$

with

$$f(k,R_i,R_o) = \left\{ \frac{2J_1(kR_i)Y_1(kR_o) - 2J_1(kR_o)Y_1(kR_i) - kR_iJ_0(kR_i)Y_1(kR_o) + kR_iJ_1(kR_o)Y_0(kR_i)}{J_1(kR_i)Y_1(kR_o) - J_1(kR_o)Y_1(kR_i)} \right\}. \qquad (15)$$

The numerical evaluation of eqs. (14-15) has been performed with a personal computer, applying the 'Numerical Recipes in Pascal' software [3]. The inner and outer radius of the DFTP are determined by the physical geometry of the pendulum, and are respectively 1.4 and 1.7 cm. Calculations are performed for only one film.
From eq. (14) it is clear that the mechanical impedance is directly proportional to the height h.

$$Z(i\omega), R(\omega), X(\omega) \propto h. \qquad (16a)$$

The influence of the storage and the loss modulus, and angular frequency has been determined with the computer program, varying the storage modulus from 10^5 Nm^{-2} to 10^{11} Nm^{-2}, the ratio of the loss modulus to the storage modulus from 10^{-1} to 10^{-3}, the frequency from 250 to 800 Hz, and the density from 10^2 to 10^4 kgm^{-3}. The conditions chosen represent a material of a predominantly elastic nature, so that gap-loading of the torsion pendulum is ensured. The frequency range does include the operational frequency range of the DFTP. With these variables the following applies:

$$|Z(i\omega)| \tilde{\propto} |G^*(i\omega)|, \qquad (16b)$$

$$\frac{R(\omega)}{X(\omega)} \cong \frac{G''(\omega)}{G'(\omega)}, \tag{16c}$$

and

$$Z(i\omega), R(\omega), X(\omega) \overset{\sim}{\propto} \frac{1}{\omega}. \tag{16d}$$

The mechanical impedance is hardly any function of the density.

References

1. F.W.J. Olver, Bessel functions of integer order, Handbook of mathematical functions with formulas, graphs, and mathematical tables, ed. by M. Abramowitz, I.A. Stegun, John Wiley & Sons 1972.
2. G.F.D. Duff, D. Naylor, Differential equations of applied mathematics, John Wiley & Sons 1966, Ch. VIII, §3.
3. W.H. Press, B.P. Flannery, S.A. Teukolsky, W.T. Vetterling, Numerical recipes in Pascal, Cambridge University Press 1989.

Summary

Dense polymeric films can be used as permeation-selective barriers which change the composition of a fluid by differences in solubility and/or diffusivity of fluid components in the membrane material. In general glassy polymers show rather high selectivities, but usually in combination with low fluxes. Since membrane fluxes are inversely proportional to the selective barrier thickness, membranes are made as thin as possible. For pervaporation membranes the approach to prepare thin membranes failed with respect to the selectivity of the membrane. In literature membrane selectivities were reported to decrease with decreasing membrane thickness. Furthermore the membrane preparation procedure by drying a polymer solution cast on a suitable support influences the selective permeation.
The drying process of a polymer solution and its effect on the membrane performance in pervaporation have been investigated in this thesis. Two time-scales are involved in both the membrane preparation and in its use during pervaporation. First a concentration profile develops in time and secondly polymer relaxation will occur due to changes in the state of swelling accompanying the development of a concentration profile.

In chapter 1 a brief introduction is given to the different modes of solvent transport in glassy polymers. The time-scale of developing a concentration profile is compared to the time-scale of polymer relaxation, applying the concept of the Deborah number for diffusion. This Deborah number for diffusion is referred to in pervaporation and in the drying process employed in membrane preparation.
Chapter 2 describes the pervaporation experiments. An important feature of the experiments applying polyacrylonitrile membranes with thicknesses below 20 μm, in pervaporation using a feed mixture of ethanol and water, is that fluxes decrease in time and that separation factors increase in time. These observations are in contradiction with the development of a concentration profile, which predicts that the total flux through the membrane can only increase in time until a steady-state flux is reached. Diffusion along a concentration gradient, Fick's first law, does not apply to the observed transient permeation in the pervaporation experiments.
The history dependence of membrane performance has been noticed in the transient state of pervaporation. Pre-swelling of the membranes, prior to pervaporation, deletes the previous history of membrane preparation.
Experiments with an automated pervaporation set-up are new in its kind. The direct analysis of the permeate from the vapour phase allows higher sampling rates of the permeate compared to the usual pervaporation equipment. Large changes in flux and membrane selectivity are noticed especially within the first quarter of an hour after starting the pervaporation process.
Chapter 3 is a general discussion of the diffusive transport of a single solvent in a glassy polymer. The gradient in the chemical potential is used as the driving force for

permeation instead of a concentration gradient only. The chemical potential of the solvent is a function of the solvent concentration in the membrane and of the volume deformation imposed onto the polymer matrix due to a change in solvent concentration. Two coupled partial differential equations are used to describe the local change in time of solvent volume fraction and tensile stress. The boundary conditions account for the solvent uptake and polymer relaxation at the membrane interfaces. The swelling of the membrane interface has been considered for the ternary system polyacrylonitrile/water/ethanol, corresponding to the membrane material and feed mixture applied in the pervaporation experiments described in chapter 2.

In chapter 4 the drying process has been simulated numerically assuming that volume relaxation can follow the drying process. A Deborah number of drying is introduced and the time-scale of the drying process is compared to the polymer relaxation time. Knowledge of the dry film thickness of a cast polymer solution, the relaxation time of the dry polymer and the solvent diffusion coefficient at zero solvent volume fraction allows an estimation whether or not drying proceeds in a polymer solution/film that maintains local equilibrium. Excess free volume will be entrapped in the polymer matrix when the process of volume relaxation is too slow compared to the drying process.

In chapter 5 the dielectric experiments during drying of a polymer solution, applying the comb electrode configuration, are described. Significant changes are observed in the glassy state of the plasticized polymer film due to the high dipole moments of the solvents used. A model is proposed to describe the solvent mass transfer in the glassy state of a polymer towards the membrane interface where evaporation can take place. The calculated solvent mass transfer coefficients are an exponential function of the bulk solvent concentration, which explains the self-decreasing rate of the drying process. From the analysis of the calculated solvent mass transfer coefficients, which range from 10^{-10} to 10^{-8} ms^{-1}, it is concluded that the drying of a polymer solution is too fast compared to volume relaxation when applying the glassy polymers polyethersulfone and polyimide, the solvent dimethylformamide and when final film thickness are below ≈ 10 μm.

In chapter 6 the mechanical properties of a drying polymer solution are monitored in a non-invasive way with the drying-film torsion-pendulum. This new apparatus is very sensitive to very thin films of a glassy polymer. A drawback of the method is encountered in the various requirements imposed onto the material that is used to support the cast polymer solution. For this reason only a limited number of experiments has been carried out with water soluble polymers. A significant change in the drying curve, i.e. the resonance frequency of the pendulum plotted versus time, represents the vitrification of the polymer solution. In the glassy state gradual changes in the resonance frequency are measured and they are attributed to an increase in the shear modulus of the polymer when the resonance frequency is increasing in time, or they are attributed to a decrease in the polymer film thickness when the resonance frequency is decreasing in time.

Samenvatting

Dichte polymere films kunnen worden gebruikt als permeatie-selectieve barrières die de samenstelling van een vloeistof- of gasmengsel veranderen op basis van verschillen in oplosbaarheid en/of diffusiesnelheid van de verscheidene componenten in het membraan. In het algemeen vertonen glasachtige polymeren relatief hoge selectiviteiten, maar deze gaan gewoonlijk gepaard met lage fluxen. Daar de fluxen door het membraan omgekeerd evenredig zijn met de dikte van de selectieve barrière maakt men membranen zo dun mogelijk. De benadering om dunne membranen te maken heeft, m.b.t. de selectieve permeatie in het pervaporatie proces, niet tot het beoogde resultaat geleid. In de literatuur wordt melding gemaakt van een afnemende selectiviteit met afnemende membraandikte. Verder beïnvloedt de bereidingswijze van het membraan, d.w.z. het drogen van een polymeeroplossing gestreken op een geschikte ondergrond, de selectieve permeatie.
Het droogproces van een polymeeroplossing en het effect daarvan op de transporteigenschappen van het membraan zijn onderzocht in dit proefschrift. Twee tijdschalen zijn van belang in zowel de membraanbereiding als het gebruik in pervaporatie. Ten eerste ontwikkelt zich in de tijd een concentratieprofiel in het membraan en ten tweede treedt er polymeer relaxatie op ten gevolge van veranderingen in zwelgraad die ontstaan juist dóór de ontwikkeling van het concentratieprofiel.

In hoofdstuk 1 wordt een korte introductie gegeven over de verschillende wijzen van oplosmiddeltransport in glasachtige polymeren. De tijdschaal karakteristiek voor de ontwikkeling van een concentratieprofiel wordt vergeleken met de tijdschaal die hoort bij polymeer relaxatie, aan de hand van het concept van het Deborah getal voor diffusie. Zowel in het pervaporatieproces als in het droogproces gebruikt in de membraanbereiding, wordt gerefereerd aan dit Deborah getal voor diffusie.
Hoofdstuk 2 beschrijft de pervaporatie experimenten. Karakteristiek voor deze experimenten, waarin polyacrylonitrile membranen met een dikte kleiner dan 20 μm en een voedingsmengsel voor pervaporatie van ethanol en water worden toegepast, is dat fluxen afnemen met de tijd en dat scheidingsfactoren toenemen met de tijd. Deze waarnemingen zijn in tegenspraak met de ontwikkeling van alleen een concentratieprofiel, waarbij wordt voorspeld dat de totale flux door het membraan slechts kan toenemen met de tijd totdat er een stationaire flux is bereikt. Diffusie langs een concentratiegradiënt, de eerste wet van Fick, kan niet worden toegepast op de waargenomen niet-stationaire permeatie in de pervaporatie experimenten.
De afhankelijkheid van de voorgeschiedenis op de membraan transporteigenschappen is waargenomen in de niet-stationaire toestand van pervaporatie. Het voorzwellen van de membranen, voorafgaand aan pervaporatie, wist de voorgeschiedenis van membraanbereiding volledig uit.
Experimenten met een geautomatiseerde pervaporatie-opstelling maken gebruik van

een nieuwe meetmethode. De directe analyse van het permeaat vanuit de dampfase staat snellere bemonsteringen van het permeaat toe vergeleken met de gebruikelijke apparatuur voor pervaporatie. Grote veranderingen in flux en membraanselectiviteit worden waargenomen, vooral in het eerste kwartier nadat het pervaporatieproces is gestart.
Hoofdstuk 3 is een algemene discussie van het diffunderen van een enkel oplosmiddel in een glasachtig polymeer. De gradiënt in de chemische potentiaal wordt gebruikt als de drijvende kracht voor permeatie in plaats van enkel een concentratie-gradiënt. De chemische potentiaal van het oplosmiddel is een functie van de concentratie van het oplosmiddel en van de volume-vervorming opgelegd aan de polymeer matrix ten gevolge van een verandering in de concentratie van het oplosmiddel. Twee gekoppelde partiële differentiaalvergelijkingen worden gebruikt om lokaal de verandering in volumefractie van het oplosmiddel en rekspanning te beschrijven. De randvoorwaarden houden rekening met de opname van het oplosmiddel en polymeer relaxatie aan de membraanoppervlakken. De zwelling van het membraanoppervlak is geanalyseerd voor het ternaire systeem polyacrylonitrile/ water/ethanol, welke overeenkomt met het membraanmateriaal en het voedingsmengsel gebruikt in de pervaporatie experimenten zoals beschreven in hoofdstuk 2.
In hoofdstuk 4 is het droogproces numeriek gesimuleerd onder aanname dat volume relaxatie het droogproces kan bijhouden. Een Deborah getal voor het droogproces wordt geïntroduceerd en de tijdschaal van het droogproces wordt vergeleken met de relaxatietijd van het polymeer. Kennis van de droge filmdikte van een gestreken polymeeroplossing, de relaxatietijd van het polymeer en de diffusiecoefficiënt van het oplosmiddel bij een oneindig kleine concentratie van het oplosmiddel, maakt een schatting mogelijk of het drogen al dan plaatsvindt in een polymere oplossing/film die lokaal nog zijn evenwicht behoudt. Een teveel aan vrij volume wordt ingesloten in de polymere matrix wanneer het proces van volume relaxatie te langzaam is vergeleken met het droogproces.
Hoofdstuk 5 beschrijft de diëlectrische experimenten, m.b.v de kamelectrode configuratie, tijdens het drogen van een polymeeroplossing. T.g.v. het hoge dipoolmoment van de gebruikte oplosmiddelen worden significante veranderingen waargenomen in de glastoestand van de geplastificeerde polymere film. Een model wordt gegeven dat het transport van het oplosmiddel beschrijft in de richting van het vrije oppervlak waar verdamping kan plaatsvinden, in de glastoestand van het polymeer. De berekende stofoverdrachtscoëfficiënten zijn een exponentiële functie van de concentratie van het oplosmiddel in de bulk. Dit verklaart het zichzelf vertragende droogproces. Uit de analyse van de berekende stofoverdrachts-coëfficiënten, welke variëren van 10^{-10} tot 10^{-8} ms^{-1}, wordt geconcludeerd dat het drogen van een polymeeroplossing te snel gaat vergeleken met volume relaxatie wanneer de glasachtige polymeren polyethersulfon en polyimide, het oplosmiddel dimethylformamide en filmdiktes onder $\approx$ 10 μm worden toegepast.
In hoofdstuk 6 worden de mechanische eigenschappen van een drogende polymeeroplossing gevolgd m.b.v. een drogende-film torsieslinger, die het

droogproces niet beïnvloedt. Dit nieuwe apparaat is zeer gevoelig voor zeer dunne films van een glasachtig polymeer. Een nadeel van deze methode zijn de eisen die worden opgelegd aan het materiaal dat de gestreken polymeeroplossing moet dragen. Om deze reden zijn slechts een beperkt aantal experimenten uitgevoerd met wateroplosbare polymeren. Een significante verandering in de droogcurve, d.i. de resonantiefrequentie van de torsieslinger uitgezet tegen de tijd, geeft de verglazing van de polymeeroplossing weer. In de glastoestand worden geleidelijke veranderingen in de resonantiefrequentie gemeten en deze worden toegekend aan een toename van de afschuifmodulus van het polymeer wanneer de resonantiefrequentie toeneemt met de tijd, of ze worden toegekend aan een afname van de filmdikte van het polymeer wanneer de resonantiefrequentie afneemt met de tijd.

Levensloop

Richard Bouma werd geboren op 23 september 1967 te Zuidhorn. Aan het Lambert Franckens College te Elburg behaalde hij in 1985 zijn VWO diploma. In 1985 begon hij de studie Technische Natuurkunde aan de Technische Hogeschool Twente. Van september 1989 tot en met november 1989 verrichte hij zijn stage bij het Joint Research Centre van de Europese Gemeenschap te Ispra (Italië). De afstudeeropdracht werd verricht binnen de vakgroep Reologie van de faculteit Technische Natuurkunde, onder leiding van prof. dr. P.F. Mijnlieff, en betrof de bepaling van dynamisch-mechanische moduli uit de analyse van de spanningsrespons op niet-harmonische deformaties. Per 15 december 1990 begon hij als onderzoeker in opleiding in dienst van NWO aan het in dit proefschrift beschreven onderzoek. Het onderzoek werd verricht binnen de vakgroep Membraantechnologie van de Universiteit Twente onder leiding van prof. dr. C.A. Smolders en later prof. dr. ing. H. Strathmann. Vanaf maart 1995 is hij werkzaam aan de Università degli Studi della Calabria (Italië) in de onderzoeksgroep van prof. dr. E. Drioli.

Dankwoord

Ter afsluiting van dit proefschrift wil ik een woord van dank richten aan een ieder die in de afgelopen vier jaren heeft bijgedragen tot dit werk.
Een deel van het experimentele werk is verricht door anderen. Zandrie Borneman heeft de geautomatiseerde pervaporatie opstelling aan de praat kunnen krijgen. Het draaiende houden van deze opstelling en het waar mogelijk verbeteren van de opstelling was zeer zeker geen eenvoudige taak. De geleverde inspanning heeft in ieder geval zeer bruikbare resultaten opgeleverd. Ook Paulien Pulskens en Eric Velthuizen hebben zich bezig gehouden met pervaporatie. De asymmetrie van de droogstap in de membraanbereiding en de invloed van zwelling en ontzwelling van membranen op de scheidingseigenschappen was al zichtbaar in jullie werk.
Bij de diëlectrische metingen heeft Edwin Valstar de basis voor de meetprogrammatuur gelegd. Michiel van der Veldt heeft de eerste metingen uitgevoerd en een analyse van de meetfouten opgezet. Tijdens de eerste metingen werden uit de experimentele data bij zeer hoge frequenties negatieve diëlectrische constantes berekend. Dit is de directe aanleiding geweest tot het analyseren van de weerstand in de gebruikte electrode configuratie.
Naast het experimentele werk waren er regelmatig besprekingen met prof. dr. ing. H. Strathmann, prof. dr. C.A. Smolders, prof. dr. P.F. Mijnlieff en dr. ir. Th. van den Boomgaard. Of ik nu met één van u sprak of we kwamen met zijn vijven bij elkaar, de discussies waren vaak boeiend en leerzaam.
De dimensionele stabiliteit van polymere schuimen lag wel ver buiten mijn onderzoeksgebied, maar met veel plezier denk ik terug aan de afstudeerperiode van Warner Nauta. In deze periode, die je deels doorbracht in Twente en deels in Zuid Limburg, heb je met enthousiasme alsmaar naar nieuwe resultaten toegewerkt en nieuwe ideeën naar voren gebracht.
Tijdens de afgelopen vier jaren heb ik meegedraaid in de vakgroep membraantechnologie. De belangstelling van jullie zijde en van de zijde van familie, vrienden en kennissen is tot grote steun geweest.

Bovenal wil ik Tea bedanken,

Richard.

ISBN 90-9007846-0